DNA functionalized soft materials: preparation, biophysical properties and analytical applications.

by

Neeshma Dave

A thesis
presented to the University of Waterloo
in fulfillment of the
thesis requirement for the degree of
Doctor of Philosophy
in
Chemistry

Waterloo, Ontario, Canada, 2012

Author's Declaration

I hereby declare that I am the sole author of this thesis. This is a true copy of the thesis, including any required final revisions, as accepted by my examiners. I understand that my thesis may be made electronically available to the public.

Neeshma Dave

Abstract

Bio-nanotechnology is the use of biomolecules to control both the structure and property of nanomaterials. No biomolecule has been employed more often than DNA as exemplified in the numerous demonstrations of DNA-directed assembly of nanomaterials. DNA has been used to covalently functionalize and assemble soft nanoparticles (e.g. liposomes) and hard nanoparticles (e.g. gold and silica nanoparticles) into a variety of hierarchical nanostructures. The majority of previous work however has focused on the latter, i.e., the assembly of "hard" nanoparticles such as gold nanoparticles (AuNPs) as oppose to the assembly of soft materials. The primary focus of this thesis is to add to the growing field of DNA-directed assembly of soft materials owing to the promise of such materials in a variety of analytical and biomedical applications. The first class of soft materials considered are liposomes which interestingly can be deformed by relatively weak intermolecular forces. In addition, DNA anchored to its surface can readily diffuse laterally within the lipid bilayer while DNA attached to inorganic nanoparticles remain fixed in position. We systematically consider the effect of varying the liposome structure, size, charge, and fluidity on liposome assemblies, in chapter 2. In addition, the interesting properties of liposomes are highlighted by a side-by-side comparison to DNA-functionalized gold nanoparticles, offering fundamental insights into DNA-directed assembly. Furthermore, hybrid DNA-directed assemblies composed of both AuNPs and liposomes are described in Chapter 3. In particular, the photothermal effects of such DNA-coupled liposome and AuNP assemblies were modulated by controlling the distance between liposome and AuNP allowing such systems to have potential application in drug-delivery. In chapter 4, the utility of liposomes is demonstrated as we exploit the fluidity of its diffuse bilayer with split aptamer functionalization for the rapid and selective detection of metabolites. The second class of soft material of interest in this thesis are hydrogels, which are cross-linked hydrophilic polymers. Because hydrogels are swollen in water, they can be used to immobilize biomolecules such as DNA for a myriad of applications. In chapter 5, the preparation and characterization of DNA-functionalized polyacrylamide hydrogels are presented. The use of such a DNA-modified hydrogel for the simultaneous detection and removal of mercury from water is subsequently demonstrated.

Acknowledgements

I would like to express my sincerest gratitude to my Ph.D. research supervisor, Dr. Juewen Liu for his guidance, dedication, and fairness. I aspire to be more like him as a researcher and leader, in the future. I would also like to extend my sincerest gratitude to my Ph.D. research committee: Dr. E. Prouzet, Dr. D. Thomas, Dr. M. Palmer and Dr. S. Tang for their guidance and support during my Ph.D. studies at University of Waterloo. I would like to extend my gratitude to Dr. P. M. Macdonald and Dr. Z. Leonakeo for their time and patience. I would also like to thank Dr. P. Radovanovic and his research group for giving me the opportunity to work with them. I would also like to acknowledge the following people for their support and guidance: Cathy van Esch, Marguerite Greavette, Dr. M. Barra, Janet Venne, Dr. H. Siu, Dr. D. Donker. I would also like to extend my deepest thanks to Dr. G. Dmitrienko, Dr. J. Duhamel, Dr. J. Honek, Dr. E. Meiering, Dr. M. Palmer and their respective research groups for use of their equipment and space during my studies.

I would like to thank my research colleagues Po-Jung Jimmy Huang, Dr. Xu Zhang, Alexander Ip, Imran Khimiji, Lu Li, and Ajfan Baeissa for all their great discussions and the great times we shared. Remember the words “All izzz well”! To the nano-engineering students who taught me much more than I taught them I would like to thank Brendan D. Smith, Kevin A. Joseph, Marissa Wu, Nishi Bhatt, Firas El-Hamed, Mehmet Murat Kiy, Ahmed Zaki, Youseff Helwa, Zachary E. Jacobi, James L. Maclean, Arsalsan Beg Menhaj, Thomas A.C. Kennedy, Romain Froidevaux and to all of the nano-engineering students I have taught from the first graduating class till now. I would to like to leave them all with a quote from my favorite scientist Mr. Spock, “Live long and prosper”! And something I have come to realize is vital for living a life you want was articulated by the late Steve Jobs:

> Your time is limited, so don't waste it living someone else's life. Don't be trapped by dogma - which is living with the results of other people's thinking. Don't let the noise of others' opinions drown out your own inner voice. And most important, have the courage to follow your heart and intuition.

I found my courage, as I hope they do also.

To this particular group of people who have always believed in my hard work, honesty and integrity I would like to thank Dr. J. Fisher and Dr. M. Chong for everything. Thank-you to the great friends I have made at University of Waterloo Mike Makanoke, Apraku David Donker, Eric Brefo-Mensah, Cullen L. Myers, Jason DaCosta, Ting Wang, Ling-Ju, Hongyu Wu and to all of those that I shared a laugh with, debated with and yes shared downloads with**.** To the custodian staffs in C2 and ESC for their friendly greetings and their great kindness to a student working late at night thank-you Maria,

Joe, Dave and Tony, for taking care of our labs and our buildings. To my 90 year old friend Arthur who never forgets to say hello as I have walked up and down University Avenue.

To my mum and dad, Priyawadan and Kalpana Dave, I would like to say thank-you for working so hard for me and for always being proud of me. To my mum thank-you for always telling me what other career paths would have been a better choice! And yes mum I finally finished! I would also like to thank my sister, Krishma and my brother, Anooj who have never understood why I stayed in school for so long but have always supported me and loved me for it. I would also like to extend my sincerest gratitude to Elena and Antonio Puzzo who accepted an unconventional daughter-in law. Last but certainly not the least, I would like to thank my best friend and life partner who has this uncanny ability to make me laugh at myself Danny Puzzo. Thank-you for everything you have done for me and the hundreds of thousands of kilometers between Toronto and Waterloo you have travelled. I will never be able to repay you but thank-you for always encouraging me and guiding me. This is not just my achievement but it is our achievement. Malto tiamo! I would also like to thank Henrietta Lacks for her contribution to humanity and I am very sorry for the injustice you and your family suffered.

Dedication

To Danny, my parents, Krishma and Anooj for their love and support.

Table of Contents

List of Figures

List of Tables

List of Abbreviations

3σ/slope	three times the standard deviation of the noise
A	adenine
AgNPs	silver nanoparticle
APS	ammounium persulfate
AuNP	gold nanoparticles
Au-Au assemblies	DNA-directed gold nanoparticle assemblies
BDM	Branched DNA Molecule
Cd^{2+}	Cadmium ions
C	Cytosine
cDNA	complementary DNA
CHO	Chinese Hamster Ovary
CMC	critical micelle concentration
cryo-TEM	cryogenic transmission electron microscopy
2D	two-dimensional
3D	three-dimensional
K_d	dissociation constant
DNA	Deoxyribonucleic acid
DNA-AuNP	DNA functionalized gold nanoparticle via gold-thiol bond
DNA-liposome	DNA functionalized liposome
ds-DNA	double-stranded DNA
ss-DNA	single-stranded DNA
FAM/F	fluorescein
FWHM	full width at half-maximum
DOPC	1,2-dioleoyl-sn-glycero-3-phosphocholine
DOPG	1,2-dioleoyl-sn-glycero-3-phospho-(1'-rac-glycerol) (sodium salt)
DPPC	1,2-dihexadecanoyl-*sn*-glycero-3-phosphocholine
G	guanine
Hg^{2+}	mercury ions
HEK	human embryonic kidney cells
HEPES	4-(2-hydroxyethyl)-1-piperazineethanesulfonate

LUV	Large Unilamellar Vesicles
Mg^{2+}	magnesium ions
MPB-PE	1,2-dipalmitoyl-sn-glycero-3-phosphoethanolamine-N-[4-(p-maleimidophenyl)butyramide] (sodium salt)
MLV	Multilamellar Vesicles
Na^{+}	sodium ions
N-PDP-PE	1,2-dipalmitoyl-*sn*-glycero-3-phosphoethanolamine-N-[3-(2-pyridyldithio)propionate] (sodium salt)
PEG	polyethylene glycol
QDs	quantum dots
QCM-D	quartz crystal microbalance with dissipation
R_0	Förster distance
Rh-PE	1,2-dioleoyl-*sn*-glycero-3-phosphoethanolamine-N-(lissamine rhodamine B sulfonyl) (ammonium salt)
SNARE	soluble *N*-ethylmaleimide-sensitive factor attachment protein receptors
SPR	Surface Plasmon Resonance
SSB	single-stranded binding protein
SUV	Small Unilamellar Vesicles
T	thymine
T_m	melting temperature
T_c	phase transition temperature
TCEP	Tris(2-carboxyethyl)phosphine
TMR/R	TAMRA, Carboxytetramethylrhodamine dye
TEG	tetraethyleneglycol
TEMED	N,N,N',N'-tetramethylethylenediamine
Tris	tris(hydroxymethyl)aminomethane

Chapter 1.0 Introduction

1.1 Introduction.

Soft materials, such as lipid bilayers and hydrogels are interesting for the study of biological systems such as cell membranes and tissue engineering. These rather simple molecules or assemblies can be used as a model to study sophisticated biological tasks such as exocytosis, endocytosis, cellular signaling, biomolecule or solute migration, and transportation. Therefore, understanding the biophysical principles behind the operation of these systems can be potentially used to design artificial systems for analytical and biomedical applications. One of the most popular molecules to control the structure of nanomaterials and impart function is DNA. In the past thirty years, the function of DNA has been expanded from purely genomic functions to non-natural functions such as structural directing agent, catalyst, and ligand. Interfacing DNA with soft materials might further our understanding to generate new hybrid materials and devices.

Studying DNA-functionalized liposomes is motivated by several factors. First, from a biophysical perspective, the cell membrane is associated with various proteins, allowing complex processes such as membrane fusion to take place. While various fusion proteins and peptides have been identified, it remains difficult to have a molecular level understanding of the movement of protein and key lipids. Although DNA is not part of the natural cell membrane structure, the programmability of DNA hybridization can help us gain further insight into the fundamental bilayer rearrangement mechanism. Second, new physical principles may be elucidated by comparing soft liposomes with hard inorganic nanoparticles, by means of precise control of inter-particle distance by DNA. Last, molecular recognition and targeting properties of DNA alone can be used for making biosensors, and liposomes are ideal for signal amplification and drug containment. Therefore, a combination of DNA and liposomes would allow potential for new applications in sensing and more importantly drug delivery. Similarly, stimuli-responsive hydrogels have been used for detection of a variety of analytes, which has generally been achieved by monitoring a transition from swelled to collapsed gels, or sometimes a gel to sol transition. The commonly used stimuli include temperature, pH, ionic strength, light, and electric field. DNA functionalization of the hydrogel may allow hydrogels responsive to a diverse range of other chemical and biological stimuli to be prepared. Therefore, hybrid nanomaterials can be used to create effective sensors. In this chapter, the general structures and properties of DNA, aptamers, and the soft materials liposomes and hydrogels are introduced in detail.

1.1.1 Deoxyribonucleic acid (DNA).

Proteins are widely employed for catalysis and molecular recognition studies.[1-7] The successful synthesis of oligonucleotides using solid-phase DNA synthesis, which affords routine synthesis of a variety of sequences with greater than 100 nucleotides bearing desired chemical modification, transformed DNA from a purely (genomic) genetic material to a biological tool and building block capable of highly versatile function. This transformation is certainly evident in the field of nanotechnology, which has developed methods to interface DNA with soft materials, resulting in a number of interesting DNA-based structures and devices.[8-10] For example, DNA has been used as a template to assemble inorganic nanoparticles to form oligomers,[4] random aggregates,[5] crystals,[11-10] and two-dimensional structures.[2,12]

With the discovery of polymerase chain reaction (PCR), nucleic acid biotechnology has undergone a revolutionary change. PCR-based combinatorial selection methods have allowed for the isolation of DNA sequences with both catalytic and molecular recognition properties, i.e., aptamers.[13-15] This has allowed DNA to acquire novel chemical and biological functions. Therefore, DNA offers a number of advantageous properties that render it attractive for use in a variety of applications.[16] Firstly, DNA is relatively stable. Although increasing temperature can result in DNA duplex melting, rehybridization can be easily achieved by simply decreasing the temperature. This is not the case for some enzymes and proteins that denature irreversibly when temperature is increased, such as Taq polymerase. Second, the simple Watson-Crick base pairing rules allows for the facile prediction of DNA secondary structures with minimal information regarding the DNA three-dimensional (3D) structure. Lastly, solid-phase DNA synthesis and PCR allow for the synthesis of virtually any sequence with pre-specified modifications, which is particularly relevant to areas such as biosensing.

Deoxyribonucleic acid is made-up of four nucleotides. A nucleotide contains a purine or pyrimidine base, deoxyribose sugar and phosphate groups. The four nucleotides are adenine, thymine, guanine and cytosine (A, T, G, C). Adenine and guanine contain purines and cytosine and thymine consist of pyrimidines. In an oligonucleotide, the individual nucleotides are linked by the 3′-hydroxyl group of the 2′-deoxyribose and phosphate group of one nucleotide to the 5′-hydroxyl group of another nucleotide. This results in the formation of phosphodiester linkages that ultimately forms the sugar-phosphate backbone of DNA. Watson and Crick base pairing of DNA refers to the mutually specific formation of base pairs via hydrogen bonding between adenine and thymine on the one hand, and between guanine and cytosine on the other, as shown in Figure 1.1. Such highly specific binding capability of DNA renders it particularly attractive for use in molecular recognition experiments as well

as for applications that require sub-nanometer precision.[16a] Since the DNA phosphate backbone carries a negative charge, polyanionic DNA in aqueous solution adopts a molecular structure referred to as the B-form double-stranded (ds) DNA. It is pre-dominately the B-form DNA with 10 base pairs per turn every 3.4 nm was discovered by Watson and Crick and this is the form that we studied in this thesis. The other forms are A-form and Z-form DNAs which occur predominately in high salt solutions. This information is necessary in determining the length and stability of the studied duplex. The duplex is considered a rigid rod, which once heated above its melting temperature results in the formation of two flexible single-stranded (ss) DNA molecules. The melting temperature of dsDNA has been studied as a function of sequence length, the number of base pairs, and various amounts of guanine to cytosine content.[16b]

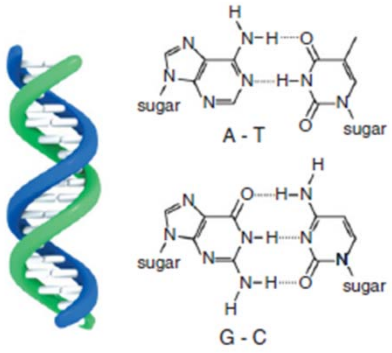

Figure 1.1 Molecular structure of double-stranded DNA duplex made-up of four nucleotides. A nucleotide contains a purine or pyrimidine base, deoxyribose sugar and phosphate group. The four nucleotides are adenine, thymine, guanine and cytosine (A, T, G, C). Adenine and guanine consists of purines and cytosine and thymine consist of pyrimidines. Figure adapted with permission from ref (18n). Copyright from Wiley Publishing Group.

1.1.2 Solid-phase synthesis of DNA.

DNA synthesis using solid-phase synthesis was first developed by Khorana and coworkers in the 1960s.[17a] In 1983, following several years of trying to achieve better efficiency and longer oligonucleotides, successful synthesis was achieved using phosphoramidite monomers and tetrazole catalysis.[17b,c] The advantages of using phosphoramidite are several. For one, this monomer is a nucleotide containing protection groups such as trityl groups added to the amine, hydroxyl, and phosphate groups. Protection groups prevent side-reactions and they can be easily removed after synthesis. The

linkage to the solid support, which consists of 5 micron pore glass beads with holes and channels (CPG), is made through the 3′ carbon on the sugar group. The oligonucleotide synthesis then progresses through 3′ to 5′ linkages. Each added nucleotide undergoes five steps; i.e., deprotection, coupling, capping, stabilization, and cleavage. For deprotection, the first step is to remove the trityl group on the 5′ carbon of the pentose sugar attached to the solid-support. This is achieved by treating the nucleoside with trichloroacetic acid (TCA), exposing a reactive hydroxyl group to which the next base is added. The coupling step involves treatment of the nucleotide with tetrazole to form a tetrazolyl phosphoramidite intermediate, which reacts with the nucleoside attached to the bead resulting in the desired 5′ to 3′ linkage. It is primarily the efficiency of this step that has allowed for the synthesis of longer oligonucleotides with a coupling efficiency exceeding 99%.

The third step is capping, which removes the coupling failures. This is achieved by adding an acetylating reagent made-up of acetic anhydride and N-methyl imidazole, which reacts with only free hydroxyl groups to irreversibly cap the DNA. The fourth step, stabilization, is achieved by adding iodine and water, which leads to oxidation of the functionality phosphite to phosphate, affording a stabilized phosphotriester bond. This step will occur everytime a new nucleoside is added to the oligomer. Following addition of the desired number of nucleotides, the 5′ end is protected with a trityl group and every base except thymine has a protection group. Adenine and cytosine are protected with benzoyl groups, and guanine with a N-2-isobutyryl group. After DNA synthesis, the oligonucleotide is cleaved off the solid support and deprotected, which results in free hydroxyl groups at both the 3′ and 5′ ends. Deprotection of the oligonucleotide backbone via base hydrolysis using ammonium hydroxide at high temperature results in the formation of single-stranded DNA sequence. This methodology allows for the synthesis of oligonucleotides in high yield, and quality (see Figure 1.2).

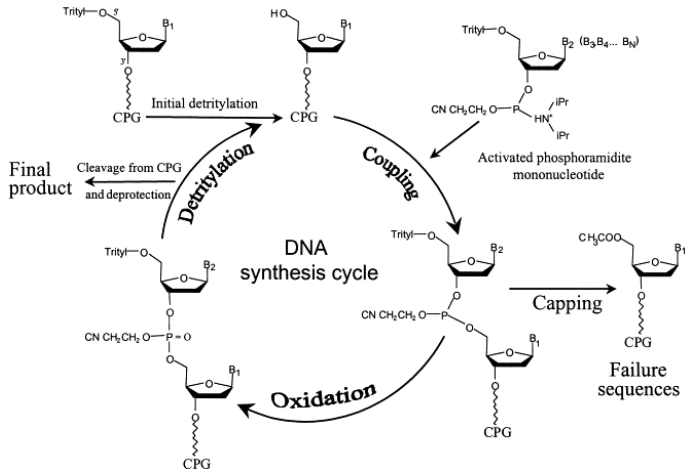

Figure 1.2 Solid-phase synthesis of oligonucleotides which undergoes five steps deprotection, coupling, capping, stabilization, and cleavage to achieve the final oligonucleotide synthesized where CPG is the solid-support.

The advancement in solid-phase DNA synthesis has tremendously influenced nanotechnology. One example is the coupling of DNA to nanomaterials for the construction of diverse two- and three-dimensional (2D and 3D) meso- and macroscopic assemblies of nanomaterials. Seeman and coworkers were the first to prepare DNA containing branched junctions with complementary sequences referred to as "sticky ends" to the arms of the DNA, which resulted in the formation of 2D and 3D DNA structures in the presence of DNA ligase.[18a,b,c] Seeman and coworkersused the the same solid-support oligonucleotide synthesis system to build 2D and 3D assemblies of DNA during the DNA synthesis to overcome the yield and purification issues required in the abovementioned solution-based method.[18d] This allowed them to construct truncated DNA octahedrons made up of 2550 nucleotides with a molecular weight 790 kDa.[18e] In addition, Bergstrom and coworkers also used DNA to build complex structures by using tetrahedral linker with arylethnylaryl spacers which allow for the assembly of DNA macrocycles.[18f]

Although DNA alone can be used to build complex 2D and 3D structures, the low yields of such structures and difficulty in working with small volumes led to the use of DNA as a template or scaffold. This was demonstrated by Coffer and coworkers[18g,h,i,j] who utilized DNA to stabilize Cd^{2+} ions by simply mixing calf thymus DNA with Cd^{2+}. Addition of 1 molar of Na_2S to the same solution resulted in the formation of CdS nanoparticles with an average size of 5.6 nm. Further studies determined that increasing adenine content allowed for control of CdS nanoparticle sizes, which of course affects their

respective photophysical properties. Braun and coworkers grew silver wires on a DNA template with significant adenosine content, using silver ion deposition followed by reduction with hydroquinone.[18k] The wires were 100 nm in diameter and 12 μm long. Tour and coworkers utilized the phosphate backbone of DNA to form electrostatically stabilized complexes with C_{60} fullerene molecules containing a positively charged *N*,*N*-dimethylpyrrolidinium iodide moiety in dimethyl sulfoxide (DMSO).[18l]

A major drawback in using DNA as a template as well as to build pure DNA-based nanostructures is that such nanostructures are still relatively expensive since milligram quantities are prepared using automated synthesizers and kilogram quantities would be required for potential device integration such as Lab-on-a-chip devices. Thus, one focus of DNA nanotechnology is directed towards employing the biomolecule to assemble other nanomaterials into complex architectures. One of the first demonstrations of DNA-directed assembly was performed with gold nanoparticles (AuNP) in 1996.[18m] Such DNA-based AuNP assemblies have now found widespread use in the fields of analytical, biomedical and sensing.[5,18m] The aforementioned assemblies are the primary focus of this thesis.[18m] In particular, in chapters 2 and 3, we discuss in detail the DNA-directed assembly of soft and hard nanomaterials.

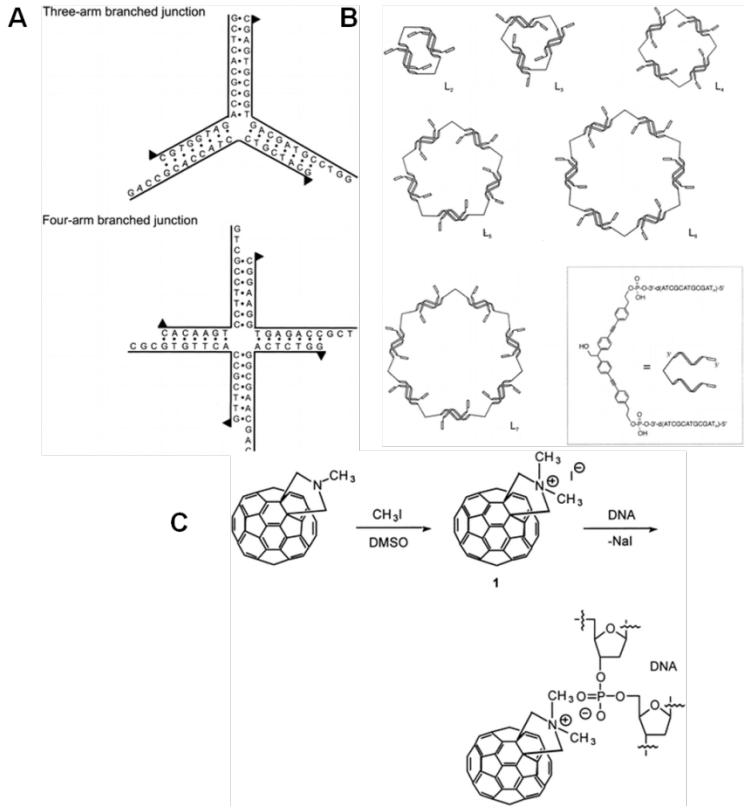

Figure 1.3 Utilization of DNA to construct 2D and 3D nanostructured materials using (A) branched DNA, (B) molecular weight of DNA to generate octahedrons and (C) C_{60} fullerene molecules to electrostatically complex to the backbone of DNA. Figure adapted with permission from ref (18m). Copyright from American Chemical Society.

1.1.3 Aptamers.

The development of solid-phase DNA synthesis and PCR technology together have allowed artificial nucleic acids for catalytic or selective binding purposes to be reliably and reproducibly synthesized.[19a] These artificial nucleic acids or nucleic acid ligands are generated by an *in vitro* selection method called systematic evolution of ligands by exponential enrichment (SELEX). In a typical SELEX experiment, a combinatorial library of nucleic acids undergoes multiple cycles of partitioning and amplification.[13,14] This process generally involves three steps as highlighted in Figure 1.4. Step one involves DNA-target binding. In step two, bound DNA are isolated from those that are unbound. Lastly, bound DNA are replicated using PCR. Nucleic acid ligands identified using SELEX have been termed aptamers, a name derived from Latin, which is translated to mean "to fit". Aptamers are nucleic acids

that bind small molecules with high affinity, where the binding constant, K_d, ranges from pM to μM concentrations with high specificity. Since the invention of SELEX, a number of aptamers have been discovered for proteins and small molecules. In addition, the expansion of SELEX to more complex systems such as proteins, cell surfaces,[19b] and human plasma,[19c] has allowed for the identification of aptamers for specific sites on proteins or receptors.

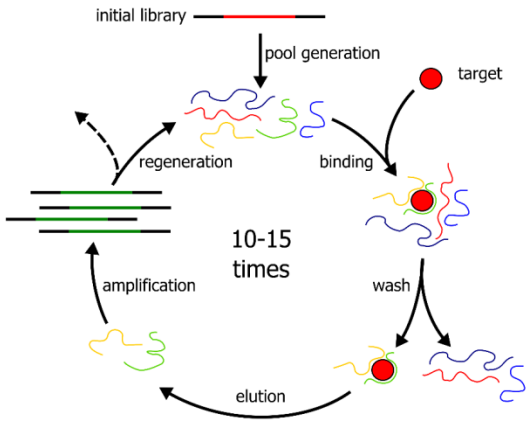

Figure 1.4 In a typical SELEX experiment, a combinatorial library of nucleic acids undergo multiple cycles of partitioning and amplification. This process involves three steps. Step one is to identify the DNA ligand sequences that bind to the target and in step two those DNA ligands bound are isolated from those that are unbound. Last method is the amplification of the eluted bound ligand DNA.

Aptamers aspire to have similar properties as antibodies for use in next-generation therapeutics.[7] Comparison of the two technologies reveals that there are several limitations. Firstly, aptamers are isolated using *in vitro* methods. Antibodies, in contrast, are isolated by *in vivo* methods. Irrespecitve of the origin, anything that is foreign in the body can potentially create an immune reaction. Secondly, similar to antibodies, aptamers can be easily synthesized on a large scale using the solid-phase phosphoramidite chemistry described above. A major obstacle that both aptamers and antibodies suffer from is cellular uptake. To date, antibodies empolyed for therapeutic purposes binds to the extracellular or cell surface target. Antibodies also have a limited shelf-life as they are prone to denaturation. Aptamers possess a significantly longer shelf-life owing to the stability of the phosphodiester bond. More importantly, dyes or functional groups can be easily bound to the aptamer with minimal effect on activity. In contrast, introducing functional groups onto antibodies typically results in mixtures of products and

reduced activity. Antibodies are stable in serum and due to their large size do not undergo renal filtration *in vivo*. These limitations for aptamers have been overcome by modification with poly-ethylene glycol (PEG), for example, which inhibits nuclease degradation of the aptamer in serum with subsequent renal filtration *in vivo*.

Aptamers are envisioned for use in a range of therapies. These include activating or deactivating receptors as treatment, as well as, diagnosis of a medical condition via detection of heavy metals or metabolites.[7,19a] One example where receptors are activated by an aptamer to combat disease is in the treatment of wet macular degeneration. In this case, the aptamer was selected to target vascular endothelial growth factor (VEGF), which is an endogenous pro-angiogenic protein involved in repairing damaged cells to activate blood vessel formation in order to combat the disease. This approach was especially encouraging due to the long lifetime of the aptamer in the ocular region. The success of such aptamers has encouraged studies in which aptamers are brought across the cell membrane for more targeted treatment. Aptamers are also used for the detection of a range of small molecules as well as highly toxic metals.[19e-j] One of the key advantages of using aptamers is that they can be isolated to target small molecules. Antibodies, on the other hand, are difficult to isolate for small molecules because of their inherent molecular structure.

Figure 1.5 shows four aptamers that target small metabolites and highly toxic metals. The (Figure 1.5A) secondary structure of a thrombin binding aptamer that folds into a G-quadruplex. Thrombin is an important serine protease and is often used as a model protein to test aptamer binding. Figure 1.5B and C present the structure of adenosine and cocaine aptamers, respectively. Figure 1.5D shows a thymine rich DNA capable of binding Hg^{2+} to form T-Hg^{2+}-T base pairs, which we employed to prepare a highly selective Hg^{2+} sensor as discussed in detail in chapter 5.

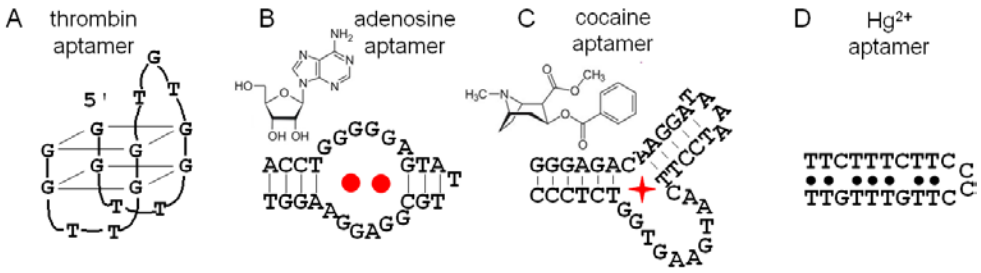

Figure 1.5 Examples of DNA aptamers for (A) thrombin, (B) adenosine or ATP, (C) cocaine and (D) mercury ions. In (B), each aptamer binds two adenosine molecules. In (D) there are seven Hg^{2+} binding sites in each DNA. Figure adapted with permission from ref (16). Copyright © Royal Society of Chemistry.

1.1.4 Fluorescently modified DNA.

The simple base pairing rule of DNA hybridization implies remarkable programmability. The relative ease of DNA synthesis has allowed various DNA probes to be customarily prepared allowing DNA to be used in genomics, bioanalytical chemistry and nanotechnology.[19k-o] For example, DNA has been used in gene chips, polymerase chain reactions, molecular beacons, and functionalized to nanoparticles. Non-immobilized probes such as molecular beacons have also been widely used for DNA/RNA detection in medical diagnosis,[19w,x] real-time PCR, and biosensor development.[19p] Over the past 15 years, a number of improvements have been made on the beacon fluorophore,[19q,r] quencher,[19s] and the backbone[19t-v] to enhance signal, decrease background, and increase specificity and stability. Molecular beacons are engineered DNA hairpins with the two ends labeled. One end contains a fluorophore and the other end contains a quencher, respectively.[19m,s,w] The molecular beacon in the hairpin formation has a low fluorescence signal. In the presence of target DNA, which is complementary to the loop region of the beacon, fluorescence signal increases. This increase is due to the formation of a more stable DNA duplex which results in the separation of the fluorophore and quencher. Such probes have become increasingly attractive.

1.2.1 Liposomes.

The biocompatibility, facile manipulation of size and surface charge of liposomes coupled with the ability to load both hydrophobic molecules in the lipid bilayer and hydrophilic molecules in the inner core or lumen render such materials increasingly popular for a variety of medical applications.[20] For example, the anticancer drug doxorubicin in polyethylene glycol (PEG) grafted liposome has demonstrated increased patient survival for breast-carcinoma metastases. This has been predominately due to prolonged circulation lifetime of liposome-doxorubicin with subsequent accumulation in tissues with increased microvascular permeability.

There are 15 liposome based drugs commercially available or in phase III of their clinical trials. This is a demonstration of the unique properties of liposomes making it one of the few nanomaterials which have achieved clinical application. One of the most active areas of liposome drug delivery research is pertaining to the development of liposome drugs to be administered by inhalation. Several companies currently have a number of inhaled liposome lung cancer vaccines in clinical trials. This targeted approach has been championed as a superior alternative to chemotherapy, which in some cases

needs to be stopped prior to eradicating the cancerous tumor owing to adverse toxicity to other parts of the body.

Bangham and coworkers were the first to report the formation of vesicles (i.e., liposomes) upon addition of phospholipids to an aqueous solution (Figure 1.6A).[21] Hydrophobic molecules can be readily loaded into the bilayer region marked by **1**, while hydrophilic molecules can be entrapped in the compartment marked **2** where the bilayer thickness is approximately 5 nm (Figure 1.6B). Liposome formation is governed by two factors lipid solubility and shape. Critical micelle concentration (CMC) indicates the concentration above which complex structures such as micelles or bilayers will form. Bilayer-forming lipids have a much lower CMC values then other amphiphiles, which have CMC values ranging from 10^{-2}-10^{-4} M.[22,23] The primary factor that governs what type of structure is formed is the shape of the lipid. In general, the cross-sectional areas of the polar head group (A_p) and hydrophobic tail group (A_{np}) of a lipid are compared to predict the complex structure it will form. If $A_{np} > A_p$ then complex structure with positive curvature forms inverse micelles. On the other hand if the opposite is true then structures pertaining to negative curvature will form micelles. Bilayers are formed only when both A_p and A_{np} are similar resulting in zero curvature. The majority of bilayer-forming lipids can be modeled as rods. The most commonly used phospholipids are zwitterionic phosphatidylcholine (PC) and phosphatidylethanolamine (PE), negatively-charged phosphatidic acid (PA), phosphatidylglycerol (PG), and phosphatidylserine (PS) (Figure 1.7). Cationic lipids are uncommon in nature but can be prepared synthetically, such as the commonly used 1,2-dioleoyl-3-trimethylammonium-propane (DOTAP).

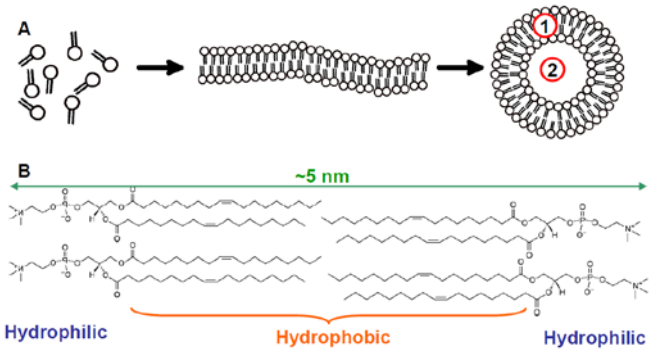

Figure 1.6 (A) Schematic shows self-assembly of lipid molecules into lipid bilayers and liposomes. Both hydrophobic and hydrophilic molecules can be contained in liposomes as respectively marked by 1 and 2. (B) The thickness of a lipid bilayer is around 5 nm and molecular structure of the amphiphilic DOPC is shown.

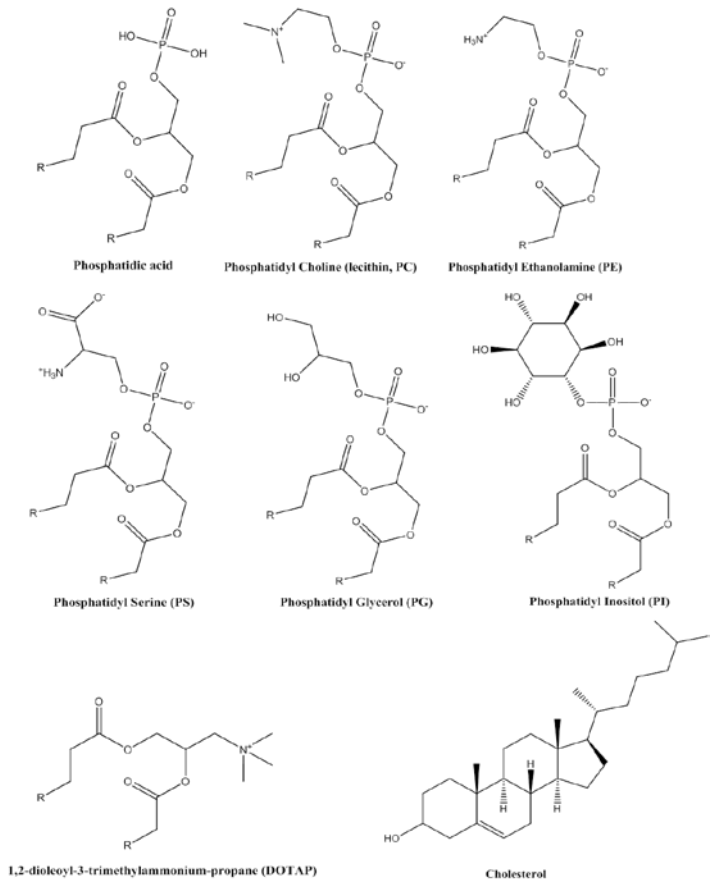

Figure 1.7 The general types of phospholipids and cholesterol typically used to make liposomes.

1.2.2 Preparation of Liposomes.

Liposomes are classified according to their size and the number of bilayers they possess. Small unilamellar vesicles (SUV) fall in the size range of 15 to ~50 nm, while large unilamellar vesicles (LUV) can go up to one micron in size. Giant unilamellar liposomes (GUVs) typically exceed a few microns and can be resolved using optical microscopy. Various methods have been developed to prepare each type of liposome. In general, lipids are dissolved in an organic solvent such as chloroform, which is subsequently fully evaporated by rotary evaporation spray drying, low pressure evaporation for several hours in the presence of a neutral desiccant, or gentle nitrogen flow on top of the sample followed by overnight incubation in a vacuum oven. The resultant film is solubilized using cyclohexane with small amounts of ethanol and frozen using dry ice. This frozen mixture is then incubated for several hours under high

vacuum to remove the organic solvent and water. This is referred to as lyophilization. Hydration of the resulting film induces liposomes owing to osmotic pressure effects, which causes the bilayer lamellae to separate into liposomes. The hydration must be performed above the lipid phase transition temperature, denoted T_c. In the case of lipid mixtures, rehydration should occur at a temperature above the highest T_c of any of the lipids in the mixture to ensure complete dispersal of the dry lipid film. Hydration under mechanical agitation results in the formation of micrometer sized multilamellar vesicles (MLV). These suspensions appear cloudy due to intense light scattering by larger liposomes.[20] In order to transform MLVs into unilamellar vesicles, many methods have been developed such as sonication, membrane extrusion, detergent depletion, and solvent injection.[24,25] High-energy sonic fragmentation is used to generate SUVs. In this case, the MLV suspension is exposed for several minutes to a titanium tip probe sonicator at a particular temperature. However, the possibility of introducing contaminating metal particles released from the sonicator tip is one of the disadvantages of this method. To minimize this problem, the suspension can be subsequently filtered through a micron pore size filter to remove residual titanium particles.[26]

Extrusion, on the other hand, allows the formation of homogenous SUVs and LUVs with precise size control. In this case, the MLV suspension is forced through a polycarbonate filter membrane with a defined pore size. Filter membranes with pore sizes ranging from 50 nm to 1 μm are commercially available where two membranes can be stacked together allowing for uniform size distribution of liposomes. Extrusion using membranes with a pore size >200 nm often yields a polydisperse suspension of multilamellar liposomes. Unilamellar liposomes with a narrow size distribution can only be produced with membranes with a pore size less than 200 nm. Extrusion is typically carried out repeatedly (> 20 cycles) to convert all large particles to the desired SUVs. In addition to manual extrusion, a high yield of SUVs can be produced with a high pressure French press. This scalable method can be applied to a variety of lipids and lipid mixtures and the extruded SUVs are always larger than the vesicles formed via sonication.[24] However, it is noteworthy that all of the extrusion/sonication operations need to be carried out above T_c before the desired size of liposomes are prepared. SUVs have low encapsulation efficiency of hydrophilic reagent metal blackhead extractor since the aqueous space per mole of phospholipids lies in the range of 0.2 to 1.5 liters (e.g. 0.1-1.0% encapsulation). Addition of cholesterol and charged lipids into the lipid mixtures can increase the aqueous volume. Finally, there is a limit to the size of reagent that can be encapsulated, typically the the molecular weight should not exceed 40,000.

To form LUVs, in addition to extrusion, reverse-phase evaporation (REV) can also be used. In this method, the lipid or lipid mixture is first dissolved in an organic solvent, to which a buffer is added

with subsequent sonication.[27] This mixture then undergoes rotary evaporation under reduced pressure forming a gel-like material forming liposomes. One of the disadvantages of the REV method is the exposure of the encapsulating reagent to an organic solvent, which could result in denaturation of proteins to be encapsulated. One of the popular methods to form GUVs is electroformation, which applies an alternating electric field to a lipid film causing swelling and fluctuations in the bilayers leading to the separation of the lamella and the formation of giant vesicles.[28,29]

1.2.3 Lipid Phase Transition.

In addition to charge, the phase behavior of a lipid also strongly influences its properties. Below the phase transition temperature, the hydrophobic tails are extended and the lipids adopt a gel-like state; whereas above T_c, the lipids are quite mobile and adopt a liquid crystalline or liquid-like state (Figure 1.8A). T_c, which is primarily a function of the acyl chain length, can be precisely determined using differential scanning calorimetry (DSC). For example, lipids such as DOPC have a double bond situated in each hydrophobic tail that forms a kink, which prevents efficient packing of the lipids tails, resulting in a lower T_c value of -20°C. On the other hand, DPPC has no kinks and thus can pack better, resulting in a high T_c of 41°C. In general, the T_c value decreases considerably in the presence of unsaturated acyl chains, branched chains, or bulky side groups.

The lipid bilayer is hydrophobic and thus inhibits the passage of polar or charged compounds into the liposome. Permeability of the bilayer membrane is a function of temperature and is the greatest at the T_c of the lipid. For example, DPPC is highly permeable at ~41 °C, while DOPC can retain its content for a long time at room temperature. At T_c, lipid packing is constantly changing from the gel-like to liquid-like state, thus causing increased permeability. Cholesterol as an additive has a significant influence on the lipid T_c.[23] For high T_c lipids such as DPPC, cholesterol disrupts lipid packing and results in a lowering of the T_c, which makes the liposome more liquid-like. The addition of cholesterol to fluid DOPC increases liposome elasticity, allowing the liposome to behave as if in a gel-like state.[30,31]

In cases where the liposome is made up of a mixture of both high and low T_c lipids, lateral phase segregation or domain formation may take place. For example, saturated lipid tails with more than four methylene unit difference results in non-ideal mixing leading to lateral phase separation. If the lipids differ by only two methylene units, they are usually completely miscible.[24] A commonly used lipid mixture to achieve lateral phase separation consists of DOPC/DPPC/cholesterol. Certain dyes can be

selectively dissolved in the domains, allowing for the observation of lipid phase separation using fluorescence microscopy. For example, by increasing the percentage of DPPC, the area of the domains stained with Texas Red DPPE is significantly reduced (Figure 1.8B) since the dye, prefers to dissolve in the less ordered DOPC phase.[32] This unexpected behavior stems from the large size of the dye which does not allow for efficient lipid packing. Domain formation has become an increasingly important topic in biophysics for better understanding cell membrane behavior. Its applications in nanotechnology, however, have still not been widely explored.

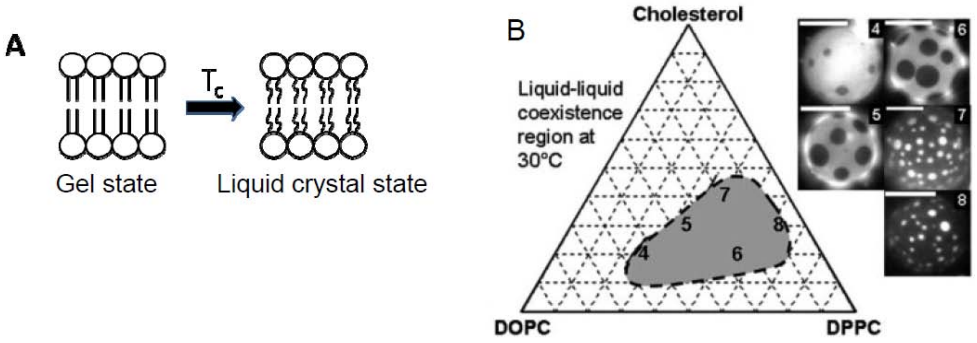

Figure 1.8 (A) Schematic showing the phase transition behavior of a lipid bilayer. (B) Phase diagram of the DOPC/DPPC/Cholesterol tri-component mixture. The region encased by the dashed line is liquid-liquid immiscible region. The GUVs composition in micrographs 4-8 are: 4), 2:1 DOPC/DPPC + 20% Chol; 5), 1:1 DOPC/DPPC + 30% Chol; 6), 1:2 DOPC/DPPC + 20% Chol; 7), 1:2 DOPC/DPPC + 40% Chol; and 8), 1:9 DOPC/DPPC + 30% Chol. Scale bars are 20 μm. Figure adapted with permission from ref (16). Copyright © Biophysical Society.

1.2.4 Nonmedicinal Applications of Liposomes.

Liposomes are also promising for use in areas other than therapeutics, such as liquid chromatography (LC), capillary electrophoresis (CE), immunoassays and biosensing technologies. In addition, liposomes are being used in single-molecule spectroscopy, imaging, cell biology, liposome-nanotube networks, and in nanobioreactor systems.[21] Since the liposome structure resembles cell membranes, liposomes have also been used to study the interactions of lipids within the bilayer with DNA,[21b] proteins,[21c]permeability of ions,[21d,e] drugs,[21f] and the mechanism by which pesticides[21g] and antibiotics[21h] interact with the surface. The surface of the liposome can be conjugated with oligonucleotides, aptamers, and other bio-recognition elements using lipids with reactive head groups such as an amino group in PE, a carboxy group in N-glutaryl-PE, a maleimide group in maleimidomethyl cyclohexane-carboxamide (MCC)-PE, maleimidophenyl butyramide (MPB)-PE, a disulfide in pyridyldithiopropionate (PDP)-PE, and a hydroxyl group in cholesterol as well as polyethylene glycol (PEG).[21i,j] The general methods used to conjugate such biorecognition elements to the liposome depends on the functional groups of the element and the lipid bilayer.

1.3 Hydrogels.

Wichterle and Lim were among the first in the 1960s to propose the use of a hydrophilic polymer poly(2-hydroxyethyl methacrylate) in the preparation of contact lenses.[34a,b] Since their proposal, hydrogels have been used in a variety of biomedical and pharmaceutical applications. It is important to distinguish between gels and hydrogels. Gels are semi-solid materials where a small amount of solid is dispersed in a large amount of liquid.[34a] On the other hand, hydrogels are crosslinked network of hydrophilic polymers. They can absorb and retain a large amount of water, up to several hundred fold of their gel dry mass.

For biomedical purposes, in comparison to other soft materials, hydrogels closely resemble tissue with respect to their soft and rubber-like structure, as well as their ability to hold high water content. In addition, hydrogels do not absorb proteins from bodily fluids in part due to their low interfacial tension. Moreover, the ability to control the drug loading and drug release from the hydrogels allows for their use as drug delivery vehicles for administration via a variety of pathways.[34a]

Hydrogels are often referred to as “smart” or “intelligent” gels since their physical or chemical behavior changes in response to external stimuli. In general, hydrogels are classified according to the types of crosslinkers used.[34c] In one case, the crosslinking is achieved via non-covalent interactions such

as hydrophobic, ionic or hydrogen bonding. For example, alginate hydrogels are made up of mannuronic acid and gluconic acid, which are cross-linked together by divalent calcium ions. Removal of calcium ions results in gel dissolution. This type of gel has been used for encapsulating proteins as well as for growing cells for potential tissue engineering.[34d-i] In addition, polymer blends can be used to form a hydrogel. For example, the carboxylic acid groups of poly(acrylic acid) and poly(methacrylic acid) form hydrogen bonds with poly(ethylene glycol), resulting in the formation of hydrogels in acidic pH.[34j,k] Pure DNA-based hydrogels are also known.[34l] Covalent crosslinkers are very commonly employed in the epreparation of more robust hydrogels. Such are formed by polymerizing monomers in the presence of cross-linking agents, which are molecules that contain more than one polymerizable functional group. For example, poly(acrylamide) hydrogels are formed by simply polymerizing acrylamide monomer and a bis-acrylamide crosslinker, e.g, *N,N′*-methylenebisacrylamide. This polymerization proceeds in solution upon addition of initiator (ammonium persulfate) as shown in Figure 1.9. A variety of hydrogel structures, such as monoliths, thin films, microparticles and nanoparticles, can be easily synthesized using any of the above-mentioned methods described for the preparation of hydrogels.[34a,C] The motivation for synthesizing different physical sizes and shapes of gels stems from their different cargo loading capacity, release kinetics, and mechanical properties. For example, micro- and nanoparticles are useful for drug delivery applications while thin films are ideal for cell-culturing as well as for the preparation of various fast response transducers.

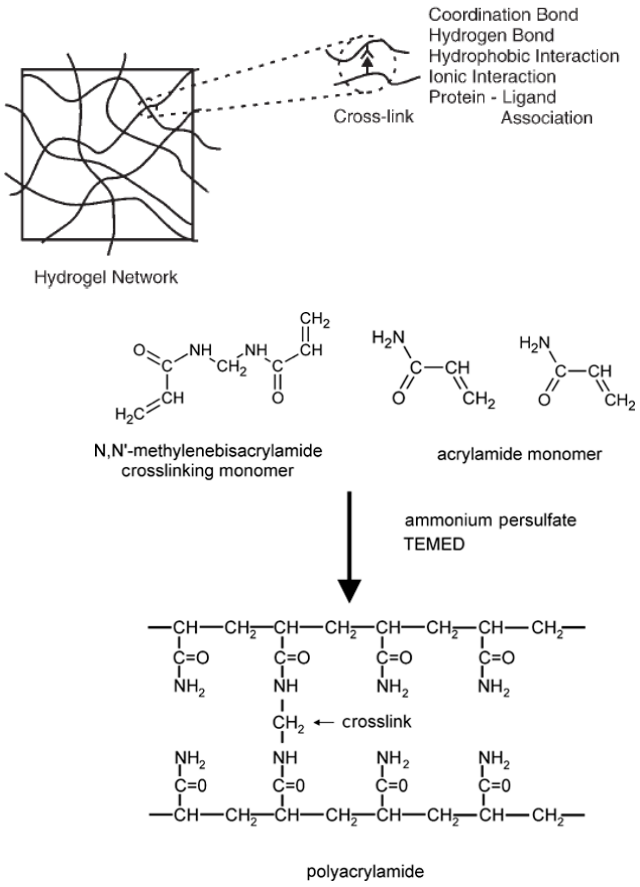

Figure 1.9 Hydrogels are classified according to the type of non-covalent or covalent cross-linker. An example of covalent cross-linker is the generation of poly(acrylamide) hydrogels. Figure adapted with permission from ref (34c). Copyright from Wiley Publishing Group.

Hydrogel volume can be manipulated by a variety of stimuli such as solution conditions, temperature, pH, ionic strength, solvent composition, light, and electric field. A well studied example are the hydrogels polymerized using the monomer N-isopropylacrylamide (NIPAm), which show a large temperature-dependent volume change.[34c,n,o] In solution, the amide groups of NIPAm hydrogels hydrogen bond with water and the isopropyl groups undergo hydrophobic interactions with each other. If the temperature is below a critical value, referred to as the lower critical solution temperature (LCST), water-polymer interactions dominate causing the gel to swell. Above this temperature, the hydrogen bonding between the gel and water weakens and polymer-polymer interactions via isopropyl groups dominate inducing a decrease in gel volume. In another example, at elevated pH, polyacrylic acid hydrogels swell

due to repulsion between negatively charged polymer chains. Swelling in this system can be modulated by screening the repulsive charge through control of the ionic strength. Stimuli-responsive hydrogels have been exploited in various applications, including controlled drug release systems, sensors, and other smart systems.[34p-s] Although significant progress has been made in the design of responsive hydrogels, the choice of stimuli remains limited. For bioanalytical and biomedical applications, hydrogels responsive to small molecule metabolites, nucleic acids, or proteins are particularly sought after. Toward the end of this doctoral thesis, we propose in chapter 5 the use of aptamers for covalent functionalization within a hydrogel for the detection of heavy metal ions.

1.4 Gold nanoparticles (AuNPs).

In the nanoscale domain, the unique optical properties of metallic nanoparticles is due to their surface plasmon resonance (SPR).[35a,b,c] Surface plasmon resonance effects are due to the oscillation of surface electrons of metallic nanoparticles upon interacting with electromagnetic radiation. As a result, the absorbance features can simply be varied by changing the size, shape, morphology and dielectric constant of the surrounding medium of the synthesized metallic nanoparticles. Citrate-functionalized gold nanoparticles (AuNPs) using the methods of Ferns and Turkevich can be easily synthesized at a large scale wand with a high degree of monodispersity.[35d,e,f] This allows for the synthesis of citrate-capped spherical nanoparticles ranging in diameter from 5 to 250 nm. Gold nanoparticles play a particularly important role in bionanotechnology because they are nontoxic, stable, conductive, catalytically active, and electron dense.[35g] AuNPs possess unique optical properties in terms of extremely high extinction coefficients, distance dependent color, and outstanding fluorescence quenching ability. Finally, thiol-containing biopolymers such as proteins and nucleic acids can be chemisorbed onto AuNPs giving rise to both colloidal stable and functionalized nanoconjugates.[35h,i,j] These nanoconjugates are usually achieved by using citrate reduced 13 nm AuNPs stabilized by negatively charged citrate ions. For functionalization of thiol modified DNA to AuNPs, the negatively charged DNA is repelled by AuNPs. This charge repulsion even at a high concentration of NaCl for screening the charge led to AuNP aggregation in the absence of high DNA density. This problem was solved by a method called “salt aging” where NaCl was added stepwise to a mixture of DNA/AuNPs. [35k,l,m] Chemisorbed DNA not only enhances AuNP stability such that even more NaCl addition therefore further increases DNA loading. This process typicall takes 1-2 days resulting in the formation of stable nanoconjugates. Since 1996, the programmable nature of

DNA was first demonstrated allowing synthesize AuNP oligomers,[35n,o] random aggregates,[5] periodic structures[35p,q] and crystalline superlattices.[35r,s,t]

1.5 Research goals.

Previous studies have shown that DNA can be used as a tool to grow and assemble inorganic nanoparticles. The majority of previous work, however, has focused on the assembly of "hard" nanoparticles such as gold nanoparticles (AuNPs) as opposed to the assembly of soft materials. The primary focus of this thesis is to add to this growing field of DNA-functionalized and DNA-directed assembly of soft materials, which are promising in a variety of analytical and biomedical applications. The soft materials studied are liposomes and hydrogels. Soft materials such as liposomes differ from inorganic nanoparticles in several important ways. Firstly, liposome are formed as a result of the self-assembly of lipid molecules bound together by non-covalent interactions. Owing to such weak lipid-lipid interactions, liposomes can be easily deformed, while inorganic nanoparticles cannot be deformed by forces operative at the molecular level. Second, the physical properties of liposomes can be easily manipulated by simply changing the charge of the lipid headgroup to positive, negative, or zwitterionic. The composition of the phospholipid tail can also be tuned, which influences the lipid phase transition temperature. Third, by changing lipid curvature and composition, fusion can be selectively promoted or inhibited. Finally, due to the fluidity of the bilayer membrane, DNA sequences bound to liposomes are relatively mobile and can reorganize on the membrane surface in response to external stimuli. For inorganic nanoparticles, however, the immobilized ligands cannot diffuse easily on the particle surface. My doctorial research addresses the fundamental biophysical aspects of DNA-functionalized lipid bilayers and hydrogels and their interactions with various chemical species using DNA as a molecular recognition ligand and as a structural directing agent.

1.6 Thesis outline.

This thesis consists of six chapters with a common focus of studying DNA immobilized liposome and hydrogel and their analytical and biomedical applications. A synopsis for each chapter follows:
Chapter 2 describes the preparation of DNA-directed liposome assemblies via addition of linker DNA. The melting transitions of these liposome assemblies as a function of lipid charge, size, fluidity, and

attached DNA are systematically studied and compared to the analogous properties of DNA-directed AuNPs assemblies. Such a fundamental study is lacking in the literature.

Chapter 3 uses the same methodology outlined in chapter 2 to obtain reversible and programmable assembly of DNA-functionalized liposomes and gold nanoparticles (AuNPs), where both temperature and radiation are used for controlled liposome release by tuning the specific linker DNA separation between the nanomaterials. Using this method to inhibit or induce liposome content release has not been studied in detail in the literature.

Chapter 4 and 5 describes the preparation of soft material-immobilized aptamers. In chapter 4, the preparation and characterization of split aptamer-functionalized liposomes and their responsiveness to external stimuli is studied. For comparison, the same DNA aptamer was also immobilized on silica nanoparticles where the lateral mobility was eliminated. Chapter 5 describes using monolithic and microparticle hydrogels for covalent immobilization of a thymine-rich DNA or aptamer for simultaneous detection and removal of heavy metal mercury.

Chapter 6 discusses the conclusions in each chapter of this doctoral study, contributions of this research to the overall scientific community, and recommendations for future studies.

Chapter 2.0
DNA-directed hard and soft material assemblies.

The results presented in this chapter have been published as part of:

Neeshma Dave and Juewen Liu "Programmable Assembly of DNA-Functionalized Liposomes by DNA", ACS Nano, 5, 1304–1312, 2011.

2.1 Introduction.

2.1.1 Research objective.

Bio-nanotechnology involves using biomolecules to control both the structure and properties of nanomaterials. A well studied example is DNA-directed assembly of gold nanoparticles (AuNPs). A number of studies have considered the effect of melting temperature as a function of AuNPs physical properties i.e. size, DNA density and interparticle spacing.[38a,k,81] Similar studies in the case of another distinct class of soft nanomaterials, i.e., liposomes, have also been demonstrated. Although assemblies formed using soft and hard materials display cooperative melting behavior, a characteristic feature of DNA-directed nanostructured materials, comparing both hard (e.g., AuNPs) and soft (e.g., liposomes) DNA-directed assemblies is still lacking. As will be highlighted below, we describe the preparation and characterization of DNA-directed liposome assemblies. We study the melting temperature as a function of liposome physical properties and compare them to the analogous properties of Au-Au assemblies.

2.1.2.0 DNA-directed gold nanoparticle assemblies.

One method to achieve Au-Au assemblies involves surface functionalization of the AuNP, which can be readily achieved by treating the gold surface with molecules bearing high affinity functional groups such as thiols, phosphines and amines.[38b] Functionalizing AuNPs with capping agents containing reactive head-groups allows for subsequent conjugation to a variety of biomolecules such as oligonucleotides, proteins and antibodies.[38k] One of the popular methods to achieve nanoconjugates involves the functionalization of AuNPs surfaces with oligonucleotides/DNA. This is achieved by mixing citrate-capped AuNPs with alkanethiol-terminated oligonucleotides, which replace the citrate on the AuNP surface, resulting in the formation of covalent gold-thiol bond (Au-S). A dense monolayer is subsequently obtained by adding salt (NaCl), which shields neighboring DNA (see Figure 2.1). Using

this salt-aging method, the surface of 15 nm diameter AuNPs can be passivated with ~250 oligonucleotides.[83] AuNPs with diameters from 2 to 250 nm have been optimized for DNA functionalization.[83,93b]

Mirkin and coworkers were the first to compare the thermodynamic properties of molecular DNA free in solution to those of DNA grafted onto 13 nm AuNPs via concentration-dependent melting studies. Addition of a dye-labeled complementary DNA (cDNA) resulted in hybridization with the molecular DNA probe and the nanoparticle probe. Subsequent melting studies showed a binding constant two orders of magnitude higher for DNA-AuNPs compared to DNA in solution.[89] To determine whether enhanced stability stemmed from DNA density on the AuNP surface, melting studies comparing 13 nm AuNPs with densely packed DNA (30 pmol/cm^2), and large silica particles with a DNA surface-capping density of 1 pmol/cm^2 were conducted. The silica nanoparticles displayed the same T_m as molecular DNA, indicating that enhanced binding strength for DNA-AuNPs originated from DNA surface density. Both experimental and theoretical models have also shown that this higher binding constant stems from the dense packing of oligonucleotides on the gold surface.[51a,b] In addition, the DNA sequences chemisorbed on the surface are in close proximity with one another, such that counter ions associated with one oligonucleotide screen the negative charges on adjacent oligonucleotides. This screening increases the effective binding strength for DNA-AuNPs compared to molecular DNA alone.

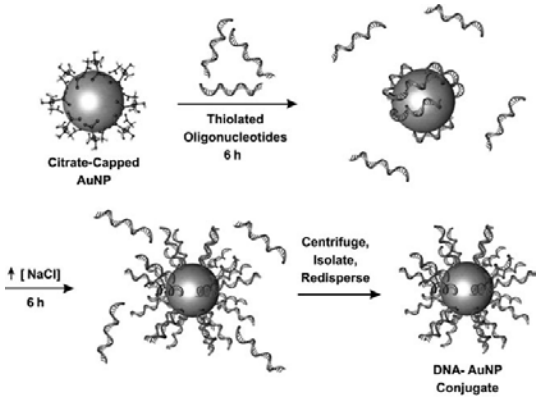

Figure 2.1 AuNP functionalization with alkanethiol-terminated oligonucleotides forms a gold-thiol (Au-S) bond where subsequent addition of salt (NaCl) results in a dense monolayer. Figure adapted with permission from ref (38k). Copyright © John Wiley & Sons, Inc.

Such DNA-directed AuNPs assemblies were first demonstrated in 1996 by Mirkin and coworkers.[36] They achieved this using two sets of nanoparticles that were functionalized with different, non-complementary sequences. A sample containing both types of particles was mixed with a DNA linker, the sequence of which contains stretches complementary to both particle-bound sequences. Bridging of the particles by this DNA linker resulted in the formation of three-dimensional (3D) assemblies via duplex formation (see Figure 2.2A).[36] Depending on the reaction conditions, assembly formation required several minutes or hours for completion. Since the aggregates or assemblies were the result of multiple duplexes between particles, such assemblies underwent dehybridization when heated above a certain temperature (T_m) or when the salt concentration was reduced. Hybridization rate is directly related to salt concentration as such this determines the degree of electrostatic repulsion between neighboring AuNPs in the formation or dissociation of aggregates (see Figure 2.2A and B). Aggregation in AuNP assemblies can be tracked by monitoring the red-shifting of their Surface Plasmon Resonance (SPR) wavelength.[52a] This SPR absorption wavelength arises from the incident photon frequency being resonant with the collective oscillation of the conduction band electrons. Upon aggregation, AuNP solution change color from red to purple/blue owing to stronger coupling of the SPRs of neighboring particles.

2.1.2.1. Cooperative DNA melting behavior.

In the absence of AuNPs, DNA duplexes alone have a broad melting profile with full width at half maxima (FWHM) ranging over 20^{o}C as shown in Figure 2.2C. The melting profiles are obtained by monitoring an absorption feature as a function of temperature where the melting temperature (T_m) corresponds to the temperature at which 50% of the duplex has melted. The melting studies of such systems are a measure of the thermal stability of the duplex, which depend on several factors such as the number of formed base pairs, sequence composition (i.e., percentage of G/C vs. A/T), sequence length, DNA concentration, and the ionic strength of the solution.[52a,95] The higher the T_m, the more energy is required to sever the hydrogen bonds between base pairs. Such fundamental studies on duplex formation alone in solution have allowed for calculations of theoretical melting temperatures using a method referred to as "nearest neighbor considerations".[52a,95]

In contrast to free DNA duplexes, DNA-directed AuNP assemblies exhibit sharp melting transitions that occur within a full width at half-maximum (FWHM) of 1^{o}C (see Figure 2.2C). The sharp melting transition associated with DNA-directed AuNP assemblies is due to the high degree of

cooperativity that exists between the DNA strands packed tightly on the surface of AuNPs. The cooperative effect of DNA in DNA-directed AuNP assemblies has been studied both experimentally and theoretically by examining the magnitude of T_m and breadth of the FWHM of the melting transitions as a function of monovalent salt concentrations, interparticle distance, surface DNA density and particle size by Mirkin and coworkers.[38k,49a,89,52a] The counterions associated with neighboring DNA sequences anchored on the AuNP surface stabilize neighboring duplexes.[52a,81] Increased salt therefore leads to an increase in T_m. In addition, increasing salt concentration also facilitates the formation of large aggregates. This has been demonstrated by the large changes in optical density during melting as determined by light scattering measurements. This is explained as follows: increased salt concentration reduces the electrostatic repulsion between neighboring DNA-AuNPs, which allows for more hybridization events to occur. Therefore, the more hybridization events that take place, the larger the dampening of the SPR of the AuNPs and the easier it is to monitor assembly and disassembly by UV-visible spectroscopy. Mirkinand coworkers also studied the effect of using spacers between the AuNP surface and DNA. In the presence of a spacer, the T_m value increased indicating formation of more linkages between neighboring AuNPs. The size of the aggregates in the absence and presence of spacer however were the same, as confirmed by TEM studies and light scattering measurements.[52a] Increasing the number of duplexes should theoretically only lead to a 5^oC increase in T_m; however, they observed a 10^oC shift in the presence of a DNA spacer. Therefore, Mirkin and coworkers concluded that in the absence of a spacer, electrostatic repulsion between neighboring particles is dominant. The next parameter was the effect of DNA density on the AuNP surface, which was directly proportional to T_m. Mirkin and coworkers varied the percentage of DNA on 13 nm AuNP surfaces and found that T_m decreased with decreasing density. In addition, the sharp melting profile broadened for low density surface-capped AuNPs. The correlation between particle size and T_m was independently verified by Kang and coworkers and Mirkin and coworkers.[52a,b] Kang and coworkers reported a direct correlation between T_m and 10 nm, 20 nm, and 50 nm AuNPs. Mirkin and coworkers observed a similar trend and proposed a cooperative model in which the enthalpy of particle-particle hybridization was determined to be a function of the number of connections between the particles. Therefore, a larger particle formed more connections, corresponding to a higher T_m (see Figure 2.3). However there is a limit. In the case of AuNPs, Mirkin and coworkers demonstrated that as the AuNPs size increased the oligonucleotide surface density increased up to 60 nm. For greater than 60 nm AuNP, the oligonucleotide surface density decreased resulting in a broader melting curve.[81] Similary, with latex particles, which have a low surface coverage of 10^{11} strands/cm^2, no cooperative behavior or sharp melting profile was observed.[52a,d]

Therefore, the cooperative effect occurs when the duplex-to-duplex distance is less than 5 nm.[51a,52a,c] Melting of Au-Au assemblies begins with removal of DNA linker, followed by removal of counter ions, which destabilize the neighboring DNA linkages that ultimately results in a "melting cascade" over a narrow temperature range. This behavior is referred to as cooperative melting.[81]

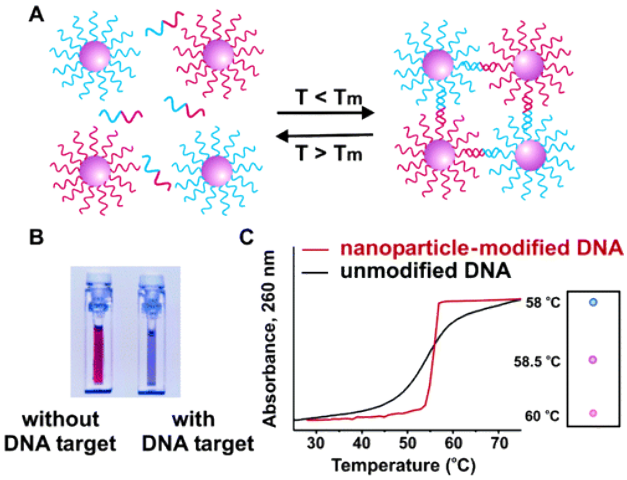

Figure 2.2 DNA-directed assemblies of AuNPs via (A) addition of linker DNA accompanying (B) a color change from red to purple. (C) The sharp melting transition for the assemblies is attributed to many linkages formed compared to molecular DNA. Figure adapted with permission from ref (38a). Copyright © American Chemical Society.

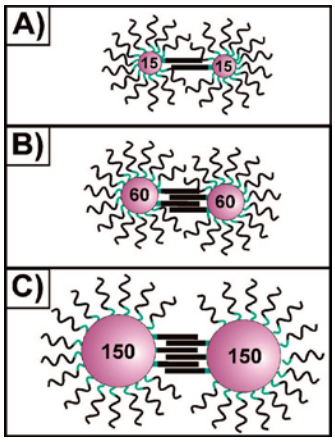

Figure 2.3 Schematic showing the number of linkages formed between neighboring DNA-AuNPs in the formation of Au-Au assemblies as a function of nanoparticle size (A) 13 nm, (B) 60 nm and (C) 150 nm. Figure adapted with permission from ref (81). Copyright © American Chemical Society.

2.1.2.2. DNA-directed crystallization of AuNPs.

Such DNA-functionalized AuNPs have been used in programmed assembly and crystallization of materials,[37] arrangement of nanoparticles into dimers and trimers onto DNA templates,[36,38g-h] bioelectronics,[36,38g-h] and in various detection methods.[38i-k] For detection purposes, DNA-functionalized AuNPs have been used for sensitive and selective colorimetric detection of nucleic acids.[38,36,54] With aptamer-functionalized AuNPs, sensitive colorimetric detection has been achieved for a wide range of analytes. The use of AuNPs for such applications offers a number of advantages over conventional organic chromophores. For one, AuNPs exhibit high extinction coefficients.[49a] For example, 13 nm and 50 nm AuNPs have extinction coefficients of 2.7×10^8 and 1.5×10^{10}, respectively.[49b] Such values are at least 3-5 orders of magnitude higher than conventional organic dyes. For this reason, only nanomolar concentrations of AuNPs are required for visual detection, whereas micromolar quantities are required for organic dyes. For example, Stojanovic and coworkers incubated dyes with an anticocaine aptamer (see Figure 2.4A).[49d] Addition of cocaine resulted in cyanine dye displacement from the aptamer pocket and formation of dimers in solution causing a shift in the absorption spectrum. A major drawback of this method was the requirement of 20 μM aptamer, significant amount of dye for sensor response and 12 hours were required for sensor response.

2.1.2.3. DNA-functionalized AuNPs as colorimetric sensors.

We now turn to aptamer-based colorimetric sensors that use only nanomolar AuNP concentrations. These exploit the distance-dependent signal of AuNPs.[36] In one AuNP-based colorimetric sensor developed by Willner and coworkers, ligand binding to aptamer resulted in AuNP assembly. Here, the AuNPS were functionalized with a 15-mer anti-thrombin aptamer containing a poly-T-spacer and mixed thrombin (see Figure 2.4B). Each thrombin molecule interacted with two aptamers allowing for AuNPs to assemble on a glass slide. To this sample chloroauric acid and NADH was added to increae the size of AuNPs resulting in an absorption shift from 540 nm to 560 nm.[49c] For signal amplification purposes, these aggregates were separated and used to grow larger DNA-directed AuNP aggregates by further addition of DNA functionalized AuNPs and linker DNA to obtain a detection limit of 20 nM. A second type of colorimetric sensor was reported by Mirkin and coworkers for Hg^{2+} detection.[93a,c] Two sets of AuNPs were prepared with DNA such that both were complementary, save for one base pair mismatch. Each sequence contained a thymine (T) mismatch. In the absence of Hg^{2+}, the aggregates undergo typical melting behavior with a concomitant solution color change to red. However, in the presence of Hg^{2+}, the formation of T-Hg-T complexes increases the stability of the assemblies. Therefore, the T_m increased by at least 10^oC from samples without Hg^{2+}. For this sensor, a detection limit of 100 nM was reported. When used in conjunction with a chip-based scanometric method, a detection limit of 10 nM was achieved (see Figure 2.4C and D). In the scanometric chip-based method, DNA sequences containing a thymine mismatch were functionalized on a glass surface and AuNPs were functionalized with complementary DNA sequences also containing a thymine mismatch. Addition of Hg^{2+} resulted in binding of AuNPs to glass surface where subsequent addition of silver solution in the presence of hydroquinone resulted in silver coating allowing for a signal to be generated such as color due to absorption or light scattering of the particles. Lu and coworkers prepared another type of colorimetric sensor consisting of assemblies that dissociated rather than stabilized upon target binding.[42b] Two sets of DNA-functionalized AuNPs were assembled via a DNA linker modified with a 17 nucleotide adenosine aptamer (see Figure 2.5). In the presence of adenosine, the aptamer underwent a conformational change that caused dissociation from the AuNP assemblies, since the remaining 5 base pairs were insufficient to maintain the stability of the assembled state. A solution color change from purple to red occurred within seconds (see Figure 2.5D) of the addition of adenosine. The sensor demonstrated good specificity, as no color change was observed in the presence of other ribonucleosides (see Figure 2.5C). Similarly responsive assembly-based AuNP sensors have also been reported for analytes such as cocaine and potassium ions.[49a,e]

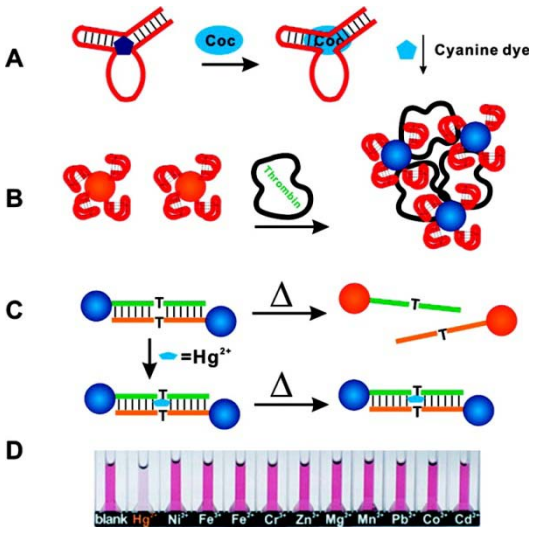

Figure 2.4 Colorimetric sensors (A) for detection of cocaine using dye replacement, (B) based on aptamer functionalized AuNPs assemblies via protein addition, which binds two aptamer molecules and (C) for Hg^{2+} detection (C) where mercury binding stabilizes the duplex formed to achieved aggregation and (D) specificity test using a scanometric method for (C). Figure adapted with permission from ref (49a). Copyright © American Chemical Society.

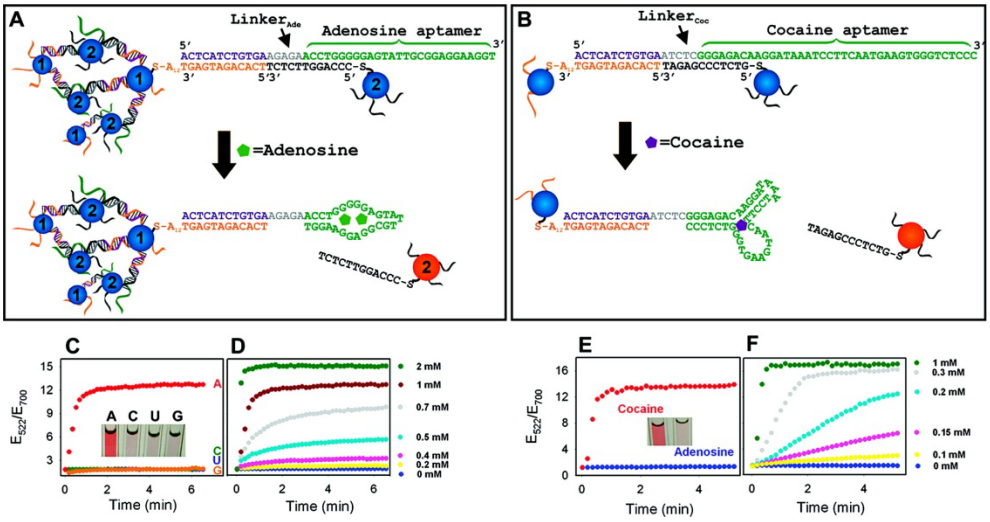

Figure 2.5 Colorimetric sensor based on aptamer disassembly where aptamer is part of the DNA linker. Schematic showing AuNPs assemblies using linker DNA containing (A) adenosine aptamer and (B) cocaine aptamer in the presence of target. The specificity test for (C) adenosine aptamer with addition of other nucleosides such as cytidine (C), uridine (U) and guanosine (G); and (E) cocaine aptamer and kinetics of color change as a function of (D) adenosine and (F) cocaine. Figure adapted with permission from ref (49a). Copyright © American Chemical Society.

2.1.3 DNA-directed liposome assemblies.

Although similar studies in the case of another distinct class of soft nanomaterials, i.e., liposomes, have been performed, a side-by-side comparison between liposomes and AuNPs is still lacking. While there are many similarities between liposomes and AuNPs in terms of their DNA-directed assembly, important differences exist which can be explained by their respective physical properties. Liposomes differ from inorganic nanoparticles in several important ways. First, liposomes are formed as a result of the self-assembly of lipid molecules bound together by non-covalent interactions. Owing to such weak lipid-lipid interactions, liposomes can be easily deformed, while inorganic nanoparticles cannot be deformed by forces operative at the molecular level. Second, the physical properties of liposomes can be easily manipulated by simply changing the charge of the lipid headgroup to positive, negative, or zwitterionic. The composition of the phospholipid tail can also be tuned, which influences the lipid phase transition temperature. Third, by changing lipid curvature and composition, fusion can be selectively promoted or inhibited.[86a,b] Finally, due to the fluidity of the bilayer membrane, DNA sequences bound to liposome are relatively mobile and can reorganize on the membrane surface in response to external stimuli. For inorganic nanoparticles, however, the immobilized ligands cannot diffuse easily on the particle surface. For these reasons, important insights can be obtained from a side-by-side comparison of such soft and hard nanoparticles. Prior to studying DNA-directed liposome assemblies, it is important to review the common methods of DNA attachment to liposomes as well as the types of DNA directed assemblies to date that have been prepared and their applications.

2.1.3.1 DNA attachment to liposome surface and formation of liposome assemblies.

DNA attachment to a liposome can be achieved via insertion of cholesterol modified single-stranded DNA (ssDNA). This type of lipid containing DNA allows for cholesterol to spontaneously insert into the hydrophobic interior of the lipid membrane and the DNA remains on the outer part of the lipid bilayer.[56] Because cholesterol is a small lipid, insertion occurs quite rapidly, however the association of the inserted DNA is relatively weak and does not allow for quantification. To allow quantification of inserted DNA, Höök and coworkers designed a dual cholesterol anchoring DNA duplex.[63,85] The duplex was composed of a 15-mer and 30-mer DNA sequences containing cholesterol groups at the 5′ and 3′ ends, respectively. Using quartz crystal microbalance with dissipation (QCM-D), Höök and coworkers demonstrated that addition of cholesterol-modified ssDNA to a phospholipid bilayer

coated on a SiO_2 surface was saturated by 100 nM single cholesterol-modified ssDNA, whereas only 5 nM of the dual cholesterol was required for saturation. From this pronounced difference, we can conclude that both cholesterol moieties of the doubly modified duplex were inserted into the liposome. This led to studies where DNA containing a polyethylene glycol (PEG) spacer between the cholesterol group and DNA sequence was used for insertion into pre-made liposomes. Typically this is achieved by treatment of a cholesteryl-PEG containing a succinic anhydride at the end of the PEG moiety with *N*-dimethyl-aminopyridine, resulting in the formation of an active ester, which reacts with 5′ aminohexyl modified DNA. This was first demonstrated by Sugaware and coworkers using a PEG modification with a molecular weight of 4400 g/mol. They successfully incorporated cholesteryl-PEG-DNA into giant vesicles.[55d] Studies on such PEG-containing DNA has led to the commercial availability of cholesteryl-tetraethyleneglycol (TEG) labeled oligonucleotides, in which the TEG chain is significantly shorter, with a molecular weight of only 240 g/mol. The short TEG spacer between the membrane and the DNA allows for better control in the formation of DNA-directed liposome assemblies. In addition, cholesteryl-TEG-DNA does not condense the membrane lipid, as is often observed in cases where cholesterol is used.[55e,f,86a] For example, Banchelli and coworkers demonstrated successful DNA insertion into a liposome using the cholesterol-TEG DNA. Greater than five hundred 18-mer DNA or 18 oligonucleotide containing DNA sequences were inserted per 70 nm POPC liposome.[86a] The inserted DNA behaved as a random coil at low surface densities but adopted an extended and rigid conformation at high density. Using this DNA attachment method, DNA-directed liposome assemblies were formed by Beales and Vanderlick. In this study, two sets of non-complementary DNA anchored to the liposomes were mixed together.[57] Similarly to the design first presented by Mirkin and coworkers[36] they added a DNA linker in which half of the sequence was complementary to one liposome-anchored DNA and the other half was complementary to another set resulting in the formation of liposome-liposome assemblies, which appeared as white fluffy flocculates.[55b] These flocculates dissolved into a clear solution upon heating and reappeared upon cooling. Monitoring these vesicles after melting using light scattering measurements displayed the same polydispersity as for free liposomes in solution. Therefore, the vesicles were completely unbound after melting. A detailed study demonstrated that at least 39 DNA molecules per liposome were required to achieve aggregation. When this number rose to approximately 155, white flocculates appeared, presumably due to DNA linked liposome assemblies.

To determine whether insertion of DNA led to lipid mixing, two sets of liposomes were prepared containing different dye-modified lipids and then assembled. Confocal microscopy revealed no transfer of dye-modified lipids after formation of aggregates. However, liposomes labeled with the same dye

were found to assemble with each other. Since non-specific, DNA-independent aggregation was ruled out, transfer of cholesteryl-TEG-DNA from one liposome to another could be a possible explanation. Occurrence of flipping is facilitated if the space between neighboring liposomes is small enough to decrease the energy barrier promoting cholesteryl-TEG-DNA exchange. Vesicle assemblies were made using large and giant unilamellar vesicles, illustrating the generality of cholesteryl-TEG-DNA method for liposome aggregation.

An alternative to cholesteryl-TEG-DNA is amphiphilic DNA, first reported by Boxer and coworkers.[55a,b] They synthesized an amphiphilic oligonucleotide by first reacting the DNA's 5′ end with an iodination reagent, $(PhO)_3PCH_3I$, thereby making this end electrophilic. Through subsequent treatment with lipid-phosphoramidite as the base lipid, followed by de-protection, cleavage, and HPLC purification, the final product was obtained.[55a,b] Addition of this DNA (dissolved in a ratio of 1:1 buffer and acetonitrile) to pre-made liposomes such as PC/DPPS at 4°C for 4 hrs resulted in the spontaneous and quantitative insertion of DNA into pre-made liposomes. Further purification using gel filtration chromatography showed very little free DNA in solution, therefore insertion was achieved. The lack of commercial availability of such amphiphilic DNA probes requires them to be synthesized and has, therefore, limited their application. On the other hand, using this type of DNA attachment method has led to the formation of DNA-directed liposome assemblies. For example, Vogel and coworkers achieved inter-liposome anchoring by using a bivalent binding amphiphilic DNA probe.[62] This was achieved by bringing two liposomes together via insertion of a single-stranded DNA probe modified at each end with two lipid anchors (see Figure 2.6A). Addition of DNA linker resulted in the formation of liposome-liposome assemblies held together by a rigid duplex. This method selectively avoids liposomes where both anchors are embedded in it, since this does not form a rigid duplex as shown in Figure 2.6A. Formation of liposome-liposome assemblies via rigid duplex demonstrated sharp melting temperature profiles with FWHM of 1^oC, which were obtained by monitoring the extinction at 260 nm as a function of temperature (see Figure 2.7A). Since such assemblies demonstrated cooperative melting behavior, melting studies can be used to differentiate mismatches, insertions and deletions in linker DNA within a couple of degrees (see Figure 2.7A). The perfectly matched linker DNA assemblies melted 10^oC above the melting temperatures of DNA linker containing single-base mismatches, insertions and deletions. Vogel and coworkers were among the first to demonstrate that DNA-directed liposome assemblies that lack visible color can be used for detection of single nucleotide polymorphisms. Interestingly, similar to Au-Au assemblies, formation of liposome-assemblies is reversible.[52a] When heated above a certain temperature (T_m), the assemblies underwent de-hybridization/melting and upon cooling re-hybridization

or assembly formation (see Figure 2.7B). This was monitored by examining the scattering of light at 260 nm as a function of heating and cooling. Therefore, liposome assemblies display cooperative melting behavior, and polymorphism similar to the archetypical DNA-directed AuNPs.

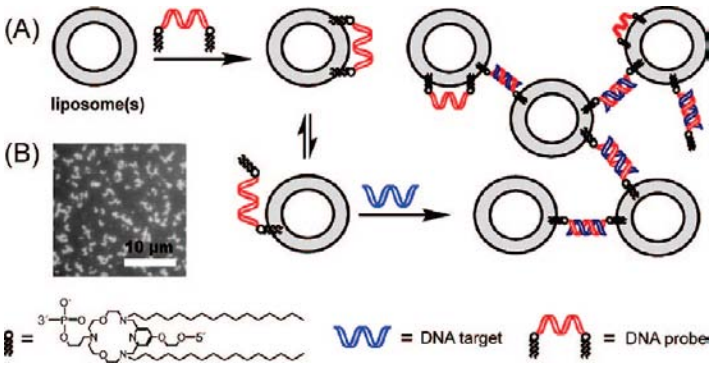

Figure 2.6 (A) DNA linker (blue) mediated liposome-liposome assemblies using an amphiphilic or lipophilic DNA probe (red). (B) Resultant fluorescence microscopy image of liposome-liposome assemblies formed on mica planer solid surface in HEPES buffer pH 7.0. Figure adapted with permission from ref (62). Copyright © American Chemical Society.

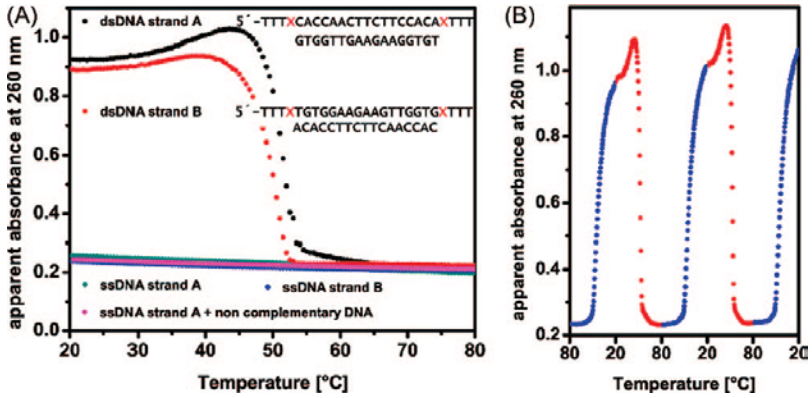

Figure 2.7 (A) The melting profiles of DNA-directed liposome assemblies (black and red), molecular DNA in the absence of liposomes (green and blue) and liposomes in the presence of non-complementary DNA linker (light red). (B) Reversibility of liposome-liposome assemblies shown by heating-cooling (blue is cooling and red is heating). Figure adapted with permission from ref (62). Copyright © American Chemical Society.

The last method to attach DNA to a liposome is via conjugation or coupling chemistry. In this approach, a small percentage (e.g. 1-5%) of a reactive lipid is included in the liposome formulation. After formation of the liposome, DNA containing a reactive functional group (thiol or amine) is treated with the liposome, resulting in covalent functionalization of DNA where the DNA is pre-dominantly attached to the outer leaflet of the bilayer. Willner and coworkers made use of a maleimide-modified phosphatidylethanolamine (MPB-PE) that allows covalent functionalization of DNA by treatment with thiol-modified DNA (Figure 2.8A).[49c] This method takes advantage of the commercial availability of both 3′ and 5′ thiol modified DNA sequences and the MPB-PE lipid. Boxer and coworkers used 1,2-dipalmitoyl-*sn*-glycero-3-phosphoethanolamine-N-[3-(2-pyridyldithio)propionate] (sodium salt) (N-PDP-PE) for functionalization of thiol-modified DNA via a disulfide bond (Figure 2.8B).[59] This disulfide exchange occurs also in the presence of activated thiol-DNA, which is achieved by treating DNA with tris(2-carboxyethyl)phosphine (TCEP) in tenfold molar excess at pH 4. The activated thiol-DNA breaks the disulfide bond, resulting in a by-product, pyridine-2-thiol and DNA linked to the lipid via a new disulfide bond. For the disulfide linkage pH affects the rate of thiol-disulfide linkage. On the other hand, MPB-PE lipid as demonstrated by both Willner and coworkers and Liu and coworkers forms a covalent thio-ether linkage that is not reversible.[48c,76a] This is the method we employ to attach DNA to the liposome. DNA-functionalized liposomes require purification prior to use to remove unreacted DNA and liposome. One method to achieve purification is gel permeation. However, commonly used short columns lack the high separation efficiency necessary for purification, and if longer columns are employed, dilution of the liposome sample readily occurs. On the other hand, DNA-induced liposome aggregation with subsequent centrifugation can also be used for purifying the DNA-liposomes. At high DNA density, the DNA sequences can induce liposome self-aggregation.[71] This occurs because of the DNA being partially self-complementary. In addition, storage at low temperature (e.g. 4°C) and in the presence of high salt (e.g. 500 mM NaCl) facilitates DNA hybridization.[76b] Aggregated liposomes can be easily harvested by brief centrifugation at 4°C. This is the method we used for purification of our DNA-functionalized liposomes. For some DNA sequences, self-aggregation does not occur readily. In these cases, ultracentrifugation can be performed at ~100,000 rpm.

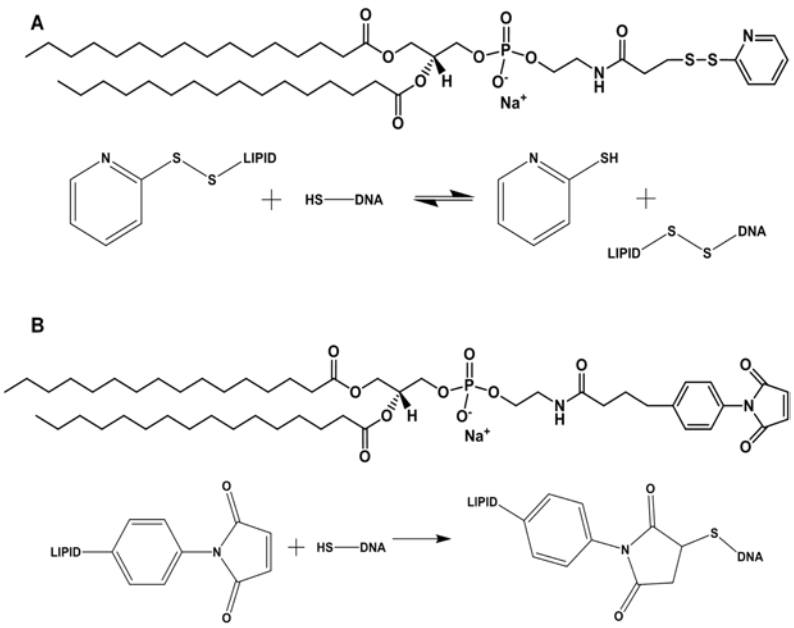

Figure 2.8 Reactive lipid head groups modified with (A) MPB-PE and (B) N-PDP-PE for conjugating thiol-modified DNA.

2.1.3.2 Applications of DNA-directed liposome assemblies.

As demonstrated above, DNA-directed liposome assemblies have been formed using different methods of DNA attachment to the liposome surface. Using this method Francis and coworkers formed DNA-directed live cell assemblies in order to better understand live cell behavior in the presence of neighboring cells.[55j] In the past, live cell adhesion receptors were used such as laminin, fibronectin or peptides containing amino acids arginine, glycine and aspartic acid. Although different types of cells could be studied, control over binding order was difficult to achieve. Utilizing DNA directed assemblies of live cells allows for more control over binding order since DNA sequences can be easily changed.

To achieve covalent attachment of DNA to cell surface, Francis and coworkers made use of metabolic oligosaccharides for introducing azides on the cellular surface.[55j,k] The oligosaccharide is peracetylated *N*-α-azidoacetylmannosamine, which is metabolized to N-α-azidoacetyl sialic acid. After incorporation into glycoproteins and transport of the latter to the cell surface, it subsequently reacts with phosphine-modified ssDNA via Staudinger ligation, a bio-orthogonal reaction, to form an amide linkage. The advantage of this method stems from the highly specific nature of Staudinger chemoselective

ligation. Live cells do not produce azide or phosphine groups, therefore the reaction only occurs if these groups are present and therefore is highly effective *in vitro*. Francis and coworkers using a microfluidic device as a support functionalized two non-complementary ssDNA sequences.[55j] Using the same Staudinger method, they attached DNA sequence complementary to one of the immobilized sequence to cells labeled with a cytosolic dye. Sequence-specific binding following incubation for 35 minutes resulted in greater than 90% binding of cells to the surface. Interestingly, for three different cell types-Chinese Hamster Ovary (CHO), Jurkat and human embryonic kidney (HEK) cells-a shear force greater than 31 dynes/cm^2 (3.1 x 10^{-4} Newton/cm^2) was measured, which is well above the stress needed for application in microfluidic technology. In order to test the behavior of neighboring Jurkat cells, viability tests were conducted by being incubated for 25 hours at 37^{o}C. 79% of bound cells were still viable similar to those that were unbound to the support. This was one of the first examples where DNA assembly was used to attach cells for potential application in tissue engineering.

An extension of this study was conducted by Bertozzi and coworkers using fluorescence microscopy.[55i] Employing the same method as described by Francis and coworkers, wherein two sets of cells modified with mutually complementary DNA molecules where mixed, resulting in the formation of large multi-cell aggregates as shown in Figure 2.9D. Similar to the studies done on liposome assemblies, the cell assembly formation was strongly dependent on DNA density. Reversibility was also demonstrated by attaching a 10-mer DNA that underwent melting at 37^{o}C. At room temperature, the assembled state was formed, whereas at T_m the assemblies became unbound. In addition, controlling binding order of different cells, an important aspect of tissue engineering, was also demonstrated. Attachment of CHO cells via DNA hybridization to a hematopoietic progenitor cell line (FL5.12), whose survival and replication was dependent on CHO, showed accelerated cellular growth after 16 hours. Therefore, DNA-directed live cell assemblies were formed successfully with control over binding order using this approach.

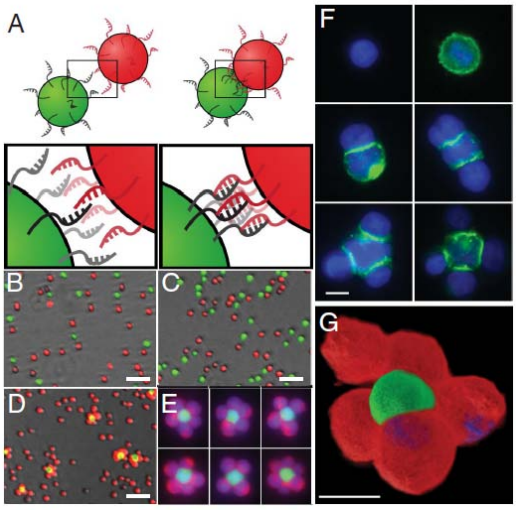

Figure 2.9 DNA directed live cell assemblies where (A) cells modified with complementary DNA sequences were mixed. (B) Non-adherent Jurkat cells stained with cytosolic stains such as fluorescein (green) or Texas red (red) were mixed at a 1:1 ratio. (C) The same cells were mixed as in (B) but labeled with mismatched DNA. (D) Mixed the same cells with complementary sequences at a ratio of 1:50. (E) Assemblies in (D) at higher magnification. (F) Cells labeled with fluorescein modified DNA (top right) assembled with cells containing non-fluorescent DNA (top left). (G) 3D assemblies encapsulated in agarose using deconvolution fluorescence microscopy. Red, Texas Red; green, fluorescein; blue, DPI. Scale B-D 50 μm and E-G is 10 μm. Figure adapted with permission from ref (55i). Copyright © National Academy of Sciences.

Another application of DNA-directed liposome assemblies is studying the fundamental cell membrane functions for analytical and biomedical applications. One such function is membrane fusion. This fundamental process influences a diverse range of biological processes such as neurotransmission, endocytosis, and viral infections.[56a] However the exact mechanism of the membrane including membrane receptors and the different kinds of lipids remains a challenge. Nevertheless, vesicle fusion is believed to occur in three steps. In the first step, docking brings the two membranes close to one another. Second, the outer leaflets merge, resulting in stalk formation and a hemi-fused vesicle state. Third, content mixing is achieved via transient pore formation or merging of the two membranes. Although the mechanism is not completely understood, the SNARE family protein (soluble *N*-ethylmaleimide-sensitive factor attachment protein receptors) is believed to play an important role for membrane fusion.[56c] Given the complexity of the protein system, Höök and coworkers employed DNA hybridization to induce liposome

fusion.[60,61] In their case, two types of liposomes were mixed containing complementary bivalent cholesteryl-modified DNA inserted into each liposome, which resulted in the formation of a duplex. The DNA was designed such that hybridization was achieved in a zipper-like fashion. Fusion was evaluated by monitoring the lipid mixing of both the inner and outer leaflets of the bilayer. The fusion rate was found to depend on DNA density and presence of DOPE and cholesterol in the liposome formulation. Alternatively, Boxer and coworkers studied vesicle fusion by mixing two sets of liposomes decorated with complementary amphiphilic ssDNA probes, as shown in Figure 2.10.[56a,b,58] By inserting a thymine spacer between the complementary region of the DNA and liposome surface, they achieved increased content mixing in the absence of the spacer. The resultant duplex formation brought the liposome in close proximity with one another. Although no zipper-like duplex formation was engineered for this system, fusion was still observed. Boxer and coworkers also observed increase in fusion as the number of DNA per vesicle increased and fusion was low when non-complementary DNA conjugates were used.

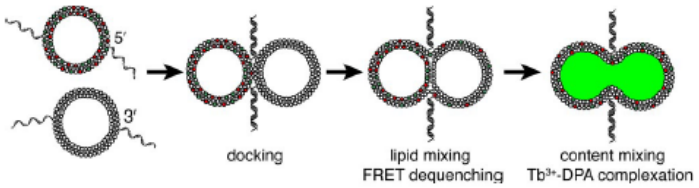

Figure 2.10 Liposome fusion achieved by mixing two types of liposomes each functionalized with complementary amphiphilic ssDNA probes. DNA hybridization leads to docking then lipid mixing followed by content mixing (dyes Tb-DPA)$^{3+}$). Figure adapted with permission from ref (56a). Copyright © National Academy of Science.

As highlighted above, several studies have been conducted on the preparation and applications of DNA-directed AuNP and liposome assemblies. Although assemblies formed using soft and hard materials have unique properties they both display cooperative melting behavior. So far a study comparing hard (i.e., AuNPs) and soft (i.e., liposomes) DNA-directed assemblies is still lacking. We herein report the preparation of DNA-directed assemblies made-up of three-components, two sets of DNA functionalized liposomes or two sets of DNA functionalized AuNPs and DNA linker. The melting

transitions of these liposome assemblies as a function of lipid charge, size, fluidity, and attached DNA are systematically studied and compared with the analogous properties of AuNPs.

2.2 Results and Discussion.

2.2.1 System Design.

As shown in Figure 2.11A, our soft system is made-up of three components, two types of DNA-functionalized liposomes and a linker DNA. The charge and fluidity of the liposomes can be independently varied by judicious selection of the base lipid. For instance, lipids such as DOPC and DPPC are zwitterionic (Figure 2.11B), and DOPG is anionic. We did not consider cationic lipids, since they are prone to aggregation in the presence of negatively charged DNA via electrostatic interactions. The phase transition temperature, T_c, of a lipid determines the liposome fluidity at room temperature. As highlighted below, liposomes prepared with DOPC and DOPG are fluid at room temperature, whereas those from DPPC are not. In a typical experiment, liposome aggregates were prepared using a concentration of 0.25 mg lipid/mL of each DNA-functionalized liposome in the presence of 2.5 μM linker DNA. As shown in the inset of Figure 2.12C, large gel-like DOPC liposome aggregates were formed in the presence of linker DNA. As expected, in the absence of linker DNA, the liposomes remain well-dispersed. To help visualize liposome assembly, 1% rhodamine-B labeled lipid was employed. Following assembly, the liposome aggregates were purified by centrifugation to remove free DNA and liposomes. As shown in the inset of Figure 2.12C, the supernatant was clear after purification, indicating that all liposomes were present in the analyte in their aggregated form. In the melting transition experiments, at temperatures above the DNA melting temperature, T_m, aggregated liposomes disassemble to produce a clear solution. As demonstrated for DNA-linked AuNPs, melting transition experiments can provide useful information.[51,52,54]

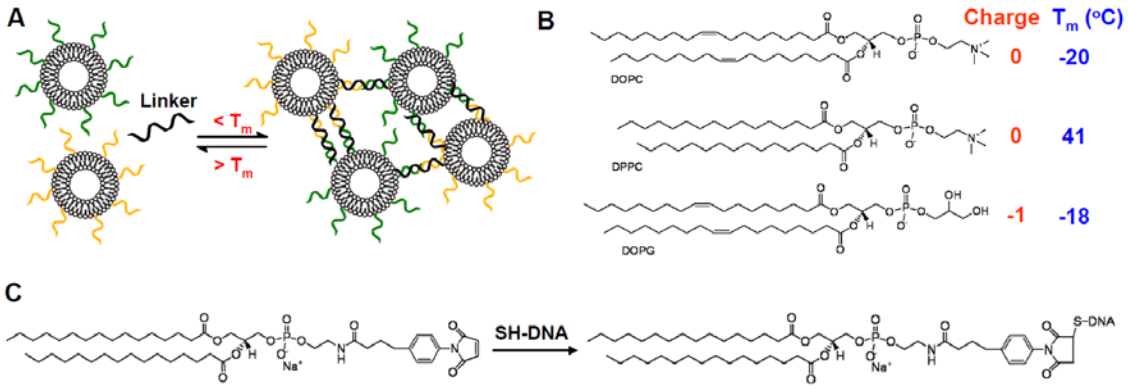

Figure 2.11 (A) DNA-directed assembly of DNA-functionalized liposomes where T_m is the DNA melting temperature of the assembled liposomes. (B) The different phospholipids used in this study and their respective T_c values are the lipid phase transition temperatures. (C) DNA functionalization chemistry via bio-conjugation of thiol-modified DNA to MPB-PE lipid in the liposome.

2.2.2 Assembly of DNA-functionalized liposomes.

In order to direct their assembly, DNA must first be linked to the liposomes. This linking is commonly achieved using one of three methods.[81] First, lipid-functionalized DNAs (e.g., with cholesterol) are incorporated during liposome preparation, resulting in DNA being present at both the inner and outer-leaflets of the bilayer membrane. However, this method requires a relatively large quantity of modified DNA and the stability of DNA insertion is low.[82] In the second method, DNA modified with certain lipids (e.g., cholesterol-TEG) can spontaneously and quantitatively insert themselves into preformed liposomes.[83,84] One limitation of this methodology is that only the 3′-end modification is commercially available for cholesterol-TEG. Many other reported lipid-DNA conjugates cannot be purchased from commercial sources and therefore must be synthesized, as described in the introduction.[62,64] We employed a third method, in which a small fraction (5%) of lipid containing a reactive maleimide headgroup (MPB-PE) was first incorporated during liposome preparation.[60] The maleimide group was then reacted with thiol-modified DNA to form a covalent linkage (Figure 2.11C). We achieved a coupling efficiency of approximately 25%, which was determined by the decrease in the DNA absorption peak at 260 nm. Since both 3′ and 5′-thiol-modified DNAs and the reactive lipid are commercially available, this method can be readily used.

A standard extrusion method using polycarbonate membrane filters was used to prepare liposomes of two sizes. In the case of DOPC liposomes, dynamic light scattering indicated the formation of liposomes with hydrodynamic diameters of 114 and 251 nm. The numbers of DNA molecules attached

to the 114 nm liposomes and the 251 nm liposomes were estimated to be 550 and 2100 per liposome, respectively. This density is slightly lower compared to DNA-functionalized AuNPs, with which greater than 8000 DNAs can be attached to each 250 nm AuNP via Au-thiol chemistry.[85]

Unlike AuNPs, liposomes without a dye label do not absorb visible light. Nevertheless, UV-visible spectroscopy can still be used to monitor the assembly process, since assembled liposomes reflect and scatter light (260-800 nm) more strongly than individually dispersed ones. A typical extinction spectrum of 114 nm DOPC liposomes is shown in Figure 2.12A (black curve). Following DNA attachment, a peak at 260 nm due to DNA absorption was observed (red curve). Upon assembly via treatment with linker DNA, the extinction between 260 and 800 nm increased (blue curve). Therefore, any wavelength in this region can be used to monitor liposome aggregation. For most studies, we selected to monitor extinction changes at 260 nm. The extinction change at 260 nm was predominantly attributed to the assembly of liposomes rather than the hypochromic effect of DNA hybridization, since the concentration of DNA was too low to contribute to such a significant change. In the case of AuNPs (Figure 2.12B), the extinction at 260 nm actually decreases upon aggregation (Figure 2.2B), which is related to the surface plasmon coupling of AuNPs.[51] In addition, the kinetics of DNA-directed assembly of liposomes provided in Figure 2.12C can also be determined by monitoring extinction. However, we chose to use 400 nm here to avoid artifacts associated with the absorption of the added linker DNA. After the addition of 2 μM linker DNA to the DNA-functionalized liposomes, the extinction at 400 nm increased immediately, indicating the formation of aggregates. A two-phase assembly process was observed where initially the extinction increased rapidly, followed by a slow phase. By fitting the curve to a double exponential increase, we obtained rates of 7.1 and 0.061 min^{-1} for the two phases ($R^2 = 0.99$). There are two models used to describe aggregation kinetics of liposomes, these being diffusion and reaction limited cluster aggregation models.[51c] In the diffusion-limited cluster model every liposome collision results in a permanent contact followed by aggregation. Whereas, in the reaction-limited model each collision does not result in a permanent contact, as such cluster growth takes longer in the case of reaction cluster model. Therefore the short reaction kinetics we obtained for our DNA-directed liposome assemblies must be governed by diffusion-limited cluster growth model.

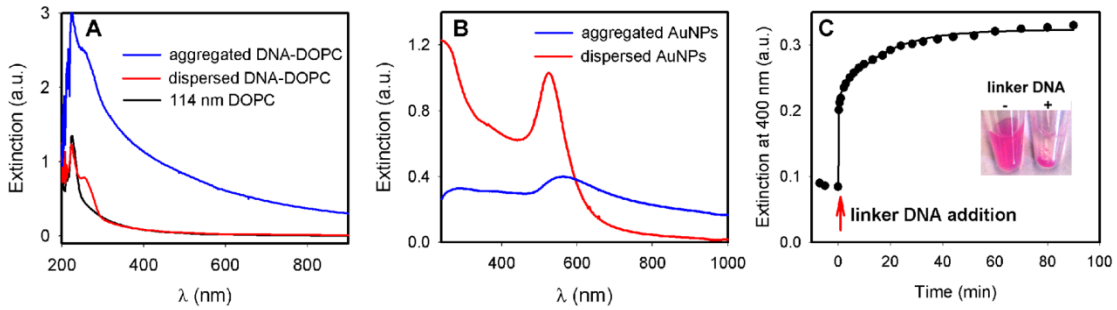

Figure 2.12 Extinction spectra of (A) unmodified (black curve), DNA-modified dispersed (red curves) and assembled (blue curves) 114 nm DOPC liposomes and (B) 13 nm AuNPs. (C) Kinetics of DNA-directed assembly of liposomes. The assembly reaction was carried out in 300 mM NaCl, 20 mM HEPES, pH 7.6 at 35°C with 114 nm DOPC liposomes. Inset shows a photograph of dispersed and assembled liposomes (with 1% rhodamine-B label). Visible precipitates are formed upon DNA-directed assembly, and the supernatant solution is clear, suggesting that few free liposomes are present.

2.2.3 Melting properties of DNA-linked liposomes.

A key feature of DNA-linked AuNPs is their sharp melting transitions,[51,52] which occur due to multivalent and cooperative DNA binding. To study melting in DNA-linked liposomes, we first tested zwitterionic DOPC with a phase transition temperature (T_c) of -20°C. The assembled liposomes were dispersed in buffers with varying salt concentrations and the extinction at 260 nm was monitored as a function of temperature. Consistent with DNA-directed assembly, an increase in T_m was observed with increasing salt concentration (Figure 2.13A). Very sharp melting transitions were observed for all of the samples considered. The sharpness of the melting transition was determined by taking the full width at half-maximum (FWHM) which was found to be 1°C or less, of the first derivative of each melting curve. The first property we considered is the effect of liposome phase transition temperature (T_c) on the melting temperature of the assemblies. Above T_c, the bilayer is fluid, allowing for fast lateral diffusion. Below this temperature, the bilayer adopts a gel-like state, which inhibits diffusion. Since the DNAs were immobilized on the lipid headgroup, the membrane fluidity may affect the local DNA density, packing, and dynamics, which may in turn affect the number of DNA linkages between liposomes as well as the T_m of the assemblies. To test the effect of lipid fluidity, DOPC with a T_c of -20°C and DPPC liposomes with a T_c of 41°C were studied (Figure 2.13A and B). The same salt-dependent increase in T_m values for all of the assemblies made with DOPC and DPPC was observed (Figure 2.13A and B). At low salt

concentrations (e.g., 6 mM), DNA melted prior to the DPPC phase transition. For the purpose of determining liposome assembly melting was after the lipid phase transition, we conducted the melt curves at 52 mM Na^+. For all of the DPPC liposome melting curves, we observed a second transition at ~41^oC (a small drop in the extinction), which coincides with the T_c of this lipid. To confirm the origin of this second transition, we monitored the extinction of non-functionalized DPPC liposomes (i.e., devoid of DNA), which again displayed a decrease in extinction at this temperature (Figure 2.14). However, non-functionalized DOPC did not show an obvious temperature-dependent extinction change. Therefore, this second transition is attributed to the phase transition of DPPC. Under our experimental conditions, the similarity in T_m between DPPC and DOPC suggests that lipid fluidity has little effect on the melting of liposome aggregates. For comparison purposes, we also conducted melting studies of 13 nm AuNPs assembled with the same linker DNA. As shown in Figure 2.13C, the resulting T_m values were very similar to those obtained for the liposome aggregates. This behavior is similar to that observed for AuNPs,[52] indicating that the melting of liposome proceeds via the same cooperative mechanism. Because the AuNPs and liposomes were different in size and will be discussed later, because nanoparticle size plays a crucial role in determining the T_m of AuNPs, this observed similarity in T_m is more of a coincidence rather than a general observation.

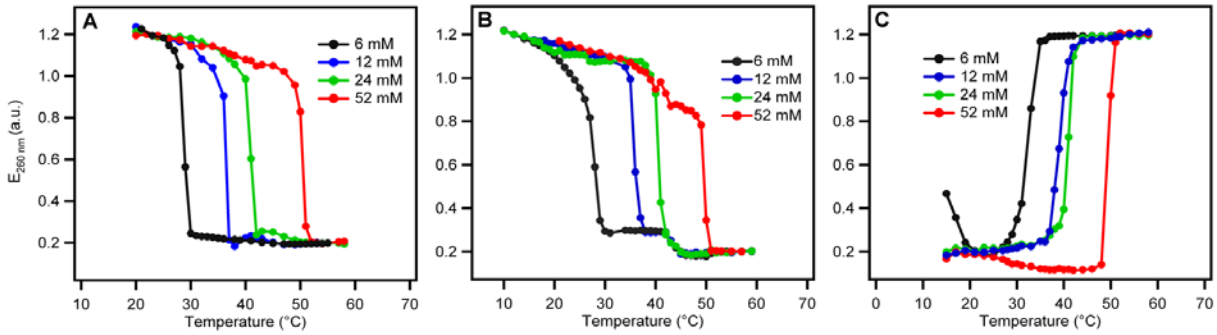

Figure 2.13 Salt-dependent melting curves of DNA-directed assembly of (A) DOPC, (B) DPPC liposomes and (C) AuNPs. All of these nanomaterials were assembled using the same linker DNA. The melting curves are normalized for comparison purposes.

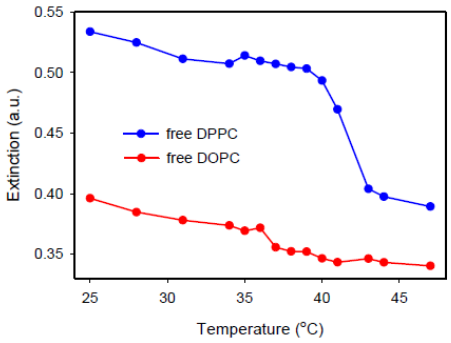

Figure 2.14 Temperature dependent extinction at 260 nm for non-DNA functionalized DPPC and DOPC liposomes (no DNA attachment). The decrease at ~41°C can be observed for the DPPC liposome but not for DOPC in 52 mM Na^+.

2.2.4 Effect of surface charge and cholesterol.

We next studied the effect of surface charge on the assembly of three different types of liposome, consisting of DOPC only, DOPG only, and an equimolar mixture of the two, respectively. The melting temperature value showed no difference when DOPG or zwitterionic DOPC or their 1:1 mixture was used. At 52 mM Na^+, all three liposome assemblies showed a sharp melting transition temperature at 50°C, as shown in Figure 2.15A. These results indicate that the liposome charge has very little effect on the melting of DNA-linked liposomes.

The interaction between charged liposomes in an electrolyte solution can be described using the Derjaguin Landau Verwey Overbeek (DLVO) theory. In the absence of DNA, long-range attractive van der Waals forces and long-range repulsive electrostatic forces govern liposome interactions. In the presence of a rigid B-form 24-mer double-stranded DNA linker, the liposomes are separated by ~8 nm. Each functionalized DNA contains a 9-adenine spacer on each end (see Figure 2.15A). Therefore, the liposomes are separated by ~10 nm in the assembled state. The interaction energy for charged liposomes separated by 10 nm has been determined to be only ~1 kBT according to already reported calculations.[86] At 298 K, this energy is ~0.6 kcal/mol. However, the 12-mer DNA base pairing free energy in our system should exceed 6 kcal/mol per hydrogen bond.[87,88] In our case, we estimated 1287 pmol of DNA per 114 nm liposome. Considering that liposomes are linked by multiple DNAs, the energy from DNA binding is even greater. Therefore, other inter-liposome forces are much smaller in comparison to the DNA hybridization energy, which may explain why liposome charge has little effect on T_m.

To further understand the effect of surface charge, the zeta (ζ) potential of the liposomes were measured. Recall that two layers of ions, referred to as the stern and diffuse layer, respectively, form at the surface of a charged colloid in an electrolyte solution. At the stern layer, which lies in closer proximity to the particle surface, surrounding ions are more strongly associated to the colloid surface than the diffuse layer. Zeta potential measurements estimate the potential at the diffuse layer, and in general, colloidal systems with ζ-potentials outside the interval -25 to 25 mV are stable. That is the more positive or negative the potential the greater the electrostatic repulsion between two colloids. At pH 7.6 with 52 mM Na^+, DOPC exhibited a ζ-potential of -7.0 mV, which is consistent with literature reports where the PC headgroup carries a slight negative charge at neutral pH.[89] Following DNA binding, the ζ-potential of the modified liposome changed to -19.7 mV owing to the negative charge carried by DNA. On the other hand, the ζ-potential for DOPG changed from -51.8 to -39.4 mV before and after DNA functionalization, respectively. This suggests that the charge density at the plane of slipping plane actually decreased for DOPG after DNA attachment. The negatively charged lipid forces the functionalized polyanion DNA to adopt an extended conformation due to electrostatic repulsion on the liposome surface. Therefore, DNA had an averaging effect on the surface charge as the ξ-potential difference between DOPG and DOPC decreased from 45 to 20 mV after DNA attachment, which may also contribute to the observed charge-independence on the melting transitions.

While the melting of DOPC and DPPC is compared in Figure 2.13, we further studied the effect of adding cholesterol. Not only is cholesterol an important component in the cell membrane, it is also known to have an averaging effect on the lipid phase transition. For instance, cholesterol can fluidize gel phase lipids as well as render DOPC lipids less fluid.[90] With 30% (w/w) cholesterol in DOPC, the melting curve still overlaps with those of pure PC liposomes in the transition region (Figure 2.15B). Therefore, it appears that neither charge nor lipid fluidity has significant effect on the melting behavior of the assembled structures. DNA hybridization alone therefore governs the melting.

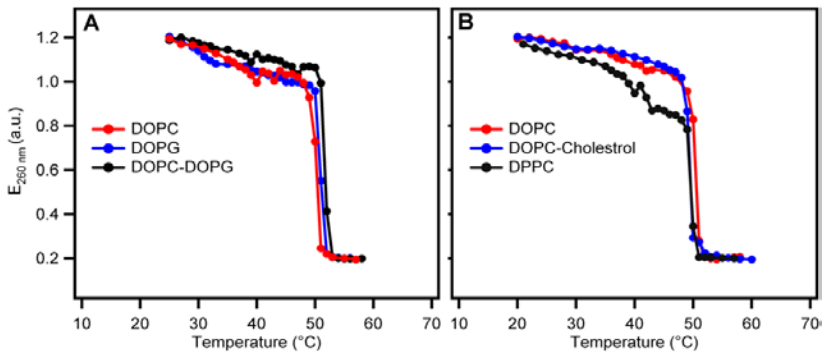

Figure 2.15 Melting curves of DNA-linked liposomes as a function of liposome (A) surface charge and (B) addition of cholesterol. All of the liposomes were assembled using the same linker DNA sequence and melting curves in 52 mM Na^+.

2.2.5 Effect of DNA spacer.

The next parameter we considered is the effect that DNA spacers have on liposome and AuNP assembly. In the case of DNA-linked AuNPs, studies have shown that such assemblies are strongly affected by the presence of a polynucleotide spacer introduced between the hybridization sequence and thiol group.[52] The interparticle distance was increased by the spacer, resulting in a higher T_m. In all of the experiments conducted thus far, a 9-adenine (A_9) spacer was used as illustrated in Figure 2.16A. To test this effect on the liposome system, thiol-modified DNAs without the A_9 spacer were used for liposome functionalization. Interestingly, little difference was observed in the T_m for liposome aggregates prepared with and without the A_9 spacer (Figure 2.16B), while AuNPs clearly showed a much higher T_m when the A_9 spacer was used (Figure 2.16C). Such behavior is attributed to sterics that are operative in the absence of A_9 spacer. This experiment illustrates an interesting difference between hard and soft nanoparticles. Soft materials (i.e., liposomes) can more easily undergo rearrangements (e.g., through liposome deformation and DNA diffusion within the bilayer) in response to the pressure and crowding induced by the assembly process. For example, Beales and coworkersreported large unilamellar vesicles (LUV) assemblies readily adopted deformed shapes in the assembled state emphasizing an important property of such soft materials.[55]

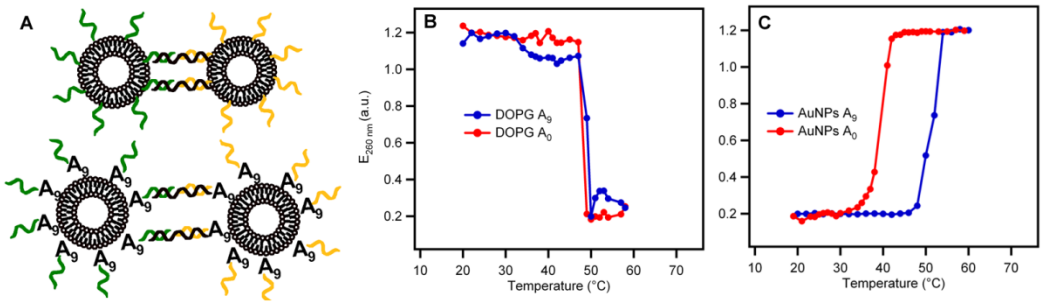

Figure 2.16 (A) Schematic presentation of the position of the nine-adenine (A_9) spacer. Melting transitions of (B) DOPG liposomes and (C) AuNPs in the presence and absence of the A_9 spacer in 52 mM Na^+.

2.2.6 Effect of liposome size.

The size-dependent properties of nanomaterials form a significant aspect of nanoscience. It has been recently demonstrated that AuNPs with diameters up to 250 nm can be functionalized with DNA.[85] It is also possible to prepare a wide range of functionalized liposomes sizes with sufficient colloidal stability. To test the effect of particle size, DOPC liposomes with average sizes of 114 and 251 nm were assembled using the same linker DNA. No significant difference in the T_m or the sharpness of the melting transition (with 52 mM Na^+, Figure 2.17A) of each size liposome was detected. On the other hand, 50 nm AuNPs melted at 12°C higher than the analogous 13 nm system (Figure 2.17B). This result is consistent with literature reports which have demonstrated that larger AuNPs show a higher T_m in DNA-linked nanostructures.[91-94] For example, Mirkin and co-workers reported a 7°C increase in T_m with an increase in AuNP size from 80 to 150 nm.[91,92] There are a number of factors that can affect the T_m of DNA-linked nanoparticles, including DNA sequence, length, DNA density on the particles, solution ionic strength, pH, and particle size. If all of the other parameters (DNA linkages and salt concentration) are fixed and only the particle size is increased, an increased T_m should be observed. This can be attributed to an increase in the contact area resulting in more DNA linkages, which has been used to explain the size dependent T_m of AuNPs.[91] The DNA density on our liposomes was about a quarter of that on AuNPs, and this may explain why our 114 nm liposomes showed a similar T_m as 13 nm AuNPs where not all DNA participate in forming linkages. Our 114 and 251 nm liposomes had on average 550 and 2100 thiol-modified DNA attached, respectively.

The number of attached DNA was determined by the decrease of the supernatant DNA absorption at 260 nm after conjugation with the liposomes. The DNA densities for both of the aforementioned liposomes were similar at about 1 nM and therefore, the observed size independent melting cannot be explained on the basis of the number of DNA linkages. Since the DNA molecules are linked to the MPB-modified PE lipid, which has a saturated lipid tail (Figure 2.11C), another possibility may be the formation of microdomains within the DOPC liposomes (T_c = -20 ^oC). The labeled DNA can then potentially be concentrated within these domains. If the size of the microdomains is independent of the liposome diameter, we can explain the observed melting behavior by considering the fluidity of the liposome bilayer. In order to test this, the melting behavior of another MPB-labeled PE lipid with an unsaturated tail and bound DNA was investigated. The new PE lipid has a T_c similar to that of DOPC, and thus microdomain formation should be inhibited in this system (given that the negatively charged DNA should be repulsive to each other). As shown in the melt curves in Figure 2.15, melting was again independent of size in this system. We thus attribute this size-independent melting behavior to the fluidity of the bilayer membrane. Unlike in the case of AuNPs, where each thiol-modified DNA is fixed in place, DNA bound to the liposome are capable of lateral diffusion. Once a DNA linkage melts, the involved DNA can diffuse away from the linkage site and minimize the probability for re-hybridization at a temperature close to T_m. This may effectively decrease the number of linkages prior to the melting transition and explain why increasing the liposome size did not increase T_m. The fact that the liposome melting profiles remained unchanged suggests that a sufficient number of DNA linkages were still present prior to the transition to allow for cooperative melting.

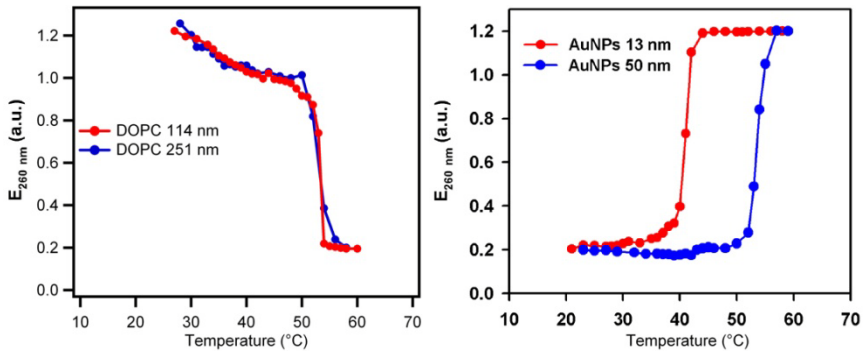

Figure 2.17 (A) Melting curves of DNA-linked 114 and 251 nm liposomes in 52 mM Na^+. (B) Melting curves of DNA-linked 13 and 50 nm AuNPs in 24 mM Na^+.

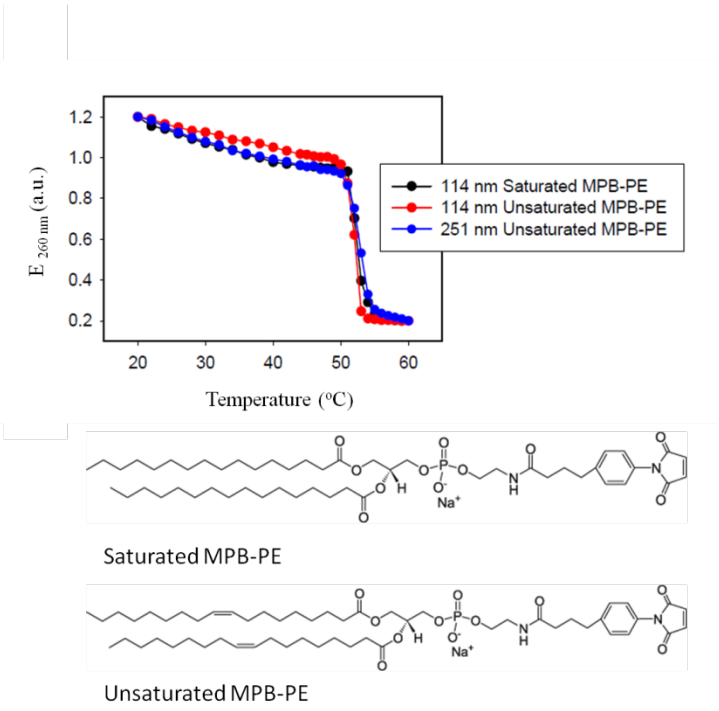

Figure 2.18 Melting curves of DNA-linked DOPC/MPB-PE liposomes functionalized with DNA.

2.2.7 Cryo-TEM studies.

To study the structure and morphology of DNA-linked liposomes, cryo-TEM experiments were performed. Both 103 nm and a mixture of 103 and 258 nm liposomes were assembled by linker DNA. Since the aggregates were very large, only the edges were imaged so that the electrons could sufficiently penetrate the structure to allow imaging. The 103 nm liposomes were spherical in shape with a membrane thickness of ~5 nm, suggestive of the presence of a unilamellar membrane (Figure 2.19A). The average size agrees well with dynamic light scattering data. Partial deformation from spherical shape can be observed in some liposomes, which may be caused by contact with nearby liposomes that occurs during aggregation. In the aggregates containing both 103 and 258 nm liposomes, both size populations can be observed with the smaller particles typically arranged around as well as bridged with the larger ones. Some of the larger liposomes appeared to be multilamellar or encapsulating smaller liposomes (Figure 2.19B). This experiment further supports that DNA-linked liposomes were reliably prepared with good programmability.

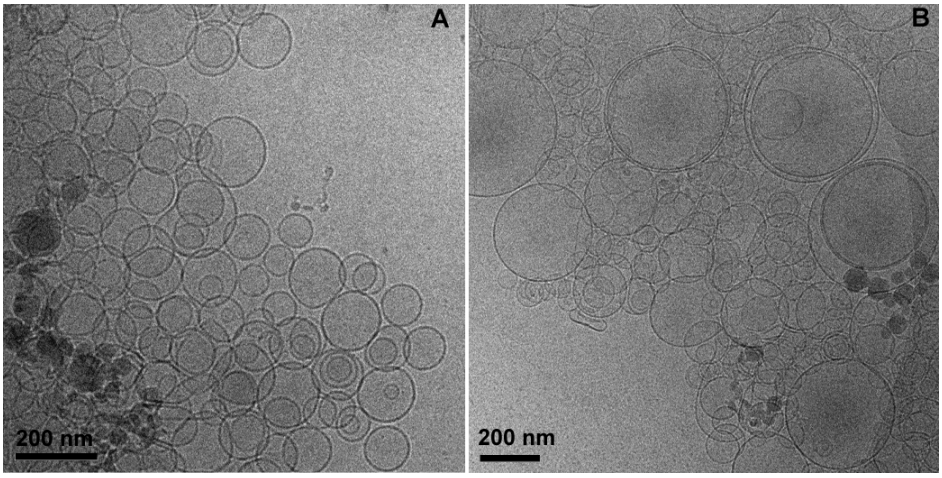

Figure 2.19 Cryo-TEM micrographs of DNA linked (A) 103 nm and (B) 103/258 nm liposomes.

2.2.8 The effect of mismatches in the linker DNA.

One important analytical application of DNA-directed assembly involves the detection of linker DNA sequence.[54,62] Because of the possible sharp melting transitions, even single base mismatches can be detected with high selectivity. We investigated the potential of our liposome system to differentiate such mismatches (Figure 2.20A). As shown in Figure 2.20B, perfectly complementary linker DNA gives a T_m of 51^{o}C. However, a single base deletion or insertion caused the T_m to drop to 48^{o}C and 49^{o}C, respectively. These results are similar to those reported for AuNP assemblies.[53] On the other hand, single nucleotide mismatches positioned in the middle of the hybridization sequence rather than the end exhibited a larger destabilization effect, which led to a decrease in T_m values in the range of 38-41^{o}C. However, in the case of AuNPs Kang and coworkers reported changes in T_m corresponding to single nucleotide mismatch present at the headof the oligonucleotide in DNA-directed AuNP assemblies. This added nucleotide interaction with the AuNP surface results in an increase in the T_m value. In the case of DNA-directed assembly of liposomes, we did not test presence of mismatch at the head of the oligonucleotide. However our DNA-directed liposome assemblies can be used for highly selective DNA detection.

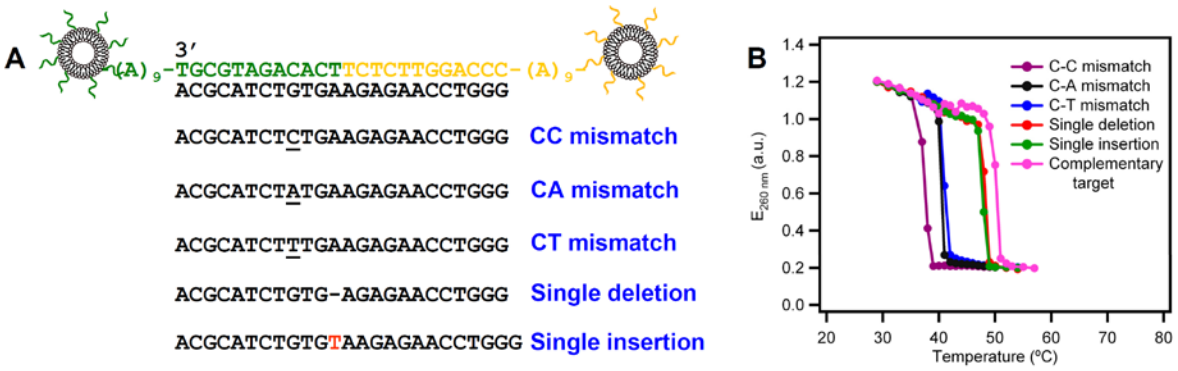

Figure 2.20 Melting curves of mismatch linker DNA sequences induce assemblies of DNA-functionalized DOPC liposomes in 52 mM Na^+.

2.3 Conclusions.

In summary, we have demonstrated DNA-directed assembly of DNA-functionalized liposomes using a three component system. The work reported herein represents the first systematic study of the physical properties of DNA-linked liposomes where various liposome formulations and DNA sequences were tested. All of the experiments were based on the same conjugation chemistry, suggesting good generality and programmability associated with the methodology we selected. The melting transitions of these liposome assemblies as a function of lipid charge, size, fluidity, and attached DNA have been systematically studied and compared with the analogous properties of AuNPs. While there are many similarities, important differences have been demonstrated which can be attributed to the soft nature of liposomes as compared to AuNPs. For example, the T_m of liposome assemblies was shown to be less affected by interparticle separation or liposome size. The fundamental understanding of such properties is expected to improve our design of new liposome-based materials for both analytical and biomedical applications, particularly considering that liposomes have many attractive properties that are lacking in AuNP systems. By now expanding DNA-directed assembly to liposomes, we can even potentially begin to consider combining AuNPs and liposomes to afford a truly multi-functional system that exploits the unique properties of both materials.

2.4 Methods and materials.

2.4.1 Chemicals.

All of the DNA samples were purchased from Integrated DNA Technologies (Coralville, IA). All of the phospholipids were purchased from Avanti Polar Lipids (Alabaster, AL). Cholesterol and chloroform were purchased from VWR. NaCl and 4-(2-hydroxyethyl)-1-piperazineethanesulfonate (HEPES) buffer were purchased from Mandel Scientific (Guelph, Ontario, Canada). Tris(2-carboxyethyl)phosphine (TCEP) was purchased from Sigma. Citrate reduced AuNPs (13 nm diameter) were prepared according to a previously published method.[82] AuNPs (50 nm) were purchased from Ted Pella Inc. The phospholipids employed in this study are 1,2-dioleoyl-sn-glycero-3-phosphocholine (DOPC), 1,2-dioleoyl-sn-glycero-3-phospho-(1′-rac-glycerol) (sodium salt) (DOPG), 1,2-dihexadecanoyl-*sn*-glycero-3-phosphocholine (DPPC), 1,2-dioleoyl-*sn*-glycero-3-phosphoethanolamine-N-(lissamine rhodamine B sulfonyl) (ammonium salt) (Rh-PE), and 1,2-dipalmitoyl-sn-glycero-3-phosphoethanolamine-N-[4-(p-maleimidophenyl)butyramide] (sodium salt) (MPB-PE).

2.4.2 Preparation of liposomes.

Liposomes were prepared using the standard extrusion method. Lipids were mixed according to designated ratios (total mass of 2.5 mg) with 5% MPB-PE in chloroform. Chloroform was first removed under a gentle N_2 flow in the fume hood followed by storage of the films under vacuum overnight at room temperature. The dried lipids were stored at -20°C prior to use. To prepare liposomes, the lipids were hydrated with 0.5 mL 150 mM NaCl, 25 mM HEPES, pH 7.6 at room temperature and sonicated. The lipid concentration was 5 mg/mL. A cloudy lipid suspension was obtained once the lipids were fully hydrated, which was then extruded through a polycarbonate membrane with two syringes 21 or more times. The membrane diameters used were 50 and 400 nm. After extrusion, the lipid solution was nearly transparent, indicating the formation of the desired liposomes. The liposomes were then immediately used for DNA conjugation experiments. Because the transition temperature of DPPC is 41°C, a water bath was heated to ~60°C to rehydrate DPPC systems and extrusion was performed at this temperature.

2.4.3 DNA conjugation to liposomes and AuNPs.

Thiol modified DNAs were activated with TCEP (TCEP:DNA=2:1 molar ratio) in 40 mM acetate buffer pH 5.0 for at least 1 hr at room temperature. In a typical reaction, 50 μL of 5 mg/mL liposomes were reacted with thiol-modified DNA (final DNA concentration ~60 μM) at room temperature overnight in buffer A. After incubation, the salt was adjusted to 500 mM NaCl and the sample was stored at 4°C for 12 hrs. The liposomes subsequently precipitated out of solution, which was attributed to the self-aggregation of the DNA-functionalized liposomes.[81] These liposomes were then collected by centrifugation (13000 rpm) at 4°C and unreacted DNA in the supernatant was removed. With rhodamine-B-labeled liposomes, we found that >95% of the liposomes could be recovered by the centrifugation step. The liposomes were then dispersed at a concentration of 2.5 mg/mL in buffer A. Thiol-modified DNAs were attached to 13 nm AuNPs according to a published protocol.[82] To attach DNA to 50 nm AuNPs, a recently reported protocol was used.[83]

2.4.4 Liposome purification and yield.

To estimate the yield following purification, 1% rhodamine labeled DOPC liposome were used. After centrifugation, the supernatant fluorescence (excitation at 540 nm and emission at 580 nm) was measured and compared to the same liposomes of known concentration from which, it was determined that the yield exceeded 95% (i.e., only less than 5% of liposome was lost during centrifugation and removal of supernatant).

2.4.5 Determination of DNA density on liposomes.

All of the liposomes were prepared from a concentration of 5 mg/mL lipid. In the case of DOPC (molecular weight = 786 g/mol), the lipid concentration was 6.36 mM. The average liposome size was determined using dynamic light scattering. For 114 nm diameter liposomes where there are an estimated 136,023 lipid molecules within each liposome. This number was obtained by assuming that there are equal number of lipids on the inner and outer leaflets and that each lipid occupies an area of 0.6 nm^2. Therefore, the liposome concentration is 46.8 nM. For 251 nm diameter liposomes, its concentration is 9.64 nM. To attach DNA, 50 μL of the above liposomes were mixed with thiol-modified DNA. The number of attached DNA was determined by the decrease of the supernatant DNA absorption at 260 nm.

1287 and 1013 pmol of DNA were attached to 114 and 251 nm liposomes, respectively. Therefore, the number of DNA was determined to be 550 for 114 nm and 2100 for 251 nm liposomes.

2.4.6 Preparation of DNA-linked aggregates/assemblies.

In a typical reaction, 0.25 mg/mL of each liposome system (functionalized respectively with 3′ and 5′-end thiol-modified DNA) in the presence of 2.5 μM of the linker DNA were mixed with a 300 mM NaCl and 25 mM HEPES solution (pH 7.6). The mixture was incubated at 50°C for 5 min and then allowed to cool slowly to 35°C. In a typical preparation of AuNPs aggregates, 4.5 nM of each AuNPs system (functionalized respectively with 3′ and 5′ -end thiol-modified DNA) was reacted with 0.2 μM linker DNA in a 300 mM NaCl and 25 mM HEPES, pH 7.6.

2.4.7 Melting curves and kinetics.

For melting temperature measurements, DNA-linked aggregates were dispersed in a total volume of 200 μL of a buffer of choice containing varying concentrations of NaCl and HEPES at pH 7.6. The aggregates were repeatedly washed (4x) by dispersing in 200 μL of the cold buffer and centrifuged to remove the supernatant at 4°C prior to the melting experiment. The measurements were performed with an Agilent 8453 spectrophotometer and the temperature was controlled by a circulating water bath. The temperature increment was every 2°C before melting and every 1°C close to T_m. The samples were allowed to equilibrate at each designated temperature for 2 min before each measurement and the rate of temperature increase was ~1°C/min. The melting curves were obtained by plotting the extinction at 260 nm as a function of temperature. To compare different samples, the melting curves were normalized linearly to have the lowest extinction at 0.2 and largest extinction at 1.2. The first derivative of the melting curve was used to determine T_m. To measure the kinetics of liposome aggregation, an equal concentration of 3′- and 5′ thiol-DNA functionalized DOPC liposomes (0.2 mg/mL) were mixed in a 300 mM NaCl and 25 mM HEPES, pH 7.6 at 35°C. A final concentration of 2 μM linker DNA was added and the extinction spectra were collected for up to 90 minutes.

2.4.8 Temperature-dependent extinction change for non-functionalized liposomes.

Freshly prepared DPPC and DOPC liposomes with no DNA on the surface were dispersed in 52 mM Na^+ buffer and the 260 nm extinction was monitored as a function of temperature (Figure 2.3). The significant drop in the DPPC extinction observed at ~41^oC, which was not observed for the DOPC liposomes, was likely due to the phase transition of the DPPC liposome.

2.4.9 Test of different reactive lipid for DNA immobilization.

The majority of the experiments in this work were performed with the reactive lipid shown in Figure 2.1C for DNA conjugation. We also used a lipid with unsaturated tails (18:1 MPB-PE) in order to test whether the unsaturation could influence the properties of the resultant liposomes. This lipid possesses a similar phase transition temperature to that of DOPC and therefore, it is unlikely to form microdomains when mixed with DOPC.

2.4.10 Dynamic light scattering and zeta potential measurements.

To estimate the size and charge of the liposomes, dynamic light scattering and zeta potential experiments were performed using a Malvern Zetasizer Nano instrument. The freshly prepared liposomes and DNA conjugated liposomes were dispersed in a buffer containing 100 mM 25 mM HEPES, pH 7.6 at a lipid concentration of 0.25 mg/mL. Zeta potential measurements were performed using 50 mM NaCl and 25 mM HEPES, pH 7.6 solution containing a lipid concentration of 0.25 mg/mL.

2.4.11 Cryo-TEM studies.

The DOPC/cholesterol liposomes (30% cholesterol with 5% DOPG and 5% MPB-PE) were dispersed in a buffer containing 40 mM NaCl and 10 mM HEPES, pH 7.6. TEM samples were prepared by a FEI Vitrobot. 5 μL of the sample was added onto a carbon coated copper TEM grid (treated with plasma to ensure that the surface was hydrophilic) in a humidity controlled chamber. The humidity was set to be 95–100% during this operation. The grid was blotted with two filter papers for 1.5 sec and quickly plunged into liquid ethane. The sample was then loaded onto a liquid cooled cold stage and

inserted into a 200 kV field emission TEM (FEI Tecnai G2 F20). The samples were imaged once the temperature was stabilized at -175°C, at a magnification of 25,000–29,000×.

Chapter 3.0
DNA-directed assembly of gold nanoparticles and liposomes for controlled content release.

The results presented in this chapter have been published as part of:

Neeshma Dave and Juewen Liu, "Protection and Promotion of UV Radiation-Induced Liposome Leakage via DNA-Directed Assembly with Gold Nanoparticles", Advanced Materials, 23, 3182–3186, 2011.

3.1. Introduction.

3.1.1 Research objective.

Controlled release of encapsulated molecules is important for many technologies, such as drug delivery, stimuli-responsive materials, and biosensors. Liposomes in particular are an ideal platform for use in controlled release applications. Stimuli such as surfactants[96a-c], peptides[97], osmotic pressure[97g,h], pH[98], temperature[99], and radiation[100] have thus far been tested to induce liposome leakage. As will be highlighted below, a combination of temperature and radiation can be used by tethering gold nanoparticles (AuNPs) to the liposome surface via DNA hybridization for controlled liposome release.

3.1.2 Stimuli-responsive liposomes.

Non-ionic surfactants are able to induce instantaneous liposome leakage via pore formation.[96a,b,c] Such liposome leakage occurs in stages. In stage I, the surfactant partitions between the liposome bilayer and the aqueous phase. However, at this point, the surfactant concentration is still below the critical micelle concentration (CMC). Increasing surfactant concentration results in saturation of the bilayer with surfactant forming mixed surfactant-phospholipid micelles, this is referred to as stage II. Pore formation occurs within stages I and II where the liposome membrane still remains unperturbed but the inherent properties of the liposome undergo a slight change. Stage III is realized once a critical ratio of surfactant to lipid is reached, which induces complete rupture of the liposome. For this reason, surfactant concentration is vital for controlling liposome leakage. Commonly used surfactants for this purpose include non-ionic surfactants such as Triton X-100, which contain a polyethyleneoxide chain as a hydrophilic component and octylphenol as a hydrophobic component.[96e,f] Studies have shown

sterilization of male fish in the presence of Triton X-100. Owing to such toxicity, surfactants are not used to induce liposome content release *in vivo*.

However, surfactants have been used for analytical applications.[96g] A liposome can contain within its core a large number of fluorophore molecules, thus facilitating signal amplification. Unlike enzyme assays where the signal increase is time-dependent, signal enhancement can be achieved instantaneously via addition of a surfactant, resulting in a signal increase of 500-1000 compared to single fluorophores. This behaviour primarily stems from the unique feature of some fluorescent dyes that self-quench at high concentrations such as calcein, fluorescein, sulforhodamine 101 and sulforhodamine B.[96h,i,j] The dye molecules form non-fluorescent aggregates due to static quenching, collisional quenching, and energy transfer from monomers to non-fluorescent dimers. When lysis occurs via addition of a surfactant, dilution of the entrapped fluorophores results in signal enhancement. If surfactants or solvents are used for lysis, a separation step is first required to ensure that only the bound liposomes are lysed. Heterogeneous assays have been developed, in which direct detection is achieved by formation of a sandwich-hybrid tethered with two antibodies which forms a sandwich using the same analyte molecule. Using immunoassay based sandwich-complex formation where the liposome is labelled with particular antibodies and encapsulated with dye have been successfully used for the detection of *Escherichia coli*, botulinum toxin, and cholera toxin.[96k,l,m] For each of these assays, the signal generated upon dye release was directly proportional to the amount of analyte bound in the sandwich complex. This method has also been used to detect astrovirus, *Bacillus anthracis*, and Dengue virus.[96n,o,p]

Liposome leakage can be achieved by peptides, osmosis, pH, ultrasound and via radiofrequency. Liposome leakage induced via peptides proceeds by pore formation, such that the peptide first inserts into the bilayer and aggregate either reversibly or irreversibly within the surface.[97a] When the peptide aggregates reach a critical size, peptide translocation occurs with subsequent pore formation. The percentage of content release is dependent on lipid/peptide ratio. Typical peptides include amphiphatic peptides such as GALA, paradaxin, and peptide HIV.[97b,c,d] Other peptides such as melittin, a 26-amino acid peptide[97e], and a variety of antimicrobial peptides made up of 12-50 amino acids that target specifically bacterial membranes have also been studied for the induction of liposome leakage.[97f]

Another method for permeabilization is based on osmotic pressure. Osmotic pressure can be controlled by simply manipulating the ionic strength of the solution. Decreasing the salt concentration of the medium results in swelling of liposomes via osmotic influx of the solvent, which increases the surface tension and liposome rupture via pore formation. On the other hand, increasing salt concentration in the

medium results in reversing osmotic flow, and therefore collapse of the liposome membrane with subsequent content release.

Incorporation of lipids in the liposomes that are sensitive to external pH is another way to induce liposome leakage.[98a] There are several physiological and pathological processes for targeted drug delivery such as endosome trafficking, tumor growth, inflammation, and myocardial ischemia that result in a decrease in pH of the surrounding.[98b,c] As a result, a tremendous amount of research has been directed towards the design of pH-sensitive liposomes.[98b,d-f] Three general approaches have been developed to achieve pH triggered content release. In the first case, neutralization of the negative charge of the carboxylate lipids within the bilayer may lead to a lamellar to hexagonal phase transition (bilayer to micelle) with concomitant content release. Leakage occurs in the aforementioned because of the reduction of surface area. This method was first demonstrated by Yatvin and coworkers[98g] who prepared liposomes made-up of phosphatidylcholine and N-palmitoyl homocysteine. A number of liposomes containing surfactants with pH-titratable carboxylate groups and a fusogenic lipid (DOPE) have since been studied.[98d] Decreasing the pH results in neutralization of the excess negative charge of the carboxylate groups results in reduction of the surface area of the headgroup and triggers collapse of the PE-rich lamella into a hexagonal phase with concomitant release of encapsulated content. A disadvantage of using this type of liposome stems from the presence of negative charges at neutral pH, which leads to interactions with plasma proteins and macrophages, resulting in the swift removal of the liposome from the circulation.[98h] In the second scenario, polymers or peptides that contain titratable acid groups are attached to the liposomes bearing pH-sensitive lipids. The protonation of the negatively charged lipids results in aggregation in the bilayer and destabilization of the liposome structure.[98a] Destabilization causes lysis, phase separation, pore formation or fusion. Peptides that exhibit this type of behaviour are the GALA family proteins.[98i] Leakage of phosphatidylcholine vesicle can be induced by protonation of glutamic acid residues initating transition of the GALA proteins from a random coil to helical secondary structure. The third scenario involves the use of neutral surfactants whose hydrolysis is catalyzed only in acidic conditions. Thompson and coworkers studied a number of mono- and diplasmenyl lipids containing acid sensitive vinyl-ether linkage between the head group and the hydrocarbon tails.[98j,k] At low pH, the vinyl ether linkage is cleaved, creating defects within the bilayer resulting in liposome content release.

Another method to achieve liposome leakage is via ultrasound.[99a] These ultrasound sensitive liposomes include a non-bilayer forming lipid such as PE which upon exposure to ultrasound undergo changes from lamellar to reverse hexagonal phase transition resulting in complete content release.[99b] The

presence of such lipids makes them easy to manipulate due to decreased van der waals packing. Schroeder and coworkers showed that by simply exposing the liposomes to low-frequency ultrasound results in the formation of pores and increased permeability due to the disruption of the lipid packing in the membrane.[99c] On the other hand, exposing liposomes to high-frequency ultrasound in the presence of inert gas such as Argon results in the formation of gas bubbles which results in an intense energy release upon bursting.

Hyperthermia treatment using radiofrequency irradiation is another method to induce liposome leakage for treatment of tumors.[99a] In this approach, a probe is typically inserted near the tumor and heat generated from the radiofrequency waves passing through the probe leads to tumor ablation. This method is currently used to treat tumors in the lungs, kidney and bones. The advantage of this method is that the tissue does not get damaged, since the temperature increase is only up to 45^{o}C. Liposomes prepared with DPPC as the major constituent have a phase transition temperature of 41^{o}C. Below 41^{o}C, the liposome adopts a more gel-like state and above 41^{o}C the liposome adopts a more liquid-like state which is more permeable allowing for complete content release. Several examples have demonstrated effective accumulation of liposome-encapsulated doxorubicin using antibodies, addition of lysolipids, and polymers can also facilitate content release.[99d] Addition of only 10% monopalmitoylphosphatidylcholine (MPPC) lysolipid to DPPC allowed content release over 24 hours with mild hyperthermic heating.[99e] Reasonbeing MPPC has a T_m of -20^{o}C addition of this lipid to DPPC lowers the mixture of the transition temperature to 34^{o}C allowing for increased content release with mild heating. Needham and coworkers showed that using dye encapsulated in liposomes containing MPPC underwent fast release was achieved at 42^{o}C.[99f] Testing such liposomes *in vivo* with the drug doxorubicin showed delay in tumor re-growth for up to 60 days. In addition, they showed that the extent of drug release was greater than with the prototypical thermosensitive liposome, DPPC, used thus far. The acceleration of content release by MPPC is due to de-stabilization of the bilayer upon MPPC partitioning.

With or without MPPC, the release of content from DPPC-based liposomes is controlled solely by melting point of the lipid. To overcome this restriction thermosensitive polymers have been demonstrated as an alternative.[99g,h,i] The advantage of these thermosensitive polymers is that their solubility can be easily controlled by simply varying their temperature. These polymers are water-soluble below their lower critical solution temperature (LCST) and are water-soluble above it. The change in solubility above this temperature stems from the behaviour of the polymer chains. Extension of the polymer chains allows the polymer to adopt a more hydrated or hydrophilic state, whereas contraction of

the polymer chains via insertion into the lipid bilayer results in destabilization of the lipid bilayer and therefore, heating results in complete content release.[99i]

An alternative method to achieve content release makes use of photosensitive liposomes that are disrupted under laser excitation. Cis-trans isomerism, photo-induced lipid fragmentation, and lipid photopolymerization have all been used to prepare photosensitve liposomes.[99j] Typically these methods rely on visible or ultraviolet light as the trigger. Although several studies using this approach have been demonstrated, the major disadvantages remain selectivity, the requirement of significant area for exposure, and the need for stable liposome formulations. One drug currently in clinical use named Visudyne^{R} consists of a photosensitive liposome. Exposure of Visudyne^{R} to light causes triggered release for the treatment of age-related macular degeneration.[99a]

3.1.3. AuNP decorated liposomes.

An alternative way to induce liposome leakage that makes use of a combination of radiation and temperature is hybridization of liposomes with AuNPs. AuNPs are commonly selected as the inorganic nanoparticle component of hard/soft assemblies, which allows for facile optical detection of the latter. In addition, the light absorbed by AuNPs is subsequently dissipated as heat; this makes Au-based nanomaterials promising candidates for use in targeted photothermal cancer therapy. For example, silica-coated Au nanoshells ablate cancerous tumors upon irradiation with near-infrared (NIR) light.[100b,c] The wavelength of light employed in this approach could be easily manipulated by changing the size of the core or the shell. Heat dissipation in such Au-based nanomaterials occurs by excitation at the plasmon resonance leading to photoexcitation of the conduction electrons with concomitant sub-picosecond relaxation by phonon scattering.[100d] This relaxation causes a quick increase in the particle surface temperature, which is then subsequently cooled via energy exchange with its surroundings.

The intimate combination of liposomes and AuNPs into a single hybrid system can therefore not only allow appreciable loading with facile imaging and detection, but also targeted release by employing the heat generated from the AuNPs photothermal effect to melt the liposome storage carriers at specific sites of interest. Prior to discussing content release studies, it is necessary to discuss the three types of liposome-AuNPs complexes that have been studied thus far (see Figure 3.1). The first system contains AuNPs within the inner phase or inside the hollow core of the liposomes.[102p,q] To achieve this, gold sol is first prepared by the addition of chloroauric acid ($HAuCl_4$) in the presence of dilute basic citrate solution with subsequent addition to liposome suspension. This method has been successfully used to study *in*

vivo distribution of liposomes by Hong and coworkers.[102p] However, a major disadvantage of this method in drug delivery applications is the potential degradation of the storage drug in the presence of a reductant. In the second method, the AuNPs are present inside the hydrophobic lipid bilayer membrane.[102d,q] This is achieved by passivating the surface of 3-4 nm AuNPs with a hydrophobic molecule such as stearylamine. Addition of these AuNPs to a chloroform solution of DPPC with subsequent rotary evaporation and hydration with buffer followed by ultrasonication results in the formation of AuNPs embedded within the bilayer.[102q] Since the membrane thickness is about 5 nm, there is a limit to the number of AuNPs that can be incorporated. The last method involves bonding AuNPs to the liposome surface.[102a,i] Controlled content release in each of the three aforementioned liposome-AuNPs assemblies has been studied by Uttri and coworkers In the first system, hydrophobic AuNPs were embedded into the lipid bilayer. In the second system, the negatively charged hydrophilic AuNPs were encapsulated inside the liposome core.[102g] Lastly, AuNP attached to the choline headgroup of the lipid produced liposomes with AuNPs present on both the inner and the outer surface. Upon irradiation with UV light, content release was observed to be greater with any of these systems than in pure liposome systems alone. For example, in the presence of 8.6 μg/mL of AuNPs embedded within the bilayer, 50% content release was achieved in 10 minutes. In the case where 8.6 μg/mL of AuNPs were encapsulated inside the liposome core, the heat generated could not be effectively transferred to the liposomes in order to induce the desired melting, and therefore only 10% content release was achieved in 10 minutes. On the other hand, only 100 pM/mL of AuNPs tethered to the liposome surface resulted in effective heat transfer with greater than 75% content release in 10 minutes. Zasadzinski and coworkers similarly demonstrated the effect of content release as a function of distance between liposomes and hollow gold nanoshells (HGN) upon NIR radiation.[101a] When tethered to liposome surfaces through a PEG thiol lipid, such HGNs demonstrated 93% content release upon irradiation. Although several Au-liposome hybrids have been reported,[101] most of these materials were prepared by exploiting non-specific and irreversible electrostatic interactions.

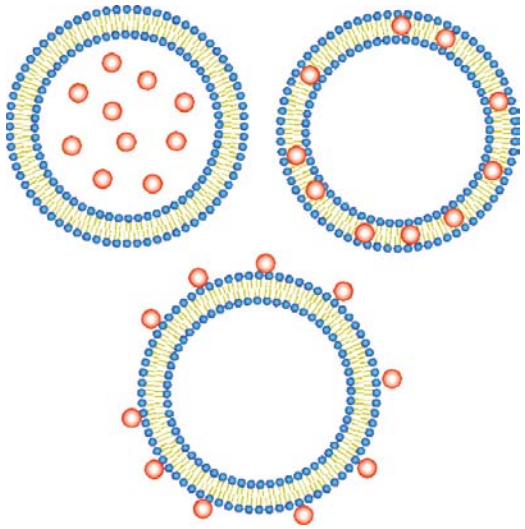

Figure 3.1 Liposome-AuNPs complexes were prepared where AuNPs are (A) encapsulated within the inner core of the liposome, (B) are embedded within the lipid bilayer and (C) are adhered to the liposome surface either via electrostatic interactions or surface functionalization. Figure adapted with permission from ref. (102a). Copyright © Elsevier Inc.

3.1.4. DNA-directed assembly of hybrid nanomaterials.

In the previous chapter, we introduced DNA-directed assembly of AuNPs and studied DNA-directed liposome assemblies. DNA can also be used to link nanoparticles differing in size or composition, which is interesting for both fundamental studies and a myriad of applications. For example, AuNPs of different sizes, 31 nm and 8.0 nm, have been assembled using DNA linkers by Mirkin and coworkers using the same three component system described before.[103a,b] Such three-dimensional (3D) assemblies displayed the same color change from red to purple during formation and sharp melting transition temperatures owing to cooperative melting behavior.[103c] Similarly, AuNP assemblies using 4.5 nm and 7.8/9.6 nm particles were formed via addition of DNA linker, resulting in the formation of two-dimensional (2D) arrays.[103d] By varying the ratio of large to small AuNPs, a variety of assembled structures were obtained. For example, bimodal arrays, hexagonal-close-packed particles, and pseudo-hexagonal lattices were obtained when the ratio of large/small AuNP particles was 0.58, 0.47 and 0.85, respectively. Similarly, Hutter and coworkers demonstrated formation of DNA-directed assemblies using AuNPs with another nanomaterial.[103e] In particular, they formed gold and silver (AgNPs) nanoparticle assemblies by mixing complementary DNA functionalized AuNPs and DNA functionalized AgNPs. The

assemblies could be monitored using UV-visible spectroscopy, since the assembly formation causes a red-shift of the AuNPs absorption wavelength with no significant change in the intensity. Such assemblies also demonstrated cooperative melting behaviour. In another case, 100 nm hexagonal phase mesoporous silica particles were passivated with amino-modified DNA and mixed with 11 nm AuNPs functionalized with non-complementary DNA, at a ratio of 106:1 of silica:AuNPs. Addition of DNA linker resulted in the formation of hybrid nanostructure materials, with TEM studies clearly showing DNA-directed silica and AuNPs assemblies.[103f]

For the purpose of multiplexing, quantum dots (QDs) have also been used. Due to quantum confinement, the QD emission wavelength can be easily changed by simply varying the size of the nanoparticle. Using Mirkin's three component system, Lu and coworkers formed AuNPs-QD 3D assemblies (see Figure 3.2).[103g] The QD surfaces were first modified with a polymer to allow modification with streptavidin, followed by biotin-modified DNA. Addition of linker DNA to a mixture of non-complementary containing DNA-AuNPs and DNA-QD resulted in the formation of 3D aggregates. Lu and coworkers used such assemblies to form an adenosine and cocaine biosensor. This was achieved by including an adenosine aptamer in the DNA linker. In the absence of adenosine, the 3D assemblies quench the QD emission, addition of adenosine induces disassembly, resulting in an increase in QD emission. Using this same methodology, a cocaine sensor was also made. Deng and coworkers similarly assembled 13 nm DNA functionalized AuNPs containing a “sticky end” that is complementary to the sticky end functionalized to 3 nm platinum nanoparticles. By changing the ratio of the particles, they were able to generate 3D assemblies which were studied using TEM.[103h] Such successful assemblies demonstrate that the three component system can be used to assemble a variety of hard and soft nanomaterials.

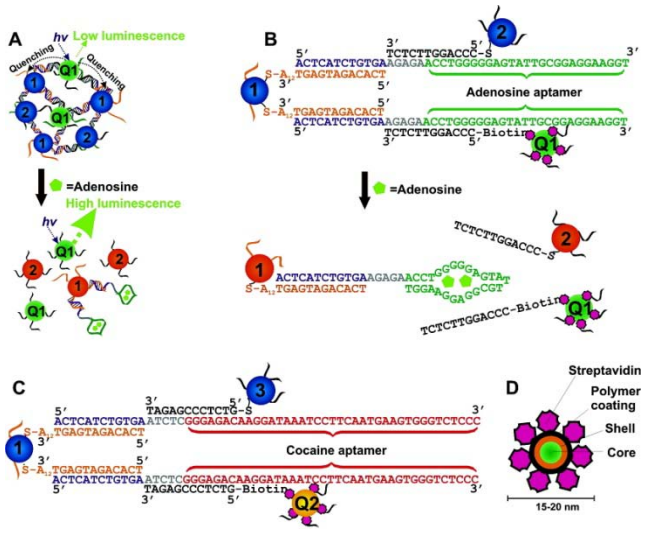

Figure 3.2 DNA-directed assemblies of (A) quantum dots (Q1) with AuNPs disassemble after addition of adenosine accompanying a Q1 emission increase. (B) The DNA sequence used to form quantum dot-liposome assemblies in the absence and presence of adenosine. (C) Similar design sequence used to form a cocaine sensor. (D) Quantum dot passivated with a polymer and modified with streptavidin allows biotin modified DNA to be used to functionalize quantum dot with DNA. Figure adapted with permission from ref (103g). Copyright © American Chemical Society.

In this chapter, the reversible and programmable assembly of DNA-functionalized liposomes and gold nanoparticles (AuNPs) is described. The optical and melting properties of the assemblies are discussed in detail. The utility of such assemblies for use in drug delivery was determined by evaluating AuNPs promoted radiation induced liposome leakage. In addition, contrary to the majority of previous reports, in which AuNPs promoted radiation-induced liposome leakage, we found that using specific linker DNA created a short and finite separation between the AuNPs and liposomes which hindered heat transfer. By tuning this separation, it was therefore possible to either promote or inhibit liposome leakage

3.2 Results and Discussion.

3.2.1 Assembly of DNA-functionalized liposomes and AuNPs.

Our system consists of assemblies of DNA-functionalized liposomes (DOPC:cholesterol:DOPG:MPB-PE, wt/wt = 10:8:1:1) and DNA-functionalized 13 nm AuNPs bound together via linker DNA (Figure 3.3). With regards to the former, DNA conjugation was achieved by

reacting the MPB-PE component of the liposome with thiol-modified DNA (DNA1). Using standard extrusion methods, 103 nm diameter liposomes were functionalized with 365 DNA strands with a coupling efficiency of ~21%. In the case of the 13 nm AuNPs, thiol-modified DNA (DNA2) was covalently functionalized via a gold-thiol linkage by salt-aging. As demonstrated below, the system described herein is different from other Au-liposome hybrids previously reported since they were prepared by non-specific and irreversible electrostatic interactions.[101,102]

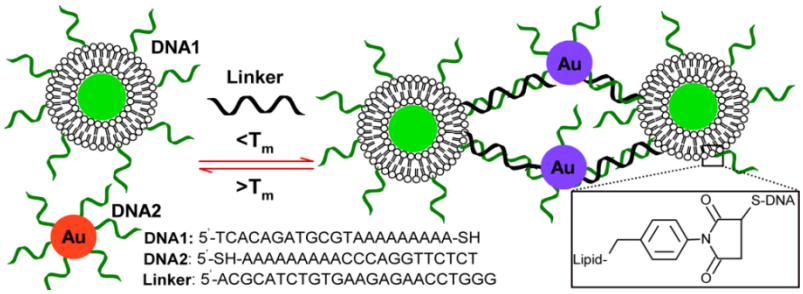

Figure 3.3 Schematic showing the assembly of DNA-directed AuNP-liposome assemblies. The sequences used in this study are also shown.

For optimization, formation of the liposome-AuNP assemblies was monitored using UV-visible spectroscopy. Free AuNPs have a characteristic extinction peak at 520 nm (Figure 3.4A) and appear red in color. Upon liposome-AuNP assembly formation, a gradual red shift of the peak at 520 nm with concomitant increase in the ratio of the assembly absorbance at 650 and 520 ratio was observed. Free AuNPs have close to zero absorption at 650 nm; therefore, even small changes due to the assembly process can be quantified by examining the ratio 650/520. As shown in Figure 3.4B, as the liposome concentration was increased from zero up to a maximum of ~0.2 nM liposome or [AuNP]:[liposome] = 20:1. After this liposome concentration was reached, the ratio decreased, with a concomitant increase in the 520 nm absorbance peak stemming from the dilution of AuNPs in the presence of significant amounts of liposome (Figure 3.5A). No color change from red to purple (Figure 3.5B) was detected in the absence of linker DNA. AuNPs-liposome assemblies were therefore only formed in the presence of linker DNA.

It should be noted that non-specific interactions between liposomes and AuNPs did not facilitate assembly formation. In order to determine the contribution of non-specific interactions, 1% rhodamine

modified lipid was included in the liposome formulation (Figure 3.6A). After incubation of 40:1 AuNPs:liposome in a 300 mM NaCl and 25 mM HEPES solution, pH 7.6, overnight, no aggregation of liposome-AuNPs was observed (Figure 3.6B). Centrifugation at 15,000 rpm for 10 min at room temperature (Figure 3.6C) resulted in precipitation of only AuNPs while liposome remained dispersed in solution. When linker DNA was included, both liposome and AuNPs were pelleted by centrifugation, with little to no free liposome remaining in the supernatant. In order to determine the presence of non-specific binding, the fluorescence of liposome containg 1% rhodamine lipid was determined both in the presence and absence of AuNPs. In both cases, the fluorescence intensities were similar as shown in Figure 3.6D, indicating minimal non-specific binding between AuNPs and liposomes. If non-specific interactions were present, fluorescence quenching originating from energy transfer to the AuNPs would be expected. To effectively determine whether assembly formation would compromise liposome integrity, we encapsulated calcein at a self-quenching concentration (100 mM) before adding the AuNPs and linker DNA. De-stabilization of the liposomes would result in calcein release and an increase in its fluorescence. Calcein leakage remained the same in the absence and presence of AuNPs (Figure 3.11), indicating that the structural integrity of the liposomes was not compromised in the formation of liposome-AuNPs assemblies.

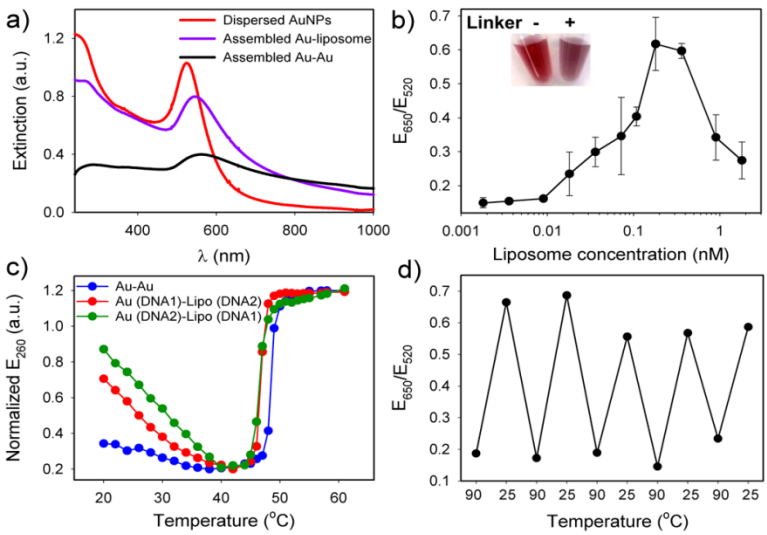

Figure 3.4 (A) UV-visible spectra of dispersed and assembled AuNPs. (B) 650/520 ratio as a function of liposome concentration for quantification of DNA-directed assembly of AuNPs and liposome. Inset shows a photograph of AuNP and liposome in the presence and absence of DNA linker. (C) Melt curves of nanostructures made-up of Au-Au and liposome-AuNP assemblies in 52 mM Na^+. (D) Reversible assembly and melting of liposome-AuNPs by monitoring the ratio of 650/520 by varying temperature from 90°C to 25°C.

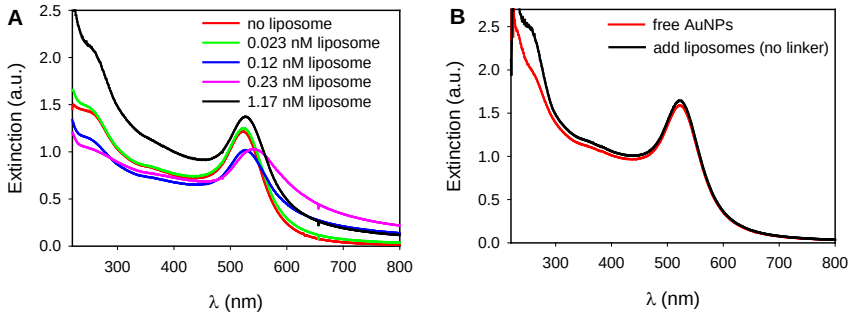

Figure 3.5 (A) Selected UV-vis extinction spectra of AuNPs assembled with varying concentration of liposomes. The plasmon peak initially shifted from ~520 nm (red curve) to longer wavelength. (B) Control experiment showing the UV-vis extinction spectra of DNA2-functionalized AuNPs (~6 nM) in the presence and absence of 0.3 nM DNA1-functionalized liposome. The buffer contained 300 mM NaCl, 25 mM HEPES, pH 7.6.

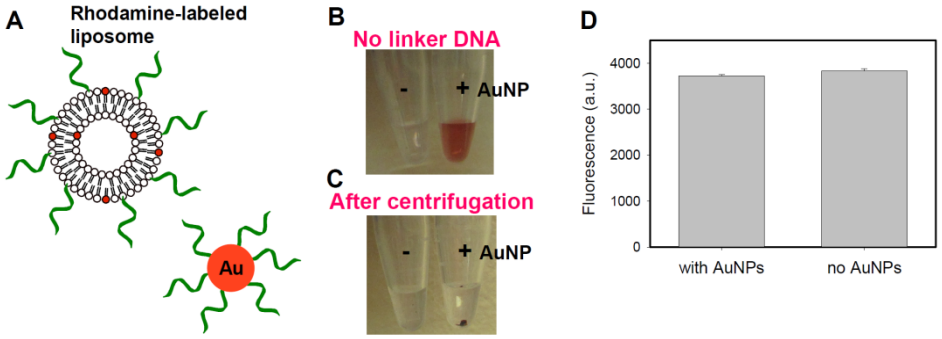

Figure 3.6 (A) Schematic of non-specific binding between DNA-functionalized liposomes and AuNPs in the absence of linker DNA. The liposome contained 1% of rhodamine modified label, which is symbolized as red dots in the bilayer. After incubating the liposomes and AuNPs overnight (B), the samples were centrifuged at 15000 rpm for 10 min resulting in (C) AuNPs precipitating to the bottom of the tube. (D) The supernatant solution fluorescence intensity of the rhodamine modified lipid.

3.2.2 Melting properties of DNA-linked liposomes-AuNP assemblies.

Sharp melting transitions are a characteristic feature of DNA-linked nanostructures.[104,105] The extinction at 260 nm was monitored as a function of temperature to study the melting of our hybrid nanostructures. As shown in Figure 3.4C, a sharp melting transition with T_m = 47°C was obtained for liposome-AuNPs and Au-Au (within 2°C) assemblies using the same DNA linker. Another characteristic feature of these DNA-linked nanostructures is the reversibility of the assembly process by varying the temperature from 90°C to 25°C. The extinction ratio (650/520) changed reversibly (Figure 3.4D) indicating that the functionalized liposomes and AuNPs were stable. In addition, particle-particle and aggregation was indeed achieved via DNA hybridization.

3.2.3 Cryo-TEM studies.

To further characterize the liposome-AuNP assemblies, cryo-TEM studies were conducted. Two vitrified samples were prepared with two different sizes of liposome (Figure 3.7A and B where 103 nm liposome was used and Figure 3.7C where 258 nm liposome was used). The liposome-AuNP assemblies were formed for each liposome size considered, suggestive of the good generality and programmability of

this method. The aggregates were very large (exceeding several micrometers in diameter), suggesting that the AuNPs and liposomes were extensively cross-linked. The AuNPs were not evenly distributed, however; they clustered along the surface contour of the liposome (Figure 3.7C), which is better seen for 258 nm liposomes. In some regions, the liposomes were completely engulfed by AuNPs (Figure 3.7B). In general, the AuNPs were more sparsely distributed in liposome-AuNPs assemblies compared to Au-Au assemblies, which may explain the smaller shift observed in the UV-visible spectrum of the Au-liposome assemblies as shown in Figure 3.4A.

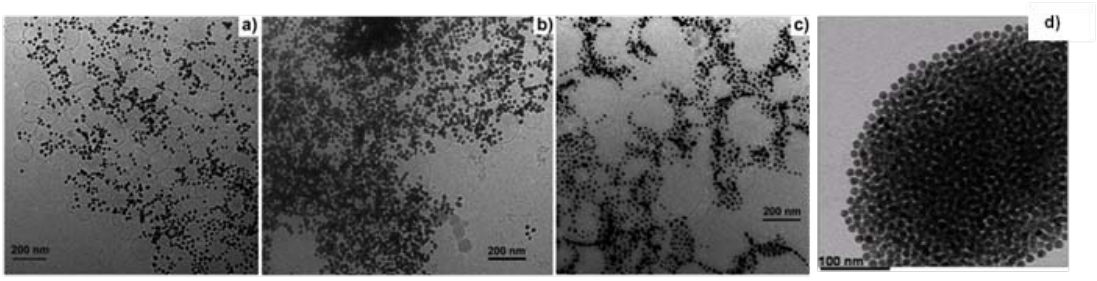

Figure 3.7 Cyro-TEM images of DNA directed DOPC liposome-AuNP assemblies where liposome sizes are for (A) and (B) 103 and for (C) 258 nm. (D) DNA directed Au-Au assemblies.

3.2.4 UV-induced liposome leakage in DNA directed liposome-AuNP assemblies.

The DNA-directed liposome-AuNP assemblies described herein can be used to investigate heat transfer at the nanometer scale. For this study, we chose to use calcein-loaded DPPC liposomes, because DPPC has a phase transition temperature at 41°C. Therefore, significant content release is only expected to occur at 41°C, and very little release should occur at room temperature. To study effective heat transfer as a function of DNA linkage, irradiation using a UV lamp (302 nm) was used. Three samples were considered, two liposome-AuNP assemblies and free DPPC liposomes. The two assemblies differed solely in one important feature, namely, the presence of linker DNA. The first liposome-AuNP assembly (Figure 3.8A) makes use of a linker DNA to create a distance of ~8 nm between the two nanomaterials. In the second liposome-AuNP assembly, the distance between the liposome and AuNPs was decreased from 8 nm by not using a linker DNA but rather by introducing a DNA sequence on the AuNPs that was complementary to the DNA1 on the liposome (Figure 3.8B).

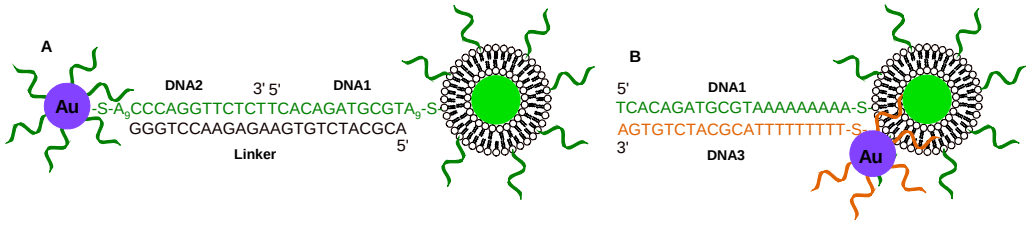

Figure 3.8 The DNA linkages in the two types of AuNP-liposome assemblies. (A) A linker DNA was used resulting in a ~8 nm distance between the AuNPs and liposomes. The underlined sequence belongs to DNA2 on the AuNP. (B) No linker DNA was used allowing the two particles to be positioned very close to each other.

To study the dependency of content release on the distance between liposome and AuNPs in the assembled state, all three samples were loaded into a 96-well PCR plate and exposed to 302 nm UV light. At designated times the fluorescence was read by a real time PCR thermocycler. Finally, the fluorescence corresponding to 100% marker release was measured after breaking the liposomes with Triton X-100. Free DPPC liposomes showed a time-dependent content release, such that ~15% calcein release was observed with an accumulative irradiation time of about 100 min (Figure 3.9D (black dots)). UV-induced liposome damage has been ascribed to pore formation caused by reactive oxygen species (ROS) induced with UV light generated.[106] The role of ROS was tested by adding 10 mM ascorbate sodium salt. This reduced, but did not abolish liposome leakage, as shown in Figure 3.10. Therefore, other factors besides ROS must contribute.

In the case of the 8 nm separated liposome-AuNP system, leakage was inhibited upon UV irradiation (Figure 3.9B and D, gray triangles). The AuNPs provided a protective effect, which could be easily changed by reducing the quantity of AuNPs in the assembled state. This is very interesting, because in majority of the previous work where AuNPs were embedded within the hydrophobic bilayer or directly adsorbed on the bilayer surface via electrostatic interactions, liposome leakage was promoted after irradiation.[102g] A possible explanation is that absorption of UV light by AuNPs in the 8 nm system converted light energy into heat via phonon scattering but because of the 8 nm distance, heat transfer via collisions with water molecules to the liposome surface could not be effectively be achieved. In order to further test whether the 8 nm distance was critical for inhibiting liposome leakage, several control experiments were conducted. We prepared liposome-AuNP assemblies in which the two nanomaterials

were in close proximity, which would allow for more effective heat transfer. For this particular type of assembly, we observed fast calcein release compared to those assemblies containing the ~8 nm DNA linker (Figure 3.9E, open squares). Therefore, the distance between the two nanomaterials was critical for achieving either induction or inhibition of liposome leakage. Next, we tested whether calcein leakage from all three samples only occurred upon UV light exposure. To study this, all three samples were incubated at room temperature in the dark. No significant leakage was observed (Figure 3.9F), suggesting that UV radiation was principally responsible for increased calcein leakage. Finally, to ensure that AuNPs attachment did not perturb the membrane releasing profile, we exposed all three liposome systems to varying temperatures and recorded the amount of calcein release at each temperature. As shown in Figure 3.9G, all three systems showed the same temperature-dependent releasing profile. That is, the fastest releasing was observed at ~40°C, which corresponds to the phase transition temperature of DPPC. This strongly supports that the membrane was not compromised in each system.

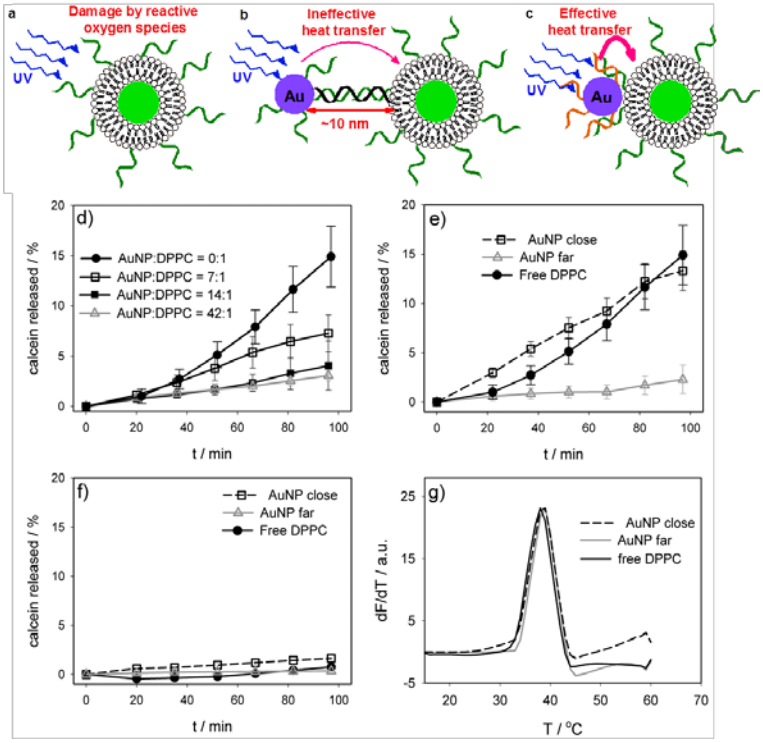

Figure 3.9 Schematic showing content release in the (A) absence and presence of AuNPs assembled, (B) far and (C) close to the liposome surface. Calcein released as a function of irradiation time (D) as the number of AuNPs are assembled far from the liposome surface. (E) Content release of free DPPC, assemblies far and close to the liposome surface. (F) All three assemblies in the absence of UV irradiation and (G) content release as a function of temperature.

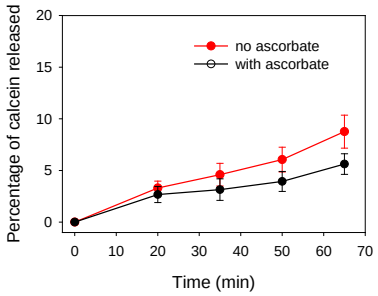

Figure 3.10 Effect of adding ascorbate on the UV radiation induced leakage of DPPC liposome.

3.3 Conclusions.

In summary, we prepared and characterized a new DNA-linked hybrid nanostructure containing both soft and hard nanomaterials. Contrary to previous reports, in which AuNPs always promoted radiation induced liposome leakage, we observed both promotion and protection effects, depending on the distance between the AuNPs and liposomes in the assemblies. This distance was easily manipulated using DNA linkages. This system is indeed promising for triggered drug release applications. For drug delivery however, the size of the aggregates must be significantly reduced and this can be potentially achieved using a reduced AuNP to liposome ratio. Although UV light was herein used for proof-of-concept, near infrared light, which exhibits increased tissue penetrability, can also be employed.

3.4 Methods and materials.

3.4.1 Chemicals.

All of the DNA samples were purchased from Integrated DNA Technologies (Coralville, IA). All the phospholipids were purchased from Avanti Polar Lipids (Alabaster, AL). Cholesterol, $HAuCl_4$, Triton X-100, and chloroform were purchased from VWR. Tris(2-carboxyethyl)phosphine (TCEP) and calcein were purchased from Sigma. NaCl and 4-(2-hydroxyethyl)-1-piperazineethanesulfonate (HEPES) buffer were purchased from Mandel Scientific (Guelph, Ontario, Canada). The lipids used in this study are 1,2-dioleoyl-*sn*-glycero-3-phosphocholine (DOPC), 1,2-dioleoyl-*sn*-glycero-3-phospho-(1′-rac-glycerol) (sodium salt) (DOPG), 1,2-dipalmitoyl-*sn*-glycero-3-phosphocholine (DPPC), 1,2-dipalmitoyl-sn-glycero-3-phosphoethanolamine-N-[4-(p-maleimidophenyl)butyramide] (sodium salt) (MPB-PE), and

1,2-dioleoyl-s*n*-glycero-3-phosphoethanolamine-N-(lissamine rhodamine B sulfonyl) (ammonium salt) (rhodamine modified lipid).

3.4.2 Preparation of liposomes.

Liposomes were prepared as described in chapter 2 section 2.4.2. For the studies highlighted in this chapter, the lipid formulation used was DOPC, cholesterol, DOPG, and MPB-PE at a weight ratio of 10:8:1:1 with a total lipid mass of 2.5 mg. In another lipid formulation, DPPC and MPB-PE were mixed at a ratio of 19:1. To prepare DPPC liposomes, the preparation method prior to extrusion was carried out at temperatures above 50°C. To prepare calcein loaded liposomes, 100 mM disodium calcein in 100 mM HEPES pH 7.6 was used to hydrate the liposomes. The hydrated liposome suspension was extruded through a polycarbonate membrane (pore diameters of 50, 100 and 400 nm) 21 times. Free calcein was removed by passing the samples through a Pd-10 gel filtration column or by centrifugation and removal of the supernatant. These liposomes were then used immediately for DNA conjugation.

3.4.3 DNA conjugation to liposomes and AuNPs.

Procedure is described in chapter 2 section 2.4.3 for details.

3.4.4 Determination of DNA density on liposome surface.

Procedure is described in chapter 2 section 2.4.5 for details.

3.4.5 Determining optimal ratio between AuNPs and liposomes for assembly.

To determine the optimal ratio between AuNPs and liposomes for assembly formation, 4 nM 13 nm diameter AuNPs functionalized with DNA2 was mixed with varying concentrations of DNA1 functionalized liposomes in the presence of 200 nM linker DNA in buffer A (300 mM NaCl, 25 mM HEPES, pH 7.6). The samples were characterized by UV-vis spectroscopy after being heated for 5 min at 50°C and then allowed to cool slowly to room temperature. The data are presented in Figure 3.2B as an extinction ratio between 650 over 520 nm as a function of liposome concentration.

For the study of non-specific binding between DNA-functionalized AuNPs and liposomes in the absence of linker DNA, 1% rhodamine modified lipid was added to the liposome formulation so that the labeled liposomes showed a red fluorescence. The AuNPs and liposomes were incubated overnight at a ratio of 40:1 in buffer A and then centrifuged at 15,000 rpm for 10 min at room temperature. The supernatant fluorescence was then measured (excitation at 540 nm) to quantify the liposome concentration via excitation at 560 nm.

3.4.6 Preparation of liposome-AuNP assemblies.

In a typical reaction, 4 nM DNA-functionalized AuNPs were reacted with 0.2 nM 103 nm DNA-functionalized liposomes in the presence of 200 nM of the linker DNA in buffer A. To prepare liposome-AuNP assemblies, the same mass concentration of liposomes were used. The mixture was incubated at 50°C for 5 min and then allowed to cool slowly to room temperature to form aggregates.

3.4.7 Melting curves.

For melting temperature measurements, the Au-Au or AuNPs-liposome assemblies were washed with and dispersed in a buffer containing 40 mM NaCl, 25 mM HEPES, pH 7.6. The measurements were performed using an Agilent 8453 spectrophotometer with an eight-channel cuvette holder. All of the samples were measured simultaneously and the temperature was controlled using a circulating water bath, as described in full detail in chapter 2 section 2.4.7.

3.4.8 UV radiation induced liposome leakage in DNA-directed liposome-AuNP assemblies.

DNA-functionalized calcein-loaded DPPC liposomes (extruded through 100 nm membrane) were first prepared according to section 3.4.1. To form aggregates with AuNPs, 300 µL of DNA2- or DNA3-functionalized AuNPs (10 nM) were concentrated down to 40 µL in buffer B. To 30, 10, or 5 µL of this AuNP solution, 1.5 µL of 5 mg/mL DPPC-DNA1 and a final of 10 µM of linker DNA were added. This mixture was left at 4^{o}C overnight to allow for aggregation. The formed aggregates were then centrifuged at 4^{o}C at 8000 rpm for 8 min. The supernatant was discarded and the aggregates were washed twice with

100 µL buffer B. Finally the aggregates were dispersed in 40 µL of buffer B. These aggregates and free DPPC (loaded with 100 mM calcein and purified by Pd-10 column) were kept on ice prior to use. For the UV irradiation experiment, 10 µL of the aggregates or free DPPC was added to 100 µL of buffer A. 5 µL of this solution was then added to each well of a 96-well PCR plate. The fluorescence was determined using a real time PCR thermocycler (Bio-Rad, CFX96) in the FAM channel (fluorescence = I_0) at 25°C. The 302 nm UV lamp of a gel documentation system (Alpha Innotech, FluorChem FC2) was used. After each 15-20 min exposure, the plate was read using PCR (fluorescence intensity = I_T). Finally, 1 µL of 5% Triton X-100 was added to each well and the plate read (fluorescence intensity = I_F). The fraction of leakage was calculated to be $(I_T - I_0)/(I_F - I_0)$.

3.4.9 Temperature-dependent calcein release.

10 µL of free calcein loaded DPPC liposomes and DPPC liposome-AuNP hybrids were loaded into a 96-well plate. The plate was sealed with a plastic cover and loaded into a real-time PCR thermocycler (CFX96, Bio-Rad). The fluorescence using the FAM channel was monitored each degree over a temperature range of 15-60°C. The holding time prior to each measurement was 30 sec.

3.4.10 DOPC-calcein leakage.

DOPC loaded with 100 mM calcein was again prepared as described above in Section 3.4.1. DOPC-calcein liposomes were mixed with AuNPs with or without linker DNA in buffer A. The sample with the linker DNA was allowed to form assemblies according to the procedures provided in section 3.4.6. The fluorescence of the samples was measured with a PerkinElmer LS55 fluorometer by exciting at 485 nm at room temperature. Triton X-100 was then added to dissolve the liposomes followed by fluorescence measurement. As shown in Figure 3.11, the fluorescence enhancements after Triton X-100 addition were 10.3 and 13.1-fold for A and B, respectively. Therefore, the difference in leakage in the presence and absence of DNA linker was only ~2%, suggesting that the assembly process did not result in liposome leakage.

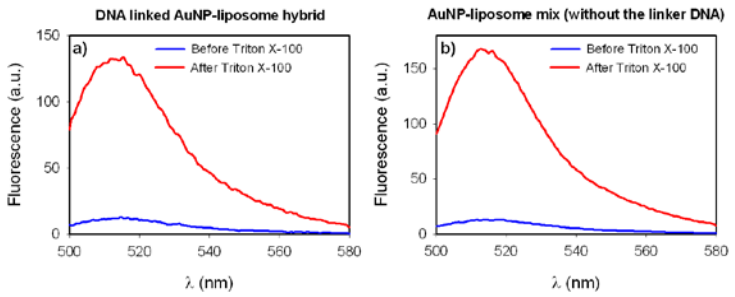

Figure 3.11 Fluorescence spectra of DNA-linked AuNP-liposome aggregates (A) and AuNP-liposome mixture without linker DNA (B) before and after treatment with Triton X-100.

3.4.11 Cryo-TEM studies.

These studies were conducted at the University of Guelph. Please see chapter 2 for a detailed description of these measurements.

3.4.12 Dynamic light scattering.

To estimate the size of the liposomes, dynamic light scattering experiments were performed using a Malvern Zetasizer Nano instrument. The freshly prepared liposomes were dispersed in a buffer containing 100 mM NaCl, 25 mM HEPES, pH 7.6 at a lipid concentration of 0.25 mg/mL. Samples after attaching DNA were also measured. The results were listed in Table 1 below.

Table 3.1 Different sizes of liposomes.

Membrane pore diameter	Hydrodynamic size (nm)
50 nm	102.8
400 nm	258.1

Chapter 4.0
Biomimetic sensing using aptamer-functionalized liposomes.

The results presented in this chapter have been published as part of:

Neeshma Dave and Juewen Liu, "Biomimetic sensing based on chemically induced assembly of a signaling DNA aptamer on a fluid bilayer membrane", Chemical Communications, 48, 3718-3720, 2012.

4.1 Introduction.

4.1.1 Research objective.

Cell membranes are fluid, and therefore membrane proteins are mobile. With some membrane proteins, such as receptors for hormones or ones that trigger endocytosis, lateral mobility is a necessary aspect of biological function. Liposomes have been used as models to study complex functions of cellular membranes such as fusion. Of particular interest has been studying the reorganization and assembly of metal chelating lipids and metal binding proteins in response to stimuli.[106,110,111] While valuable insights have been gained, it is desirable to expand the range of stimuli to other compounds such as small molecule metabolites using aptamers. As will be highlighted below, we use a split aptamer design where the aptamers re-assemble in the presence of specific external stimuli on a liposome or silica surface where surface diffusion is manipulated.

4.1.2 Sensing in the cell membrane.

The cell membrane is composed of a lipid bilayer with associated proteins. In addition to serving as a barrier that encapsulates cellular content, the bilayer, owing to an inherent fluidity, allows cell membrane proteins to reorganize and assemble in response to stimuli for complex functions such as cellular signaling and endocytosis.[106] Using such a dynamic mechanism, numerous proteins and small molecules can be detected by the cell. The detection is also reversible for some receptors as assembled receptors can disassemble at reduced stimulus concentration or after cellular uptake. It has also become clear in the past two decades that lipid composition is also important for the function of membrane proteins where lipid raft formation and phase separation are crucial for cell signaling.[107,108] Owing to the complexity of the membrane studying their assembly remains a major challenge. Liposomes have been

employed as a simplified model to study membrane mechanisms. For example, a lipid probe was prepared to contain a pyrene in the hydrophobic tail, which can act as a reporter for lateral reorganization of the lipid within the membrane by ligand binding to the Cu(II)-iminodiacetate modified head group.[110] In the presence of a poly-histidine peptide, which forms a ternary coordination complex with the Cu(II)-iminodiacetate modified head group, induces aggregation, resulting in the formation of pyrene excimers within the bilayer. The formation of such domains can be monitored by imaging the excimer fluorescence emission, which is different from the isolated pyrene monomer. While valuable insights have been gained, such as stimuli responsiveness lipid re-organization a mode by which viruses enters a live cell, it is desirable to expand the range of stimuli to other compounds such as small molecule metabolites using aptamers.

4.1.3 Aptamer based biosensors.

4.1.3.1 Aptamer-based fluorescent biosensor design.

Aptamers are nucleic acid based binding molecules that can be selected to bind to essentially any target of choice, ranging from small molecules to proteins to cells and viruses.[115a,116] The highly specific target-binding properties of the anti-theophylline aptamer, for example, allow it to discriminate against caffeine due to the presence of a single additional methyl group in the latter.[116] One of the most studied aptamers is the adenosine aptamer, first selected by Huizenga and Szostak, with a reported dissociation constant (K_d) of 6 μM.[115b] The relatively low (micromolar) affinity is typical of aptamers for small molecules; this is due to the low number of interactions between the aptamer and its target. With protein targets, binding affinities in the picomolar to nanomolar range have been reported, in keeping with a larger number of interactions between aptamer and target.[116] NMR studies on the adenosine aptamer demonstrated that it forms a non-canonical guanine-adenosine (G-A) base pair resulting from two target molecules intercalated at separate sites within the aptamer. A similar conclusion was reached by Sassanfar and Szostak, who previously had selected an RNA aptamer for adenosine triphosphate.[115c] Figure 4.1 shows the conformation change induced by binding of DNA and RNA aptamers. Both aptamers can bind the target molecules adenosine triphosphate (ATP), adenosine monophosphate (AMP), and adenosine since binding occurs via the base not the sugar or phosphate groups.

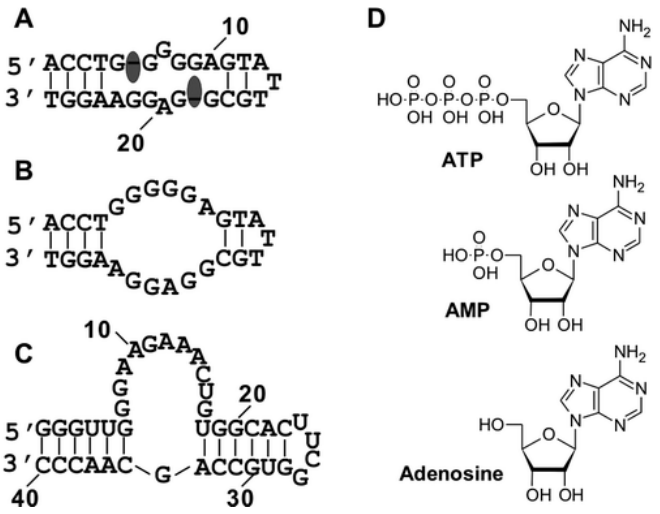

Figure 4.1 Schematic of (A) DNA aptamer with two ATP molecules and (B) drawn in the absence of the target. (C) RNA aptamer for ATP. (D) Molecular structures of ATP, AMP and adenosine. Figure adapted with permission from ref (115a). Copyright © American Chemical Society.

The modification of the selected aptamer with a variety of functional groups or fluorophores without changing their binding properties has allowed for their use as biosensors.[113] In conjunction with a conformational change induced by target binding, numerous fluorescent, colorimetric, and electrochemical sensors have been developed. Of particular interest for our study is the use of fluorophores, which can be attached to the aptamer by covalent functionalization as opposed to electrostatic, hydrophobic, and other non-covalent interactions.[115a] Fluorophores can be selected depending on their extinction coefficients, excitation/emission wavelengths, quantum yields, lifetimes, and anisotropies, for an effective sensor design. In addition, the placement of a fluorophore at a particular site on the aptamer is critical if conformational change is to induce a strong signal change. Addition of a fluorophore closer to the binding site is therefore usually preferred. For our interest, the focus is on fluorescence-based sensors. Three approaches have thus far been used for sensor design; i.e., the molecular beacon (classical), the non-molecular beacon (non-classical), and the split aptamer approach. In the molecular beacon approach, the unbound aptamer adopts a molecular beacon structure containing a loop and hairpin. The two ends of the molecule, which are labeled with a fluorophore and a quencher, respectively, are thereby placed in close vicinity. Target binding results in the formation of a loop and

hairpin structure resulting in fluorophore quenching (see Figure 4.2A) where aptamer beacon binds to a single-stranded binding protein (SSB) opens the aptamer beacon bringing the donor and quencher fluorophores in close proximity.[115e] For example, Stanton and coworkers designed a thrombin aptamer where one end was extended by 4 to 6 base pairs to form a hairpin structure (see Figure 4.2B).[115d] In the absence of the target molecule, donor fluorescence is quenched after addition of thrombin, an enzyme necessary for blood-clotting, the fluorescence increased, that is, by 2.5-fold (fluorescence increases to 100 arbitary units upon addition of target molecule). In this system, five base pairs in the stem of the beacon were included and a lower detection limit of 10 nM thrombin was detected. In the non-classical approach, the aptamers adopt a random coil structure in the absence of target and form a stable complex in the presence of target. For example, Urata and coworkers made many adenosine-based aptamer sensors, which carried fluorophore and quencher attached to each end. With such sensors, the fluorescence intensity decreased upon ligand binding; a quenching efficiency greater than 67%, and a lower detection limit of 5 μM of ligand were observed.[115e] Several examples of non-classical aptamer beacon designs have been studied for a variety of targets such as cocaine,[115f,g] PDGB[115h] (biomarker protein, platelet-derived growth factor) and potassium ions[115i] (see Figure 4.3).

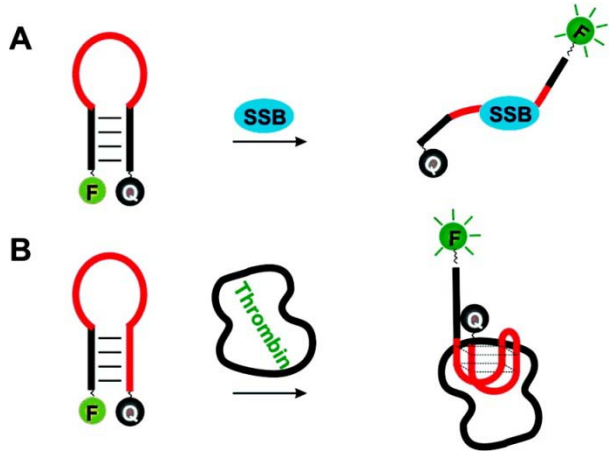

Figure 4.2 Examples of classical aptamer beacon design. These examples contain an extension (black) required for stem formation of the hairpin structure. Aptamer beacon conformational change upon binding where the target is (A) single-stranded DNA binding protein (SSB) and (B) thrombin. Figure adapted with permission from ref (115a). Copyright © American Chemical Society.

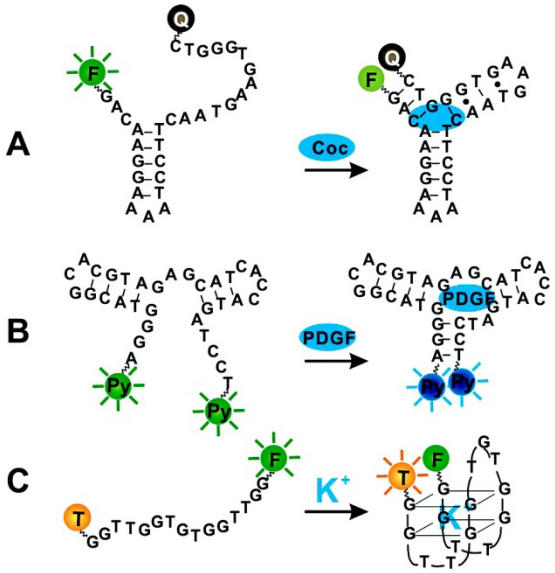

Figure 4.3 Examples of non-classical aptamer beacon design. Aptamer beacon labeled with (A) a fluorophore on one end and a quencher on the other end for target binding. Binding causes quenching of fluorophore fluorescence. (B) Aptamer beacon is labeled with two pyrenes (Py) for biomarker protein PDGF where binding results in the formation of pyrene excimer and therefore a shift in the emission wavelength. (C) Aptamer beacon for potassium ion (K^+) labeled with two fluorophores F (FAM) and T (TMARA). Figure adapted with permission from ref (115a). Copyright © American Chemical Society.

4.1.3.2 Split aptamer-based sensors.

Of particular interest to us is the split aptamer approach. Here, the aptamer is severed into two parts, one of which is labeled with a fluorophore, and the other with a quencher. Target binding causes the fragments to associate, resulting in quenching of the fluorescence emission. Stojanovic and coworkers applied this approach to the anticocaine aptamer, which afforded a novel cocaine sensor with a lower detection limit of 1 µM. In their design, no hairpin was present. Fluorescence was quenched by approximately 40% upon addition of cocaine.[128] The unperturbed aptamer had a K_d of 5 µM which increased to 200 µM when divided in half, indicating that the split aptamer affects the binding affinity; therefore, not all aptamers can be used in this way. A detection limit of 10 µM ATP and 40% quenching upon target binding was achieved by the same authors using a split ATP aptamer. Such split aptamer design shows that aptamers can re-assemble in the presence of specific external stimuli; however, to our knowledge, this split aptamer design has not been studied in sensors associated with lipid membranes.

Toward this end, we herein describe the attachment of an adenosine aptamer to a liposome as a simplified model system by which membrane attachment will affect the behavior of the aptamer and its ability to sense is investigated. The original aptamer was split into two halves, which can assemble into the full aptamer in the presence of adenosine on the lipid bilayer. However, as we highlight below, no assembly was detected when the aptamer was immobilized on a silica nanoparticle, where surface diffusion was completely inhibited. This work highlights the rapid stimulus-responsiveness of membrane-associated split aptamers, which stems from the capability of aptamer lateral diffusion in the liposome membrane. In this chapter, the preparation and characterization of split aptamer-functionalized liposomes are discussed in detail. For comparison, the same DNA aptamer was also immobilized on silica nanoparticles where the lateral mobility was eliminated.

4.2 Results and Discussion.

4.2.1 System Design and Preparation.

The system considered herein consists of adenosine aptamer bound to DOPC liposomes. Using the liposome formulation, 95% DOPC with 5% MPB-PE, we prepared liposomes with an average diameter of 142 nm according to dynamic light scattering by standard extrusion methods. We chose to use the adenosine aptamer because it is well characterized and widely used as a model for designing biosensors.[115] The splitting of the adenosine aptamer into two halves and its assembly in the presence of adenosine in solution has also been demonstrated.[116-119] In our system, we labeled each aptamer fragment with a thiol group at one end and a fluorophore at the other end. The thiol groups allow for covalent attachment to the liposome. The FAM fluorophore was attached to the 5′-end of one DNA fragment to serve as the FRET donor, and a TMR fluorophore was attached to the 3′-end of the other fragment to serve as the acceptor. After incubating the split aptamers with the liposomes overnight, the non-reacted free DNAs were removed using ultracentrifugation. The schematic provided in Figure 4.4 shows the split adenosine aptamers attached to liposome and silica-based sensors along with their respective responses.

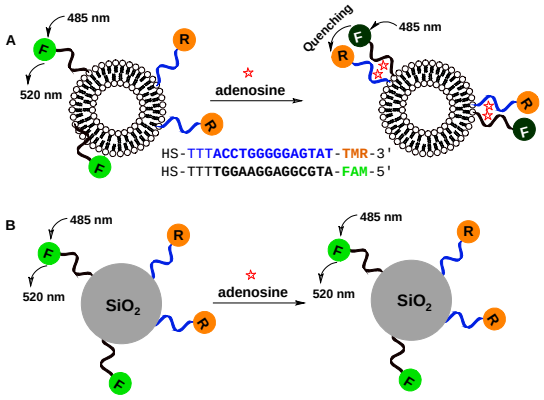

Figure 4.4 (A) Schematic of adenosine induced assembly of split fluorescent aptamers on liposome surface. (B) If immobilized on silica nanoparticles, the aptamers cannot diffuse or assemble in the presence of adenosine. F = FAM; R = TMR.

4.2.2 Optimization of split aptamer density on the liposome membrane.

In FRET-based signaling systems, the amount of signal change can be easily tuned by modulating the donor:acceptor ratio. To achieve the greatest signal change in our liposome system, we only varied the TMR aptamer concentration while keeping both the liposome and FAM aptamer concentrations the same. We considered four ratios. Addition of adenosine resulted in a decrease in the emission intensity at 520 nm upon excitation at 485 nm because both FAM and TMR are closely associated with one another upon aptamer binding (see Figure 4.8A). Therefore, the ratio of 580 nm over 520 nm upon excitation at 485 nm was plotted as a function of adenosine concentration (see Figure 4.5A). Using this ratiometric method allows even small changes to be easily detected with little background variation. Adenosine could be detected for all four ratios as shown in Figure 4.5B. The liposome system performance appears to be better with increasing TMR aptamer concentrations (see Figure 4.5B). However, as the analyte signal increased so too did the background. Therefore, we chose to use a 2:1(TMR:FAM) ratio because an almost optimal signal change was achieved in terms of FAM fluorescence quenching following adenosine addition. Further increase of TMR had a relatively small effect on the sensor performance.

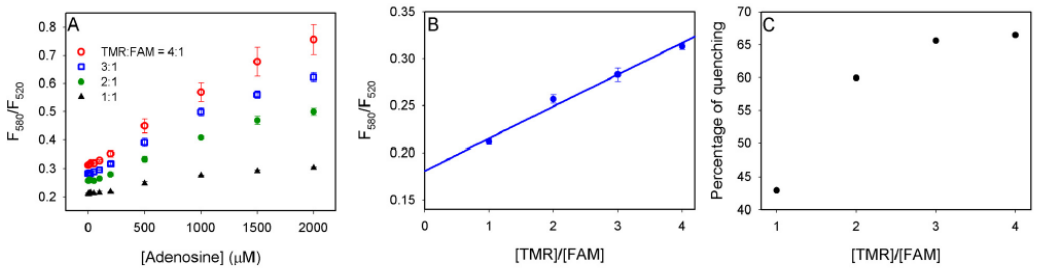

Figure 4.5 Several liposome samples were made with 40 μL of liposome with addition of 4.63 μM FAM-aptamer and different amounts of TMR-aptamer. (A) Detection of adenosine using these liposomes. (B) The initial fluorescence ratio as a function of TMR/FAM ratio shows a linear relationship. (C) Quenching of the FAM emission at 520 nm as a function of TMR/FAM ratio after addition of 2 mM adenosine.

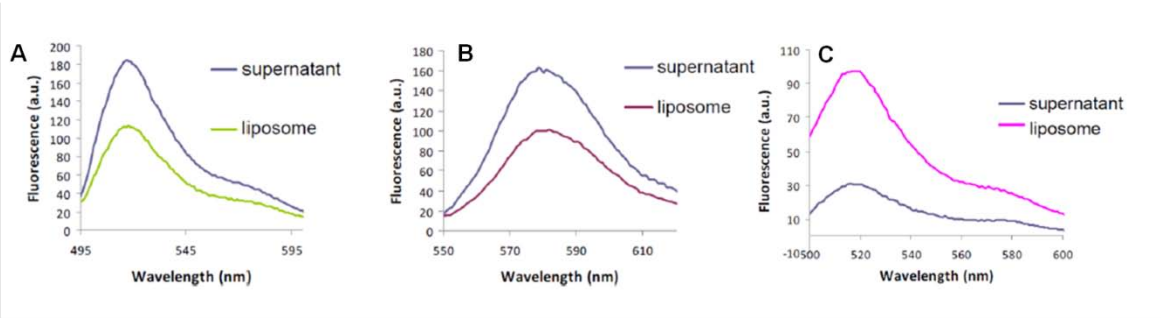

Figure 4.6 Determination of the coupling efficiency of functionalization of FAM and TMR labeled split aptamers. The liposome samples were purified by ultracentrifugation and the supernatant and liposomes were dissolved in the same volume of buffer. (A) corresponds to FAM-aptamer system (excited at 485 nm) and (B) corresponds to the TMR-aptamer system (excited at 540 nm). (C) 10x more liposome was used.

4.2.3 Immobilized split aptamer responsiveness.

To determine whether the response time was affected by immobilizing split aptamers on a liposome surface, a kinetic study was also conducted as shown in Figure 4.7. The emission at 520 nm was monitored as a function of time with sequential addition of adenosine. The spectrum provided in Figure 4.8A shows FAM fluorescence quenching and most notably, a fast response time. The split aptamers therefore quickly assemble on liposome surfaces in the presence of adenosine.

The densities of split aptamer-functionalized (FAM:2TMR) on liposome surfaces were ~60 FAM-labeled DNA and 120 TMR-labeled DNA per liposome. These values were calculated by determining the coupling efficiency as already described above. In the case of FAM, emission at 520 nm was monitored upon excitation at 485 nm. In the case of TMR, the intensity at 580 nm emission was noted following excitation at 540 nm. The supernatant and sample fluorescence spectra were compared (Figure 4.6). We determined the coupling efficiency to be 38% for the FAM-labeled aptamer and 39% for the TMR-labeled aptamer. In the case where ten times more liposome was used with the same amount of FAM and TMR aptamers, the coupling efficiency was ~76% but the surface density is lower.

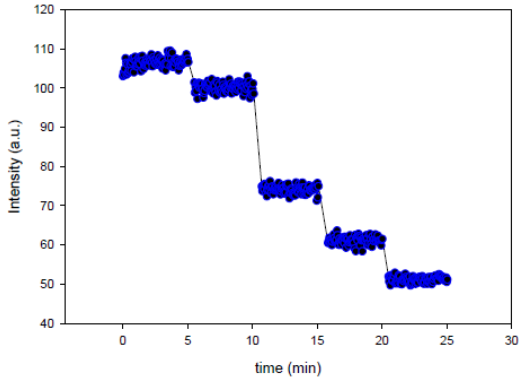

Figure 4.7 Quenching of FAM fluorescence following addition of adenosine as a function of time. Initially, no adenosine was added in the first 5 min. At 5 min 100 μM, 500 μM, 1 mM up to 2 mM of adenosine was added successively, respectively, in buffer A.

4.2.4 Adenosine detection and selectivity.

Upon excitation at 485 nm, strong FAM fluorescence at 520 nm along with a small shoulder at 580 nm from TMR was observed (Figure 4.8A). We calculated the ratio of the fluorescence intensities at 580 nm over 520 nm to be 0.25 (Figure 4.8B). This ratio was only slightly higher than that measured for the free non-immobilized split aptamers in solution (ratio = ~0.22, Figure 4.11A and B), indicating that very little energy transfer was operative because the split aptamers were well separated on the liposome surface. This can be explained by calculating the FRET efficiency. Since the liposome diameter is 140 nm, the calculated surface area is therefore 61544 nm^2. Each aptamer molecule occupies an area of ~341 nm^2. Assuming that the surface immobilized split aptamers are evenly distributed and do not interact

with each other in the absence of adenosine, the distance between each membrane-attached DNA aptamer in our system is therefore ~18.5 nm. Considering that the literature Förster distance (R_0) for the FAM/TMR pair is ~5.5 nm, at such a distance (~3R_0), the FRET efficiency between the two fluorophores should be very low. Therefore, we observe FAM quenching but no increase in TMR intensity upon excitation at 485 nm.

The ratiometric (ratio of 580/520) method was used to analyze the titration curves allowing us to view small changes quite easily. To further verify that the FAM quenching was due to aptamer assembly only, we prepared liposomes functionalized with only the FAM aptamer. Titration with adenosine resulted in a very small FAM fluorescence change (Figure 4.8C) and the ratio remained unchanged (Figure 4.8D). Therefore, the FAM quenching obtained by adding adenosine in Figure 4.8A was due to aptamer assembly, which corresponded directly to an increase in the ratio from 0.25 to 0.45 following 2 mM adenosine addition. To determine the selectivity of our split aptamer-based liposome system, we tested additional ribonucleosides. Figure 4.8C includes the fluorescence spectrum of our system when titrated with cytidine. No change in the FAM fluorescence was observed, which confirms that the use of this particular split aptamer on this particular liposome has high binding specificity. In Figure 4.8D, the fluorescence intensity ratio remained unchanged when the liposome system was titrated with other ribonucleosides.

Titration of the split aptamer-functionalized liposome with adenosine can also be used to determine the dissociation constant (K_d) of the split aptamer. Split adenosine aptamer binds cooperatively to two target molecules therefore a single dissocation constant is sufficient. This was achieved by plotting the fluorescence intensity ratios of 580 nm over 520 nm as a function of adenosine concentration. From the slope of the binding curve shown in Figure 4.8B (red dots), a K_d of 1.65 mM was calculated. Compared to a K_d of ~10 μM for the non-split original aptamer, the calculated constant is significantly larger. These results strongly suggest that by splitting the aptamer, the aptamer binding affinity is affected. The detection limit was 60 μM at three times the standard deviation of the noise (3σ/slope) (Figure 4.8B, inset). The advantage of our system over non-immobolized split aptamers stems from the confinement of the split aptamers on the liposome surface. If the two free split aptamers were dissolved in the same buffer, no change in the ratio was found (Figure 4.11A, B), which suggests that the two aptamers were too dilute to facilitate binding.

The increase in binding constant by splitting the adenosine aptamer can be explained by using thermodynamics. From a simple thermodynamics argument the adenosine aptamer binds two target molecules, whereas in the case of the split aptamer system binding results in the assembly of two

aptamers and two adenosine molecules. Therefore, the Gibbs free energy (ΔG) is expected to be lower in the case of the split aptamer system due to entropy. In relation to K_d, the Boltzmann equation correlates Gibbs free energy to K_d ($K = \ln(-\Delta G/RT)$), therefore a decrease in ΔG results in an increase in K_d. This is consistent with our findings where the K_d value increased when the adenosine aptamer was split in half.

Sensors based on splitting the adenosine aptamer have been reported previously in several systems, in which high DNA concentrations,[116] enlongated binding arms,[117,1118] or multivalent binding[119] were used to achieve binding. In each of the aforementioned examples, control of the bulk DNA concentration was crucial for the desired binding. In our liposome system, the concentration of aptamer was required only for detection, as in theory, even a single liposome should also work, as long as detection was possible. We reduced the split aptamer functionalized liposome concentration four times and titrated with adenosine and a similar adenosine-dependent binding curve was obtained (Figure 4.8E, F). In this case, we obtained a similar detection limit (70 μM) and K_d (1.6 mM). On the other hand, if the bulk split aptamer concentration was kept the same but ten times more liposome was added, an adverse effect on binding was observed as shown in Figure 4.8B (green squares). The K_d changed to 9 mM, which was six times higher than the system where the split aptamer is more concentrated on the liposome surface. We expected K_d values to remain comparable as the concentration of the split aptamers was varied on the liposome surface. One possible explanation maybe some sort of complexation of the target, adenosine, with the liposome surface. As such, this may explain the changes in K_d but requires further investigation.

To better understand the dynamics of DNA attached on the bilayer membrane, fluorescence lifetime studies were carried on a split aptamer-functionalized liposome in the absence and presence of 2 mM adenosine. Each of these samples showed very similar fluorescence lifetime decays (Figure 4.9A), with no change in their lifetime in the absence or presence of adenosine. Therefore, we attribute this to static-quenching confirming our steady-state results (Figure 4.8A) that little dynamic quenching or FRET occurred. In addition, as a control liposome functionalized with just the FAM split aptamer was also tested. The lifetime was similar to that obtained in the split-aptamer functionalized liposome case.

In the case of FAM split aptamer-functionalized liposome, a lifetime 4.05 ns was measured. The lifetime decreased to 3.85 ns in the case where both split aptamers were present. Little change of the lifetime was observed following addition of 2 mM adenosine. Therefore, the ~40% steady state quenching can only be attributed to static quenching. Similarly, no dynamic quenching was observed for the split aptamer-functionalized liposome made up of ten times more liposome (Figure 4.9B).

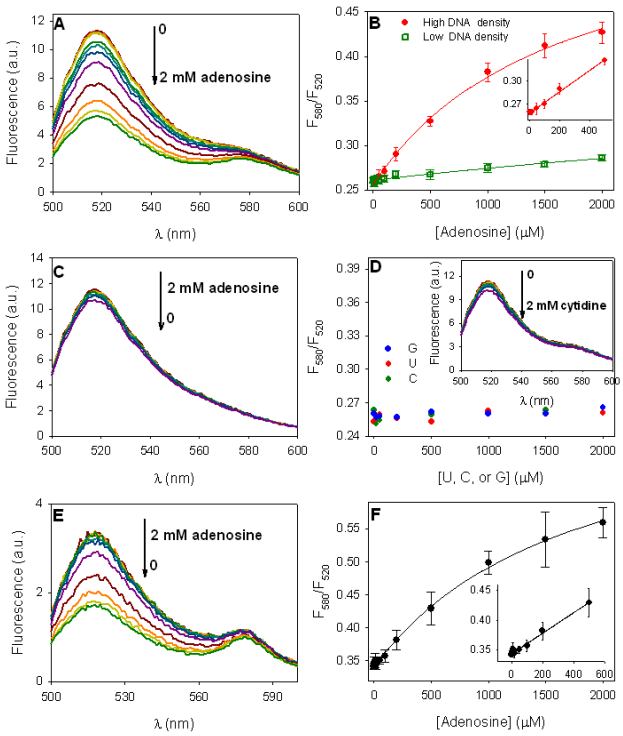

Figure 4.8 (A) Fluorescence spectra and (B) fluorescence ratio of split aptamer-immobilized liposome titration with adenosine. Inset shows the low adenosine region. (C) Fluorescence spectra of only FAM-aptamer labeled liposome titrated with adenosine. (D) Selectivity test with G, U, or C (Guanosine, Uridine and Cytidine). Inset shows fluorescence spectra of cytidine titration. Fluorescence spectra (E) and fluorescence ratio (F) of split aptamer-immobilized liposomes titrated with adenosine at low liposome concentration. Inset shows the low adenosine region.

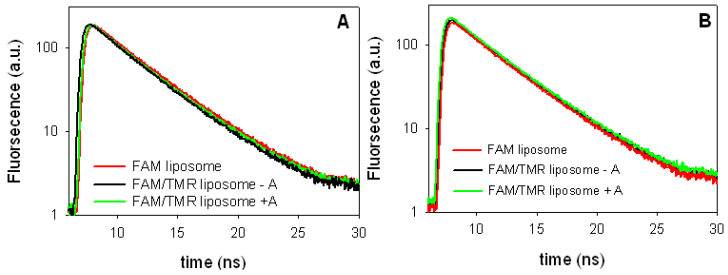

Figure 4.9 Fluorescence lifetime traces of (A) high split aptamer and (B) low split aptamer density functionalized liposomes. Three types of conditions were tested. These include only FAM split aptamer functionalized liposome and FAM and TMR split aptamers functionalized on liposome surface in the absence (-A) and presence (+A) of 2 mM adenosine.

4.2.5 Testing split aptamer assembly on different surfaces.

In order to understand the effect of lipid fluidity, we also studied split aptamer (2TMR:FAM) assembly on 1,2-dipalmitoyl-sn-glycero-3-phosphocholine (DPPC) with 5% MPB-PE liposomes. Recall that DPPC has a phase transition temperature of 41°C, and therefore is in a gel-like state at 25°C. The attached split aptamers to DPPC liposomes showed a similar K_d of 1.55 mM adenosine, although the amount of quenching was reduced compared to DOPC liposomes (Fig. 4.10C and D). The translational diffusion coefficients for DOPC and DPPC different 10^{-3} $\mu m^2/s$ and 1 $\mu m^2/s$, respectively. Irrespective of the differing phase transition temperature, DNA on DPPC remains mobile,[121] which may explain the similar K_d operative in both systems. However, the difference in quenching efficiency needs further investigating.

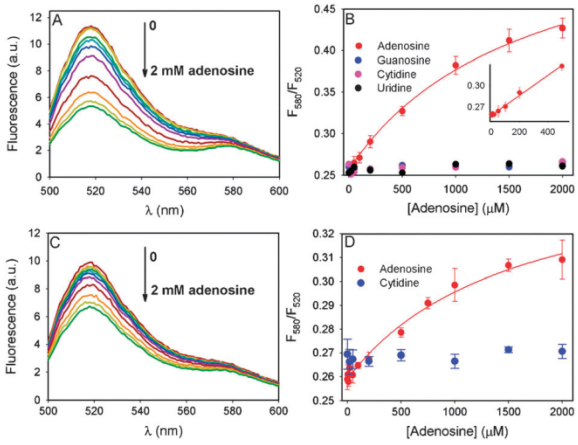

Figure 4.10 Fluorescence spectra for (A) DOPC and (C) DPPC and the fluorescence ratio for (B) DOPC and (D) DPPC split aptamer-functionalized liposome titration with adenosine and other nucleosides. Inset in (B) shows the low adenosine region.

For comparison purposes, we also tested aptamer assembly on 100 nm silica nanoparticles. Prior to assembly, amine terminated particles were treated with a bifunctional crosslinker, purified, and subsequently reacted with thiol-modified split aptamers at the same ratio (2TMR:FAM). As can be observed from Figure 4.11C and D, the split aptamers failed to bind adenosine and little change in the FRET ratio was observed. Such results were attributed to the inability of the anchored aptamers to diffuse

and re-organize themselves in response to the presence of adenosine owing to the static nature of the silica surface. The fluidity of the lipid bilayer membrane therefore facilitates effective molecular recognition.

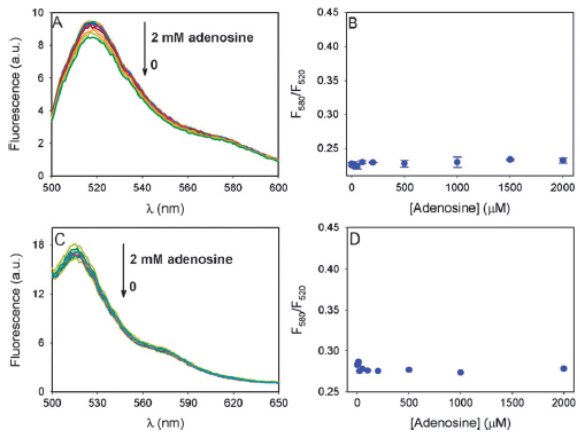

Figure 4.11 Fluorescence spectra (A) and fluorescence ratio (B) of free split aptamers in solution; titration with adenosine. Fluorescence spectra (C) and fluorescence ratio (D) of the split aptamers immobilized on silica nanoparticles titration with adenosine.

4.3 Conclusions.

In summary, we have constructed a liposome-based sensor taking advantage of the fluid nature of the lipid bilayer membrane. With some cell membrane proteins, such as receptors for hormones or ones that trigger endocytosis, lateral mobility is a necessary aspect of biological function. This concept has been utilized by liposome-based materials synthesis, drug delivery, and fusion studies. The membrane itself is also capable of achieving similar goals. Immobilization of DNA aptamer on the liposome surface allows for the construction of an effective biosensor. At the same time, this system can also serve as a model to understand various biophysical features of receptor reorganization and assembly in the cell membrane.

4.4 Methods and materials.

4.4.1 Chemicals.

All of the DNA samples were purchased from Integrated DNA Technologies (Coralville, IA). Phospholipids were purchased from Avanti Polar Lipids (Alabaster, AL). Chloroform was purchased from VWR. Tris(2-carboxyethyl)phosphine (TCEP) and maleimidobutyryloxysulfosuccinimide ester (Sulfo-GMBS) were purchased from Sigma. 100 nm silica nanoparticles modified with NH_2 were purchased from Kisker Biotech GmbH & Co. KG. Sodium chloride, 4-(2-hydroxyethyl)-1-piperazineethanesulfonic acid (HEPES) and adenosine and other nucleosides were purchased from Mandel Scientific (Guelph, Ontario, Canada). Milli-Q water was used for all of the experiments. The names of the phospholipids used in this study are 1,2-dioleoyl-sn-glycero-3-phosphocholine (DOPC), 1,2-dihexadecanoyl-s*n*-glycero-3-phosphocholine (DPPC) and 1,2-dipalmitoyl-sn-glycero-3-phosphoethanolamine-N-[4-(p-maleimidophenyl)butyramide] (sodium salt) (MPB-PE).

4.4.2 Liposome preparation.

The method outlined in chapter 2 section 2.4.2 was used to prepare liposomes. Liposome formulation for this chapter was 95% DOPC or DPPC and 5% MPB-PE.

4.4.3 Split aptamer conjugation to liposome.

Each thiol modified DNA (10 μL, 100 μM) was activated by 1 μL TCEP (10 mM) and 1 μL of acetate buffer (400 mM, pH 5) for 1 hr at room temperature. In a typical reaction, 40 μL of the freshly extruded liposome (5 mg/mL) was mixed with 2.5 μL of activated FAM split aptamer and 5 μL of activated TMR split aptamer and incubated at 4^{o}C overnight. The next day buffer A was added to achieve a final volume of 200 μL and the sample was centrifuged at 120,000 rpm for 4 hrs at 4^{o}C. The pellet was dissolved in 200 μL of buffer A.

4.4.4 Split aptamer conjugation to silica nanoparticles.

3.82 mg of Sulfo-GMBS was dissolved in 1 mL of 5 mM HEPES buffer, pH 7.6 and to this 100 μL of 25 mg/mL of amino-modified silica nanoparticles were added. After 30 min, the sample was washed three times using 5 mM HEPES and dispersed in a final volume of 32.9 μL (silica nanoparticle

concentration = ~100 nM). After incubating with activated split aptamers (similar to the procedure described in section 4.4.3 for split aptamer conjugation on liposome surface) at 4°C overnight, this sample was washed several times to remove free DNA with 5 mM HEPES (8000 rpm for 8 min for each washing). For the fluorescence study, 30 μL of the washed sample was diluted with buffer A to a final volume of 600 μL.

4.4.5 Fluorescence studies.

The steady state fluorescence studies were performed using a Varian Carey Eclipse fluorescence spectrophotometer in a quartz cuvette. 20 μL of the above prepared liposome sample was diluted to a final volume of 600 μL in buffer in the cuvette. The sample was then excited at 485 nm (fluorescein/FAM) and the emission from 500 to 600 nm were recorded. For TMR, excitation at 540 nm and emission at 580 nm was monitored. For kinetic study, the same volume of sample and buffer as described above were prepared and kinetics was monitored for a total time of 10 minutes every ~1.8 sec. The supernatants were also treated in the same manner.

4.4.6 Dynamic light scattering.

1 mL of the freshly extruded liposome sample was dispersed in buffer A (concentration = ~0.2 mg/mL DOPC). The hydrodynamic liposome size was determined to be 142.2 nm using dynamic light scattering (Zetasizer Nano, Malvern). Therefore the physical size of liposome was ~140 nm.

4.4.7 Time-resolved spectroscopy.

Fluorescence lifetime measurements were performed on a PicoQuant FluoTime 100 Compact Fluorescence Lifetime spectrometer. A 460-480 nm P-C-370 diode laser light source (PicoQuant, Berlin, Germany) was used and the lifetime measurements were performed at room temperature. Settings of the Flou Time 100 were 100% transmittance, source intensity 90 and FAM emission was isolated using a 520 ± 10 nm band pass filter (Melles-Griot, Brossard, QC). Experimental decays were numerically fit with two exponentials, with resulting χ^2 values typically below 1.3 using the PicoQuant FluoFit software.

Chapter 5.0
Hydrogel immobilized Hg^{2+} sensor.

The results presented in this chapter have been published as part of:

Neeshma Dave, Michelle Y. Chan, Po-Jung Jimmy Huang, Brendan D. Smith and Juewen Liu, "Regenerable DNA-Functionalized Hydrogels for Ultrasensitive Instrument-Free Mercury(II) Detection and Removal in Water", *Journal of the American Chemical Society*, 132, 12668-12673, 2010 .

Youssef Helwa, Neeshma Dave, Romain Froidevaux, Azadeh Samadi and Juewen Liu, "Aptamer Functionalized Hydrogel Microparticles for Fast Visual Detection of Mercury(II) and Adenosine", *ACS Applied Materials & Interfaces, 4, 2228-2233, 2012*. ***Joint first authorship.***

5.1 Introduction.

5.1.1 Research objective.

Hydrogels are crosslinked networks of hydrophilic polymers that can be used to immobilize biological molecules because approximately 90% of their volume is occupied by water. A number of stimulus-responsive hydrogels have been described in chapter 1. These hydrogels undergo a physical change from gel to sol in the presence of specific external stimuli such as temperature[139a], pH[139b-f], ionic strength[139g-i], and electric field[139j]. As will be highlighted below, we are interested in using hydrogels for immobilization of a thymine-rich DNA or aptamer for simultaneous detection and removal of heavy metal mercury.

5.1.2 DNA-containing hydrogels.

There are three methods by which DNA can be incorporated into a hydrogel. In the first case, a three-dimensional (3D) hydrogel is entirely made-up of DNA. This was demonstrated by Luo and coworkers.[139k,164m] Unlike other bio-inspired hydrogels such as peptide-based, alignate-based and DNA-polyacrylamide hydrogels the crosslinking is achieved via an efficient ligase-mediated reactions. In this case, a branched DNA molecule (BDM) with each arm made-up of a complementary “sticky end” whose sequences are palindromic undergoes hybridization in the presence of ligase-mediated reactions, T4 DNA

ligase, which serves as both a monomer and crosslinker forming three-dimensional hydrogels. Figure 5.1 shows several types of BDM that can be used to generate hydrogels with varying pore sizes. These hydrogels could be easily moulded into desired shapes and sizes. Since the polymerization occurs at physiological conditions, the authors incorporated a variety of materials such as drugs, proteins as well as mammalian cells in the liquid phase therefore eliminating the drug-loading step and potential degradation. Although these responsive gels showed many important properties required for biomedical engineering applications, the fact that the materials of interest were made purely of DNA makes application of this technology expensive.

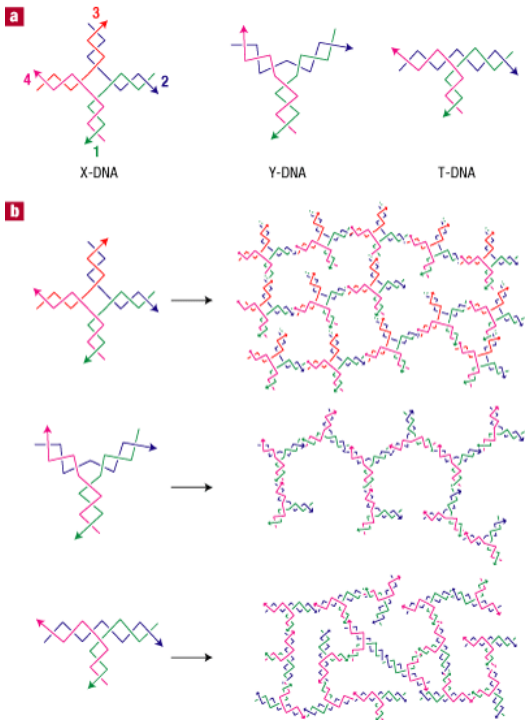

Figure 5.1 Branched DNA sequences that self-assemble in the presence of ligase to form three-dimensional hydrogels. The difference in X, Y and T DNA results in hydrogels with different porosity. Figure adapted with permission from ref (139k). Copyright © Nature Publishing Group.

In the second method, DNA sequences were modified to each monomer and addition of DNA linker resulted in the formation of polyacrylamide gels. Since the crosslinks are held together by DNA base-pairing, their formation is reversible, and the resulting gels are thermally responsive. In 1996, Nagahara and coworkers prepared a block copolymer using *N*,*N*-dimethylacrylamide and *N*-acrylaoloxysuccinimide that was suitable for conjugation purposes.[149,164] Two different DNA sequences were incorporated into the block copolymer, and subsequent addition of DNA linker resulted in the formation of a hydrogel. As shown in Figure 5.2A, reversal from a gel state to a sol state was demonstrated by heating, which induced the DNA double-strands to melt. Stimuli other than temperature can also be used to induce the gel to sol transition. For example, Langrana and coworkers demonstrated a gel to sol transition by the addition of a DNA complementary (cDNA) to the linker DNA (see Figure 5.2B).[139m] The presence of an overhang (red) referred to as a toe-hold, which has higher guanine and cytodine content in the linker DNA allows for binding of cDNA. However, this reaction took several hours for completion attributed to non-specific binding of cDNA with encapsulated quantum dots. Nevertheless, this work was one of the first demonstrations of using stimuli other than temperature to generate responsive gels. To circumvent the slow kinetics associated with using complementary DNA, Simmel and coworkers suggested using aptamers as crosslinkers.[139n] Aptamers have since been utilized in the preparation of stimulus-responsive materials with inorganic nanoparticles ranging from AuNPs,[1o-r] quantum dots[139s] and magnetic nanoparticles.[139t] Tan and coworkers were the first to demonstrate the gel to sol transition using adenosine aptamer-crosslinked hydrogels (see Figure 5.2C).[139u] In the absence of adenosine, the DNA crosslinks the hydrogel, but in the presence of adenosine triggers formation of inter-strand base pairs resulting in a sol state. This is particularly interesting because the diffusion of small metabolites is fast. In order to study the kinetics of the gel to sol transition in aptamer crosslinked hydrogel, the absorbance of AuNPs entrapped within the hydrogel was monitored upon addition of 2 mM adenosine. The AuNPs were quantitatively released within 10 minutes of the adenosine application (see Figure 5.2D and E). Although this method has extended the stimuli from temperature to DNA and small molecules, using DNA-assembled hydrogels still requires the use of mM concentration of DNA to achieve the desired function.

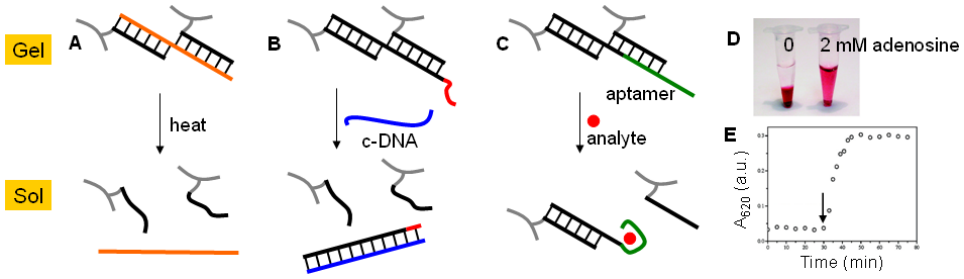

Figure 5.2 Stimuli responsive gel-to-sol transition of DNA-crosslinked hydrogels. The stimuli responsible for the transition is (A) temperature, (B) complementary DNA (c-DNA) and (C) small molecule (aptamer sequence is part of the linker DNA). (D) In order to monitor the kinetics, gold nanoparticles were entrapped inside the hydrogel and adenosine induced the gel-to-sol transition in ~15 min. Figure adapted with permission from ref (164). Copyright © Royal Society of Chemistry.

5.1.3 Hydrogels with DNA as side chains.

There are two ways to covalently incorporate DNA into hydrogels. In the first case, commercially available DNA modified with reactive functional groups (amino, biotin, acrydite, azide, and thiol) was used.[164m] For instance, amino-modified DNA can react with an ester-containing monomer or a polymer resulting in an amide bond (Figure 5.3A). The advantage of this method is that the reaction can take place either before hydrogel formation, which results in uniform DNA distribution within the gel, or after gel formation, which result in DNA functionalization at the hydrogel surface. This method does not require UV irradiation or chemical initiators for DNA incorporation.

In the second method, commercially available 5′-end acrydite-modified DNA is directly incorporated into the gel during formation (Figure 5.3B). Since the reactivity of the acrydite-modified DNA is similar to the free monomers of the hydrogel, this allows for high incorporation efficiency.[164l] Since DNA is not used to control the mechanical properties of the gel, very low DNA concentration can be used. For example, if the goal is to visually observe sensor response, low micromolar concentrations of DNA are sufficient.

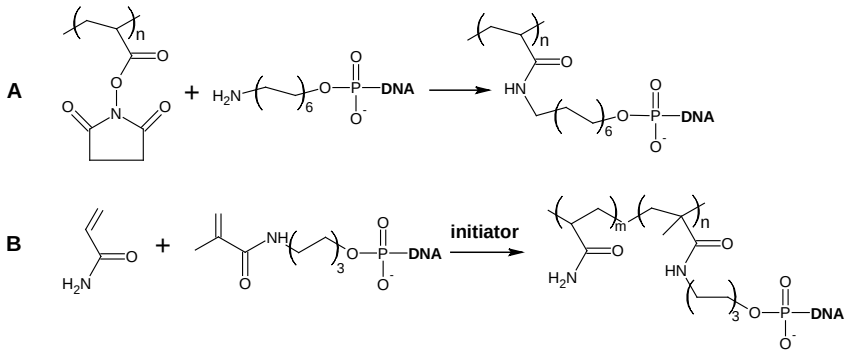

Figure 5.3 Two methods to covalently functionalize DNA in the hydrogel using (A) amino modified DNA and (B) acyrdite modified DNA during hydrogel preparation. Figure adapted with permission from ref (164). Copyright © Royal Society of Chemistry.

5.1.4 Mercury detection.

Mercury is a highly toxic heavy metal that is introduced into the environment both naturally by oceanic and volcanic emissions as well as by human-related activities such as gold mining, combustion of solid waste and fuels.[140b,145a] This environmental pollutant is especially dangerous because of its bio-accumulative properties. Inorganic mercury can be converted into neurotoxic methylmercury by marine bacteria.[140a] The introduction of this neurotoxin into natural water sources and subsequently the food chain has become a major concern, since a significant amount of the population depend on fish as their major food source. Even at low concentrations, mercury can induce severe damage to the nervous system and vital organs, such as kidneys.[140b] In order to tackle Hg^{2+} contamination, detection and removal from our natural water sources has become a paramount concern. For these reasons, new materials that are capable of both detection and removal of Hg^{2+} from environmental sources are being heavily pursued.

To date, the majority of the Hg^{2+} detection and removal tasks have been performed separately. Traditional methods for metal analysis in water rely heavily on analytical instruments, such as atomic absorption and atomic emission spectroscopy. While high sensitivity can be achieved, such instruments are only available in centralized laboratories, making on-site and real-time detection impossible for testing natural water sources in remote areas. In addition, sample pre-treatment, skilled operators as well as high operation costs are all associated with these detection methods.

Many non-immobilized sensors can effectively detect Hg^{2+} using fluorescence or absorbance changes but are unable to effectively remove Hg^{2+} because of poor sensor water solubility, poor binding affinity, and interference with other metal ions.[139,144,145a] A major advancement in Hg^{2+} detection resulted from the discovery that mismatched T-T base pairs selectively bind and are stabilized by Hg^{2+}. DNA chelates the Hg^{2+} therefore stabilizing the T-T mismatch.[145a] According to the X-ray crystal structure of 2:1 complexes of thymine and Hg^{2+}, the metal ion binds with the N3 atoms of the two thymine bases.[145b,c]

Ono and coworkers reported using a thymine-rich DNA, which they referred to as Hg^{2+} aptamer, as shown in Figure 5.4. The aptamer overcame all of the previous limitations of other sensors as it was water soluble as well as stable and selective for Hg^{2+} in the presence of other metal ions.[145a] They modified the thymine-rich DNA with a fluorophore at one end and a quencher at the other end. Addition of Hg^{2+} resulted in the formation of a DNA hairpin that brought the quencher into close proximity to the fluorophore. Using this method, they reported a detection limit of 40 nM, which was later improved to 3.2 nM by Lu and coworkers by modifying the same thymine-rich DNA such that there was a fluorescence increase after mercury addition.[148b] Because the T-T base pair is more stable than the Watson-Crick T-A (thymine-adenine)[145-147] base pair, a large number of fluorescent,[145,148] colorimetric,[149] and electrochemical sensors[150] making use of this pairing have been developed. In some cases, detection limits in the lower nanomolar range have been achieved using the same principle of a thymine-rich DNA sequence, rendering such sensors suitable for Hg^{2+} detection in drinking water, which may not contain more than 10 nM (or 2 parts-per-billion) as per regulation by the U.S. Environmental Protection Agency (EPA). For the removal of mercury and other toxic metals from water, many materials such as porous silica[151], hydrogels[152], magnetic beads and polymers[153] have been developed. These materials have large surface areas, which allow for a large number of functional groups (such as thiols and amides) per volume or weight unit of the material capable of avid Hg^{2+} binding. Simultaneous visual signal generation upon binding however still remains a problem with the aforementioned systems.[154-156] In particular, hydrogels are ideal for immobilization of biomolecules since the majority of their volume consists of water and therefore, incorporated proteins and DNA can maintain their native structure and function within the gel.[157,158] As we highlight below, the combination of Hg^{2+} aptamer and hydrogel should allow for both simultaneous detection and removal of Hg^{2+}.

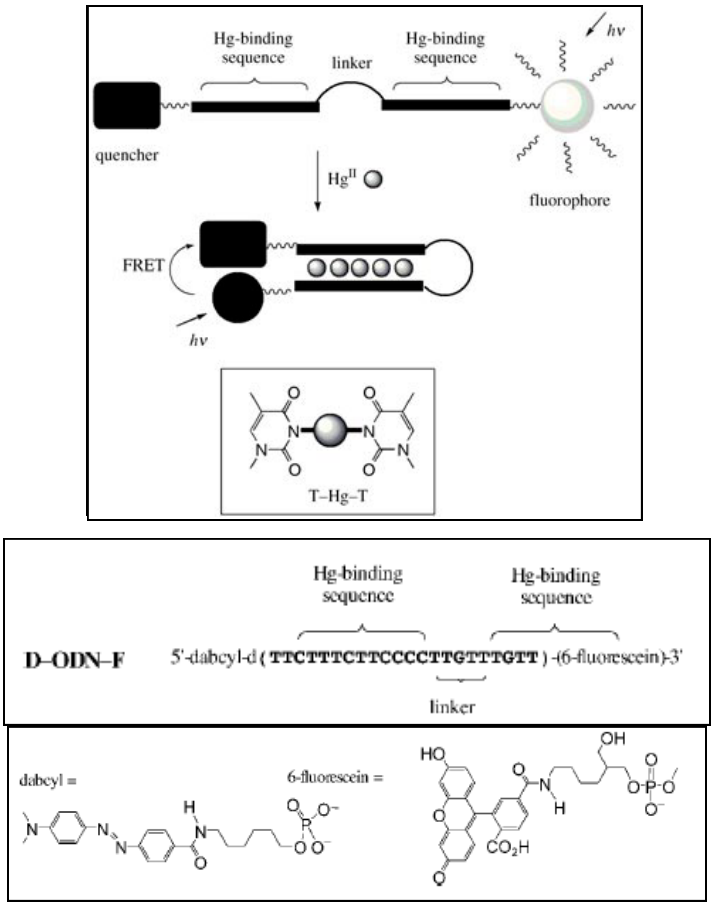

Figure 5.4 Molecular beacon thymine-rich DNA with fluorophore modified at one end and a quencher modified at the other end designed by Ono and coworkers for Hg^{2+} detection. In the presence of Hg^{2+}, the beacon forms a hair-pin structure resulting in quenching of the fluorescence. Figure adapted with permission from ref (167a). Copyright © Wiley Publishing Group.

In this chapter, a description of the preparation, characterization and application of monolith and microparticle of polyacrylamdie hydrogles covalently functionalized with thymine-rich DNA for simultaneous detection and removal of mercury is presented. In particular, we investigate response times, detection limit, and specificity of our aptamer-functionalized hydrogels. A unique property of hydrogel is that it allows for mercury enrichment unlike other soft materials such as liposomes. For example, by simply increasing the sample volume, we were able to visually detect 10 nM Hg^{2+} without performing any signal amplification steps.

5.2 Results and Discussion.

5.2.1 Visual detection in monolithic hydrogels.

A thymine-rich DNA modified with a 5′-acrydite for covalent attachment to a polyacrylamide hydrogel matrix was prepared for Hg^{2+} detection (Figure 5.5A). To monitor the Hg^{2+} binding with fluorescence measurements, a DNA intercalating dye SYBR Green I was used. To optimize the concentration of thymine-rich DNA, fluorescence measurements of the free DNA treated with Hg^{2+} were first conducted. Figure 5.6 includes the fluorescence spectrum of free 15 nM thymine-rich DNA, which adopts a random coil structure (Figure 5.6A, yellow line) in the absence of Hg^{2+}. Upon addition of Hg^{2+}, a hairpin structure is formed and a corresponding ~10-fold fluorescence increase is observed (Figure 5.6A, green line).[148c] The 10-fold fluorescence increase cannot be detected by eye. To prepare a visual fluorescent sensor, a higher concentration of DNA is therefore required. Increasing the concentrations to 1 μM DNA and 6 μM SYBR Green I affords yellow fluorescence in the absence of Hg^{2+} and a bright green fluorescence in the presence of 4 μM Hg^{2+} upon 365 nm UV lamp excitation (inset Figure 5.6B). This distinct yellow to green color change in the presence of Hg^{2+} can be used to make a visual sensor. By increasing the DNA concentration, the background fluorescence was increased. This yellow background can be explained by examining the fluorescence spectra in Figure 5.6B. Therefore, the aforementioned confirms that increased DNA content in the hydrogel system of interest is required to prepare a sensitive fluorescent Hg^{2+} sensor.

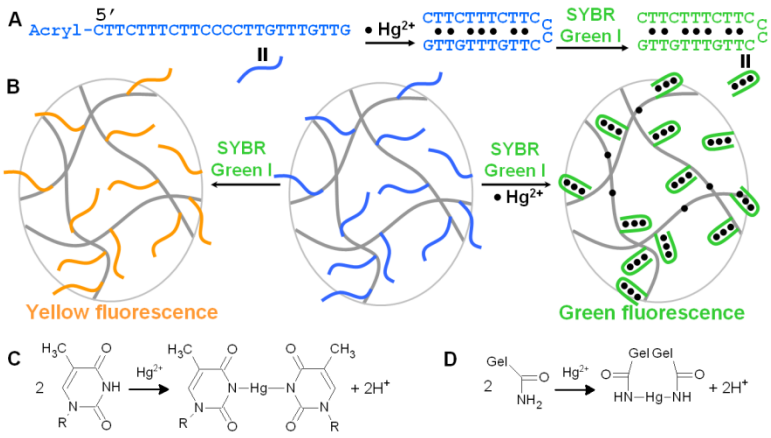

Figure 5.5 (A) The DNA sequence of acrydite modified thymine-rich DNA and fluorescence signal generation for Hg^{2+} detection. The 5′-end is modified with an acrydite group to allow for covalent attachment in the hydrogel. (B) Covalent DNA immobilization within a polyacrylamide hydrogel and interaction of Hg^{2+} and SYBR Green I produces a visual fluorescence signal. Chemical reaction of Hg^{2+} binding with (C) thymine pairs of the immobilized DNA and (D) polyacrylamide in hydrogel. Gel in (D) denotes for the hydrogel matrix.

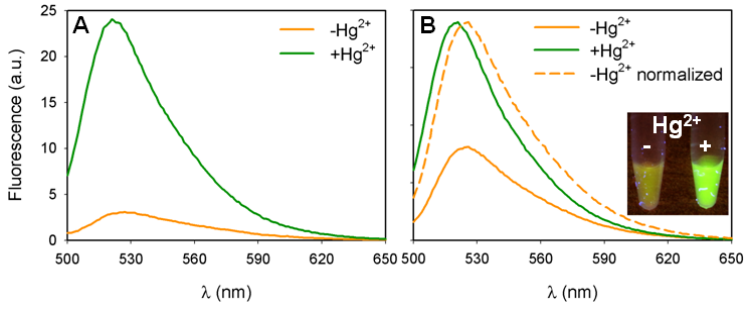

Figure 5.6 Fluorescence spectra of SYBR green I and thymine-rich DNA. (A) Thymine-rich DNA and Hg^{2+} concentration is 15 nM and 90 nM, and in (B) 1 μM and 4 μM, respectively, excitation at 485 nm. The SYBR Green I dye and DNA ratio is 6:1 in both cases. The inset in (B) is a photograph of the same sample conditions excited at 365 nm with a handheld UV lamp. The normalized curve in (B) is obtained by multiplying the yellow curve by a factor so that it has the same peak intensity as the green curve. Buffer A (20 mM $NaNO_3$ and 8 mM Tris-nitrate, pH 8.0) was used for mercury detection.

5.2.2 System design and monolithic hydrogel preparation.

The function of the hydrogel is to both immobilize DNA and capture mercury. For this reason, we selected polyacrylamide hydrogels, since they are non-toxic, cost-effective, stable, and capable of selectively binding Hg^{2+} via their amide functionalities (Figure 5.5D).[152c] The design of the Hg^{2+} binding DNA can bind seven Hg^{2+} ions per DNA resulting in hairpin-like structure. In our study, the DNA serves to only detect the presence of Hg^{2+}. If removal was also performed by the DNA, the cost of such a sensor would be exceedingly high. Using a polyacrylamide hydrogel where the estimated acrylamide concentration exceeds that of DNA by a factor greater than 10,000 allows for a significant amount of Hg^{2+} to be removed at an affordable cost as will be discussed in detail further in the document. Previously, DNA-functionalized hydrogels[159] have been fabricated using DNA as a reversible crosslinker to observe stimuli-responsive sol-gel transitions or gel volume change. While these gels have been used for the detection of target DNA and small metabolites, high DNA concentrations (1 mM) were required to crosslink the gels. In our study, we chose to use bis-acrylamide as the crosslinker at a ratio of 1:29 to acrylamide monomer and the thymine-rich DNA concentration was reduced to 10 μM. Each monolithic gel was prepared from a 75 μL solution containing the free monomers, unattached DNA, and initiator. The gels were purified by repeated soaking in buffer A (20 mM $NaNO_3$ and 8 mM Tris-nitrate, pH 8.0). To determine the amount of DNA incorporated into the hydrogel, the DNA concentration in the soaking solution was measured allowing us to estimate that approximately half of the 10 μM initial acrydite DNA is attached to the gel.

5.2.3 Optimization of hydrogel formulation and detection conditions.

We first optimized the gel formulation by varying gel concentration. High percentage thymine-rich DNA-containing gels (e.g. 10-20%) were very brittle and easily broke during harvesting. If the percentage was too low (e.g. < 3%), the resultant hydrogels were too soft and also difficult to handle. To test the sensor response, we prepared gels of 4, 10, and 20% and soaked each in 1 mL of buffer A containing 1 μM SYBR Green I with 0 or 1 μM Hg^{2+}. An hour later, the gels were excited at 365 nm using a handheld UV lamp. The fluorescence change from yellow to green for all three gel formulations can be easily observed by eye as shown in Figure 5.7A in the absence and presence of Hg^{2+}, consistent with the non-immobilized DNA results described in Figure 5.6. Detection of Hg^{2+} was achieved for all of the gel formulations; however the sensor composed of 4% gel appeared to exhibit more homogenous

fluorescence. In order to determine whether this behavior was attributed to the dye alone interacting strongly with the hydrogel backbone, 4% gels were formed without DNA and incubated with SYBR Green I. The hydrogels (Figure 5.7B) appeared transparent in the presence and absence of Hg^{2+}. This suggests that the yellow fluorescence in Figure 5.7A is due to the interaction between the DNA and the dye alone. For subsequent experiments, we selected 4% gels to achieve a uniform fluorescence and easy handling. To test the importance of covalent thymine-rich DNA attachment in the hydrogel, the same DNA sequence without the acrydite modification was used. Addition of Hg^{2+} and SYBR Green I to this hydrogel system displayed low fluorescence (Figure 5.7C), suggesting that fewer DNA strands remained within the gel upon polymerization. Covalent linkage is therefore critical for detection. Quantitative analysis of the buffer indicated that more than 84% of the DNA was lost in the first washing. To confirm whether the Hg^{2+}-induced fluorescence enhancement was due to selective binding of Hg^{2+} with the thymine bases, a hydrogel covalently functionalized with an acrydite DNA containing cytidines (C-rich DNA) instead of thymines was also tested. As shown in Figure 5.7D, only yellow fluorescence was observed in the presence of varying concentrations of Hg^{2+}, whereas in the case where the original thymine-rich DNA was immobilized, a bright green fluorescence resulted (the tube on the right in Figure 5.7D). This control experiment suggests that Hg^{2+}-induced green fluorescence is due to the specific interaction of Hg^{2+} with thymine bases as illustrated in Figure 5.7A. In order to determine the sensor response time, the kinetics of the fluorescence change upon Hg^{2+} addition were measured. As shown in Figure 5.7E, after 10 min the difference between the samples with and without 1 μM Hg^{2+} can be weakly observed. The intensity increased significantly over the course of 1 h and therefore, this duration of time was chosen as the incubation time for subsequent experiments.

To determine whether diffusion kinetics can be accelerated, we further tried to optimize the gel formulation. In the preparation of 4% hydrogels made with a final volume of 75 or 150 μL, 0.05% bromophenol blue, which has an absorption feature at 590 nm, was added prior to addition of initiator. The gels were soaked in 1 mL of buffer A and the gradual leakage of dye as a function of time was monitored using a NanoDrop 1000 spectrometer. The kinetics results are plotted in Figure 5.8A and B. For the 75 μL gels, a rate of 4.7 hr^{-1} was obtained by fitting the data to the equation $y = y_0 + a(1 - e^{-bt})$, where b is the rate and t is time. For the 150 μL gels, a rate of 0.57 hr^{-1} was obtained. Therefore, the diffusion rate increased ~8-fold by reducing the gel volume to half. For the 75 μL gels, equilibrium was reached in ~1 h. Because enhanced diffusion is observed with smaller volume particles, we prepared smaller gels with a volume of 12 μL (Figure 5.8D). However, these gels were extremely difficult to handle owing to their reduced size and the fluorescence after SYBR Green I addition appeared weaker

than in the 75 µL gels. Therefore, a volume of 75 µL for the preparation of the monolithic hydrogels proved to be optimum. We next studied the effect of gel percentage on the release kinetics of bromophenol blue. Interestingly, the release kinetics or dye release rates did not vary significantly as the gel percentage was varied from 3% to 12% (Figure 5.8C). For these reasons along with the difficulty in handling some gels, 4% gels made with a 75 µL final volume and incubation times of 1 hour were used for this study.

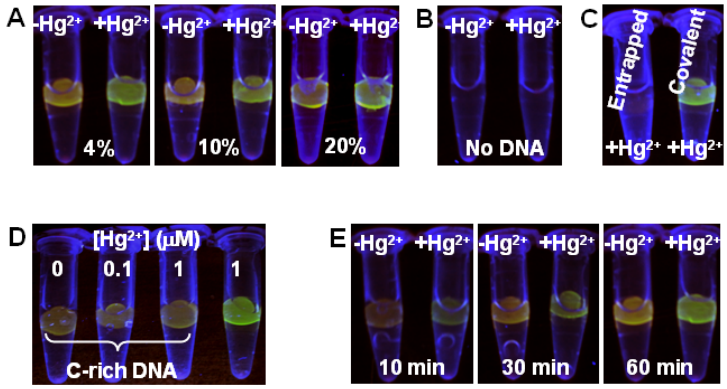

Figure 5.7 (A) Hg^{2+} detection as a function of gel percentage; (B) gels containing no immobilized DNA; and (C) gels prepared with Hg-DNA (no acrydite modification) showed a low fluorescence with addition of 0 or 1 µM Hg^{2+}, respectively. (D) Hydrogels functionalized with the cythidine-rich DNA showed only yellow fluorescence in the presence of varying concentrations of Hg^{2+}. The gel on the right is functionalized with thymine-rich DNA. (E) Gel fluorescence change as a function of time. All of the experiments were performed in buffer A (20 mM $NaNO_3$, 8 mM Tris nitrate, pH 8.0). SYBR Green I dye was added to all of the gels.

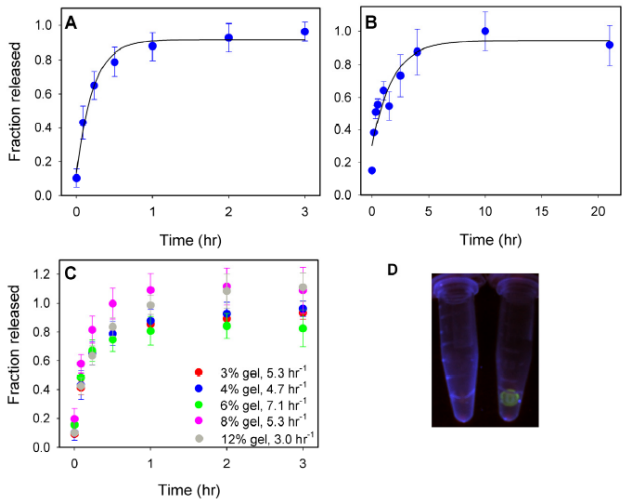

Figure 5.8 The effect of gel volume on the diffusion kinetics was studied using bromophenol blue as a model compound where the hydrogel was made with a final volume of (A) 75 µL and (B) 150 µL. (C) The effect of gel percentage on the diffusion kinetics with 75 µL gels where the respective rate of dye release are displayed in the legend. For all of the data in (A) to (C) each data point was run in triplicates. (D) A photo of 12µL gels prepared with no acrydite containing thymine-rich DNA (left) and thymine-rich DNA (right) after reacting with 1 µM Hg^{2+} and SYBR Green I dye.

5.2.4 Mercury detection sensitivity and selectivity.

The lowest Hg^{2+} concentration detectable by eye was ~200 nM Hg^{2+}, as shown in Figure 5.9A. On the other hand, by using a gel documentation system for quantitative analysis where the gels were excited at 365 nm and the emission was collected using a CCD camera bearing a green filter (Figure 5.9B) a detection limit of 75 nM at 3σ/slope could be achieved. The plot of fluorescence intensity versus Hg^{2+} concentration shows an increase in emission intensity up to ~1µM Hg^{2+} (Figure 5.9C). The overall intensity increase was relatively small. This is because of the high DNA concentration (~5 µM) attached to the gel giving it an intense yellow background fluorescence (Figure 5.6B). The sensitivity can be further improved by simply increasing the sample volume from 1 mL to 50 mL. As shown in Figure 5.9D, the detection limit was lowered to 10 nM Hg^{2+} (i.e., the toxic level in drinking water) where a visible green fluorescence was observed. At 30 nM Hg^{2+} high intensity green fluorescence was evident. In comparison to the previously reported Hg^{2+} sensors where no analytical instruments or signal amplification methods were used, the achieved sensitivity is among the highest reported thus far.[149] The selectivity was also tested by incubating the gels with various metal ions. Only Hg^{2+} produced a green

fluorescence (Figure 5.9E) and therefore, the selectivity of the DNA-based sensor is still maintained within the hydrogel matrix.

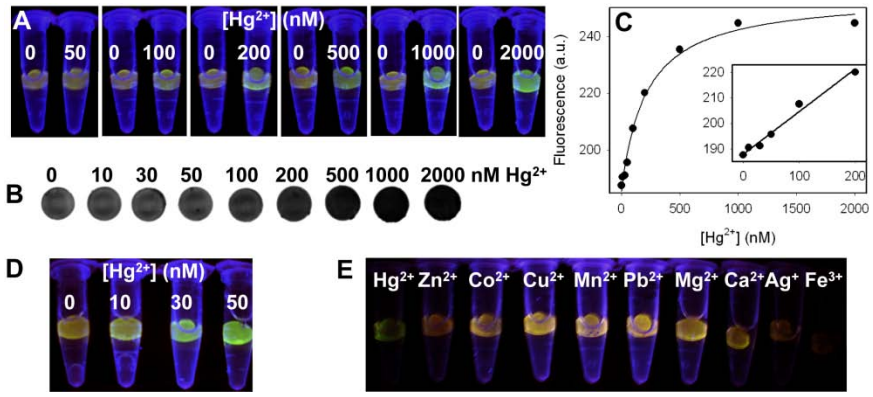

Figure 5.9 Sensor sensitivity detected using a (A) digital camera and (B) a fluorescence gel documentation system and (C) its quantification. (D) The gel sensitivity using 50 mL samples (previously in 1 mL). (E) Selectivity test with 1□M of various metal ions in 1 mL samples. All of the samples were tested in buffer A.

5.2.5 Mercury removal.

The unique volume-dependent sensitivity of our sensor as demonstrated above clearly confirms that the gel can actively adsorb and remove Hg^{2+} from water. To better understand this behavior, we studied the kinetics of Hg^{2+} removal. The Hg^{2+} concentration in the supernatant was monitored as a function of time after exposure to hydrogel. Starting with 1 μM Hg^{2+}, the concentration decreased to ~30 nM in 6 hrs with a rate of ~1 hr^{-1} (Figure 5.10A, red line), corresponding to a less than 30-fold decrease in Hg^{2+} concentration. In the absence of the immobilized DNA, the kinetics of Hg^{2+} removal was similar (black line). Therefore the polyacrylamide hydrogel predominately binds to Hg^{2+} through its amide nitrogen (Figure 5.5D).[149c] Because the monomer concentration is ~500 mM and immobilized DNA is about 0.05 mM, this concentration difference may explain why DNA did not significantly increase the kinetics of Hg^{2+} removal in our system. Due to this concentration difference the gel by itself can detect down to 10 nM Hg^{2+}. However we would not be able to see the 10 nM Hg^{2+} in the absence of thymine-rich DNA and SYBR Green dye. Therefore, the acrylamide gel matrix has a high Hg^{2+} adsorption

capacity while the DNA has a much higher Hg^{2+} binding affinity. Such a sensor simultaneously offers high sensitivity for detection and high capacity Hg^{2+} removal at an effective cost.

5.2.6 Detection and removal of Hg^{2+} from Lake Ontario water.

To evaluate the practicality of the fabricated sensor, removal of Hg^{2+} from an environmental sample was attempted. Water samples from Lake Ontario were tested, in particular. These samples do not contain Hg^{2+} as determined by ICP-MS analysis. Therefore Hg^{2+} was deliberately added to simulate contaminated natural water sources. We tested this since Lake Ontario water contains additional salts that could potentially affect mercury detection. Both DNA-functionalized hydrogel and pure hydrogel were soaked in 15 mL of the water sample with no additional salt or buffer. After soaking (gel treatment), the supernatant was collected, acidified and analyzed using ICP-MS for quantification of mercury. As shown in Figure 5.10B, the Hg^{2+} concentration decreased from 620 nM to 210 nM following gel treatment. The gels were thus capable of Hg^{2+} removal from natural water sources. Interestingly, the amount of Hg^{2+} removed exceeds the amount of Hg^{2+} that the DNA itself can bind. Therefore, at least half of the Hg^{2+} was adsorbed by the gel matrix, confirming that the Hg^{2+} removal is not limited by the DNA concentration.

We next studied whether visual detection was possible using contaminated Lake Ontario water samples. We soaked monolithic DNA attached hydrogels in 1 mL water samples with 1 μM SYBR green I and varying concentrations of Hg^{2+}. After 1 hr, the gels were imaged. As shown in Figure 5.10C, a weak green fluorescence was observed for 50 nM Hg^{2+} and an intense green fluorescence was observed for 200 nM Hg^{2+}. Although, this detection limit is slightly lower in comparison to the limit obtained in buffer A where 50 nM Hg^{2+} was quite easily detected under the same conditions (Figure 5.10D), the presence of Cl^- and SO_4^{2-} anions in the lake water compete with hydrogel for Hg^{2+}.[160] Therefore, decreased fluorescence intensity is expected. Nevertheless, detection was achieved using an environmental source.

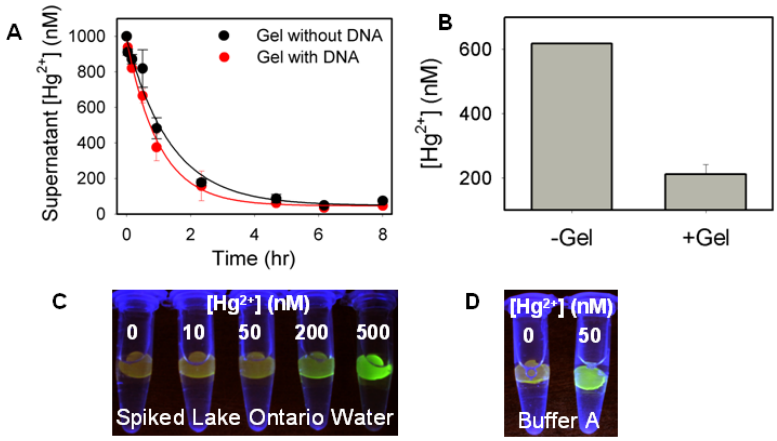

Figure 5.10 (A) The kinetics of Hg^{2+} removal in buffer A after gel treatment. (B) Mercury concentrations in spiked Lake Ontario water samples before and after gel treatment. Detection of Hg^{2+} in (C) spiked Lake Ontario water samples and in (D) buffer A.

5.2.7 Hydrogel regeneration, nuclease resistance and drying.

For on-site testing of environmental water sources, a versatile sensor requires easy regeneration along with the ability to be transported from the lab. We thus sought to determine whether our sensor could be regenerated after treatment with Hg^{2+}. This Hg^{2+} containing hydrogel was treated with 1% HCl, incubated for 3 min, and subsequently soaked in buffer A for 20 min five times over (Figure 5.11A). As shown in Figure 5.11B, the hydrogels were not fluorescent following this regeneration. Interestingly, addition of Hg^{2+} and SYBR Green I to the same gel regenerated the sensor response (Figure 5.11C). We next tested whether DNA-encapsulation within the hydrogel prevented enzymatic DNA degradation. For this, the DNA-attached hydrogel was treated with DNase 1 for 1 hr. Hg^{2+} induced green fluorescence could still be observed albeit with a reduced intensity (Figure 5.11D). In the absence of the hydrogel, the SYBR Green I intercalated DNA was no longer fluorescent within 20 min of treatment with DNase (Figure 5.11E), suggesting that the gel matrix effectively decreased enzymatic DNA degradation by possibly reducing the DNase diffusion kinetics inside the gel. Finally, another means for storing the hydrogels was studied for successful transfer from lab to an environmental water testing site. Drying provides a convenient means for gel storage and DNA protection. Thus, the gels were dried such that the dry mass is ~4% of the original hydrated gel mass. The gels could then be easily rehydrated by soaking

in buffer A to the original volume (Figure 5.11F) after for environmental detection of Hg^{2+} (Figure 5.11G).

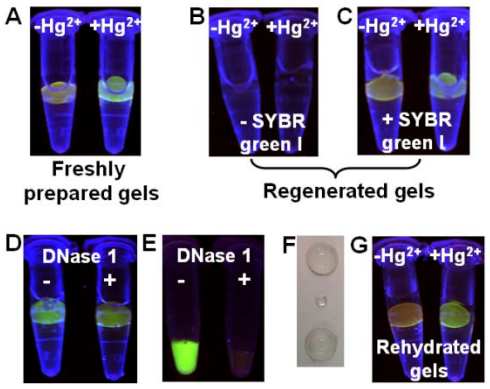

Figure 5.11 Thymine-rich functionalized hydrogels where (A) freshly prepared and (B-C) regenerated gels. Responses of the (D) gels and (E) free thymine-rich DNA complexed with Hg^{2+} after DNase 1 treatment. (F) A photo of freshly prepared (upper), dried (middle), and rehydrated (lower) gels. (G) Detection of Hg^{2+} with rehydrated gels. Hg^{2+} concentration = 1 μM.

5.3.0 DNA-functionalized hydrogel microparticles.

A major drawback of our system remains the required 1 hr gel treatment with Hg^{2+}. To increase the response time of the sensor, the performance of microparticles of the same composition were studied. It is expected that by decreasing the size of the hydrogel and increasing its surface area to volume ratio, enhanced diffusion of Hg^{2+} within the gel can be attained. Preparation of hydrogel microparticles can be achieved by emulsion templated polymerization or lithographic techniques.[165,168-170] We used the former emulsion template polymerization to prepare DNA-functionalized microparticles. In a typical synthesis, ammonium persulfate, acrydite-modified Hg^{2+}-binding DNA, acrylamide, bis-acrylamide were mixed. A water-in oil emulsion was formed by adding Span 80 as the surfactant and cyclohexane as the oil phase to the acrylamide mixture. Polymerization subsequently ensued upon TEMED treatment. After polymerization, the gel particles were precipitated by addition of ethanol, washed with ethanol and finally re-dispersed in water. Gram quantities of the gel beads could be prepared in each synthesis. Optical microscopy indicated that the formed beads were spherical (Figure 5.12A) with most in the size range of 10 to 50 μm (Figure 5.12C, black bars) and an average size of about 30 μm (calculated using mass

percentage Figure 5.12C, red bars). Staining of the DNA-attached microparticle with SYBR Green I yielded a fluorescence signal under blue light excitation (Figure 5.12A and B), and the fluorescent particles co-localized with the image obtained using the transmission mode, suggesting the DNA was inside the gel. As a control, if no acrydite-DNA was added during gel preparation, no fluorescence was observed from the beads even after the addition of SYBR Green I, confirming that the DNA-functionalized gel beads were successfully prepared.

5.3.1 Visual Hg^{2+} detection of hydrogel microparticles.

Thymine-rich DNA as shown in Figure 5.5 has been widely used for Hg^{2+} recognition. This particular DNA sequence contains seven potential Hg^{2+} binding sites. A long DNA with many Hg^{2+} binding sites can produce a larger conformational change and thus, good signal-to-background ratio. In the absence of Hg^{2+}, this DNA adopts a random coil configuration and binds to SYBR Green I producing weak yellow fluorescence. In the presence of Hg^{2+}, the DNA forms a hairpin structure, upon which SYBR Green I can bind strongly to afford intense green fluorescence. As shown in Figure 5.12D, this expected result was obtained after incubating the gel beads with 5 μM SG with or without 10 μM Hg^{2+} under excitation 470 nm excitation in 20 mM $NaNO_3$, 10 mM HEPES, pH 7.6 (buffer B). To confirm that the fluorescence originated from the gel instead of free DNA in solution, the two tubes were centrifuged and imaged again (Figure 5.12E); the fluorescent beads were pelleted at the bottom and the supernatant solution was observed to be non-fluorescent. This result confirmed that the gel beads were indeed capable of visual detection.

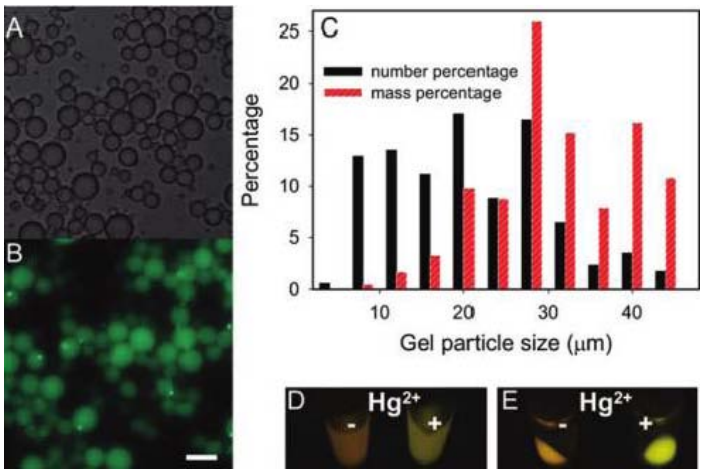

Figure 5.12 Hydrogel microparticle characterization using optical microscopy under (A) transmission light and (B) fluorescence mode where scale bar is 40 μm. (C) Representative size distribution of the prepared microparticles. Fluorescence of the gel beads in the absence or presence of 10 μM Hg^{2+} in the case where the beads are (D) uniformly dispersed in buffer and (E) after centrifugation. Buffer B (20 mM $NaNO_3$, 10 mM HEPES, pH 7.6) was used for mercury detection**.**

5.3.2 Kinetics of signal change.

The main motivation for the development of the hydrogel microparticles was to improve response by reducing diffusion distances. The thickness of the previously reported monolithic gels was ~2 mm, whereas the average size of the gel particles was only~30 μm. Given the >50-fold difference in size, the diffusion time is expected to decrease significantly in the microparticle system. To measure signaling kinetics, hydrogel microparticles were dispersed in a cuvette. As shown in Figure 5.13A, a fast increase in the fluorescence signal was observed after addition of SYBR Green I. The signal was stabilized in about 30 sec. Addition of 1 μM Hg^{2+} resulted in an additional fluorescence increase, which stabilized in ~ 3 min (rate of signal increase = 1.0 min^{-1}). For comparison, the free DNA was also tested under the same conditions and it reached equilibrium more rapidly for both additions (Figure 5.13B). Compared to the~1 h needed for the monolithic gels, as mentioned above, the improvement on the signaling kinetics was greater than 20 fold.

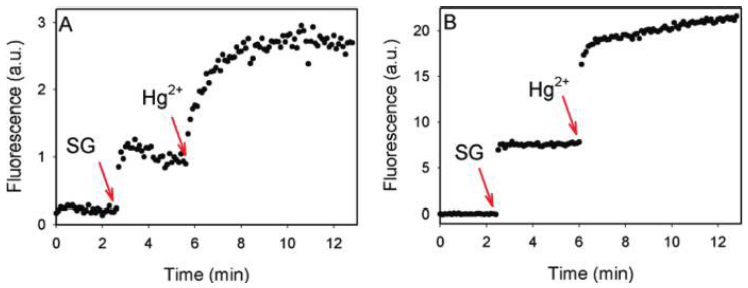

Figure 5.13 Fluorescence signaling kinetics of (A) DNA-functionalized microparticles or (B) free thymine-rich DNA. The arrows indicated the time points when SYBR Green I (100 nM) and Hg^{2+} (1 μM) were respectively added. All of the experiments were done in buffer B.

5.3.3 Mercury detection and storage.

To characterize the sensor performance, we mixed the gel beads with various concentrations of Hg^{2+} and observed the resulting structure using a fluorescence microscope (Figure 5.14A−F). The fluorescence intensity was significantly increased in the presence of Hg^{2+}. The signal was quantified and plotted in Figure 5.14G. The lower inset shows the response in the low concentration region. By visual inspection of the gel beads, even 10 nM Hg^{2+} can be visually detected (the upper inset of Figure 5.14G). 30 nM Hg^{2+} produced a significantly better distinction. Since the human eye cannot detect 10−30 nM SYBR Green I fluorescence, this sensitive visual detection suggested Hg^{2+} enrichment within the gel. For example, visual detection of Hg^{2+} using non-immobilized DNA was achieved only in the presence of greater than 500 nM Hg^{2+} (Figure 5.14I). To test the reproducibility of synthesis, we prepared three separate batches of DNA-functionalized gel beads, and similar sensitivity was observed for each batch. Therefore, although the size distribution of the gels was relatively large, the performance was not affected. To test specificity, the gel beads were incubated with various metal ions at a concentration of 10 μM, of which only Hg^{2+} showed significant fluorescence enhancement (Figure 5.14H). Although Ag^{+} also produced some fluorescence increase, this fluorescence was quickly bleached during imaging and thus could not be quantified. Therefore, high selectivity was maintained after gel immobilization. We further performed detection in Lake Ontario water samples and a similar visual detection limit of~30−50 nM Hg^{2+} was achieved (see Figure 5.14). As described above, $Hg(ClO_4)_2$ was added to simulate contaminated water. To 1.2 mL buffer A, 100 μL of Hg^{2+} sensitive hydrogel beads and varying concentrations of Hg^{2+} were added. These samples were incubated for 20 min on a rocker after which 100 nM SYBR Green I was added and incubated for an additional 5 min. The tubes were then centrifuged for 2 min and 1 mL of the supernatant was removed. To the gel beads, an additional 250 nM SYBR Green I

was added. Similar to that in pure buffer, ~30-50 nM Hg^{2+} could still be visually detected in Lake Ontario water samples. The photograph of the gels is shown in Figure 5.15.

An important feature of hydrogel microparticles lies in their ease of handling as their aqueous dispersions can be readily added to a solid substrate and dried. We cast a small array using a micropipette to dispense 2 μL gel beads onto a glass slide. After drying overnight, a thick film formed with the diameter of each spot being ~ 4 mm (Figure 5.16A). The dried beads were then rehydrated with buffer B containing 5 μM SG in the absence or presence of 2 μM Hg^{2+} (Figure 5.16B). The spots without Hg^{2+} showed orange fluorescence, whereas the spots with Hg^{2+} were yellowish green. The fluorescence intensities of these samples were quite similar. For comparison, freshly prepared gel beads were also spotted. These samples showed an intense green fluorescence only in the presence of Hg^{2+} (Figure 5.16C). To better understand the effect of drying, a micrograph of the gel beads after rehydration is provided in Figure 5.16D. The spherical shape of the beads was evident, indicating that the overall structure of the beads was not damaged with drying. The smeared features appearing on the micrograph stems from focusing issues. The increased background fluorescence after drying (Figure 5.16B) is attributed to changes in gel internal structure, which might be relieved by adding preserving agents such as sucrose or trehalose.

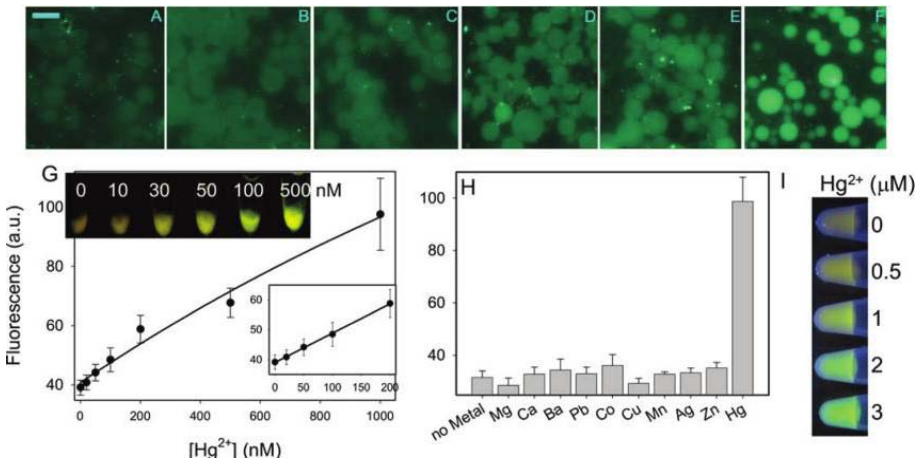

Figure 5.14 Fluorescence micrographs of the gel beads exposed to varying concentrations of Hg^{2+}. (A) 0, (B) 50, (C) 100, (D) 200, and (E) 500 nM, and (F) 1 μM where scale bar is 40 μm. (G) Quantification of signal intensity from the microscope micrographs. The lower concentration region is shown in the bottom inset shows a digital camera picture of gel beads exposed to various concentrations of Hg^{2+}. (H) Selectivity test with 10 μM various metals ions but the mercury concentration was 1 μM. (I) Visual detection of Hg^{2+} using non-immobilized sensor or free thymine-rich DNA. All of the experiments were conducted in buffer B.

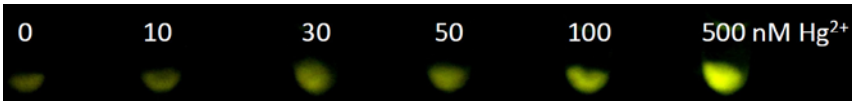

Figure 5.15 Sensor sensitivity detected using a digital camera in contaminated Lake Ontario water samples with varying concentrations of Hg^{2+}.

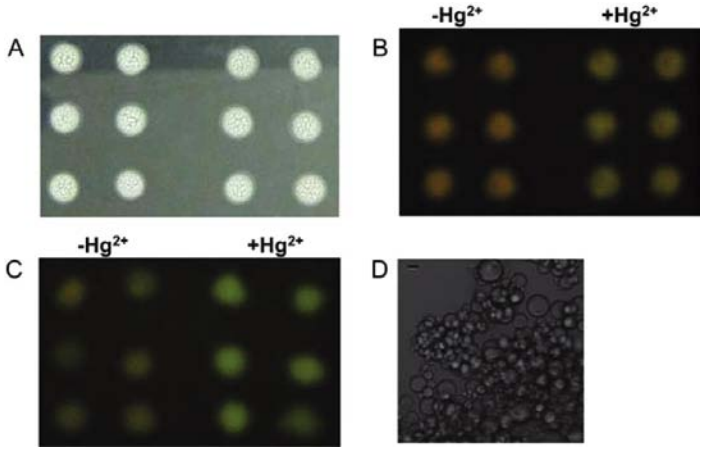

Figure 5.16 (A) Photograph of a dried array of hydrogel microparticles. The diameter of each spot was about 4 mm. Fluorescence micrograph of the dried gels (B) after rehydration and (C) freshly prepared gels in the presence (the six spots on the right) and absence (on the left) of 2 μM Hg^{2+}. (D) A micrograph of the rehydrated gel beads where the scale bar is 20 μm.

5.4 Conclusions.

In summary, we prepared and characterized a DNA-functionalized polyacrylamide hydrogel that can effectively detect and remove Hg^{2+} both in buffer and mercury contaimated lake water samples. The ability to increase sensitivity by using a larger sample volume distinguishes this gel-based sensor from previously reported systems. The immobilization method is also applicable to other nucleic acids, aptamers, proteins, and small molecule chelators for environmental and biomedical applications. However, a major drawback of our system remains the required 1 hr gel treatment with Hg^{2+}. To increase the response time of the sensor, we evaluated the performance of microparticles of the same composition. It is expected that by decreasing the size of the hydrogel and increasing its surface area to volume ratio,

enhanced diffusion of Hg^{2+} within the gel can be attained. In comparison to monolithic gels, microparticle hydrogels diplayed much faster kinetics of signal generation. At the same time, the microparticle gels can be easily handled. Therefore, such hydrogels are useful soft materials for analytical applications. The dissociation constant (K_d) of the Hg^{2+} and Pb^{2+} aptamers are in the low nM region and close to quantitative binding can be achieved. Therefore, immobilizing μM DNA probes inside gels could eventually accumulate μM metal ions to produce a sufficient signal necessary for visual detection. In other words, these metal sensors are ultimately limited by the detector (i.e., the human eye).

5.5 Material and Methods.

5.5.1 Chemicals.

All of the DNA samples were purchased from Integrated DNA Technologies (Coralville, IA). Acrydite-thymine-rich DNA (Acrydite-5′-CTTCTTTCTTCCCCTTGTTTGTTG); Hg-DNA has the same sequence as acrydite-Hg-DNA or thymine-rich DNA without the acrydite modification; C-rich DNA: (acrydite-5′-CCCCCCCCCCCCCCCGCCCGCC). 40% acrylamide:bis-acrylamide = 29:1 gel solution, bromophenol blue, ammonium persulphate (APS), N,N,N′,N′-tetramethylethylenediamine (TEMED), and DNase 1 were purchased from VWR. Mercury perchlorate, copper sulfate, zinc chloride, manganese chloride, cobalt chloride, lead acetate, magnesium chloride, calcium chloride, Span 80, acrylamide, and bis-acrylamide were obtained from Sigma-Aldrich. Sodium nitrate and tris(hydroxymethyl)aminomethane (Tris) were purchased from Mandel Scientific (Guelph, Ontario, Canada). 10,000× SYBR Green I in dimethyl sulfoxide (DMSO) was purchased from Invitrogen.

5.5.2.0 Synthesis of DNA-functionalized monolithic hydrogels.

The hydrogel was prepared by mixing the following solutions: 40% gel solution (29:1), $NaNO_3$ (2 M), tris nitrate (pH 8.0, 0.5 M), thymine-rich DNA (0.5 mM), and water. This mixture contained a final gel percentage of 4% and final concentration of 100 mM $NaNO_3$ 50 mM Tris nitrate pH 7.6 (buffer A) and 10 μM DNA. To initiate polymerization, a fresh initiator solution was made. The initiator solution was prepared by dissolving 50 mg (APS) in 500 μL water and 25 μL TEMED. The volume of the initiator was 5% of the final mixture. A 96-well plate was used for gel preparation. 75 μL of the gel

solution was added to each well. The gels were polymerized for 1 hr at room temperature and then soaked in buffer A (20 mM NaNO3, 8 mM tris nitrate, pH 8.0) three times (each soaking step was for a duration of at least 3 hr) to remove free monomer, initiator, and unincorporated DNA. For some experiments, different gel percentages of DNA were prepared. The final concentration of DNA within the gel was determined using a SYBR green 1 assay.

5.5.2.1 Determination of DNA concentration within monolithic hydrogels.

In a typical gel preparation, 10 µM DNA was added. However, not every DNA molecule was found to covalently bind to the gel. To determine the concentration of covalently attached DNA, the following experiments were performed. First, a solution containing 300 nM cDNA (5′ CAACAAACAAGGGGAAGAAAGAAG) with varying concentration of thymine-rich DNA in 20 mM $NaNO_3$, 2 mM $MgCl_2$, and 30 mM tris nitrate, pH 8.0 was prepared. These two DNA sequences are complementary and form a duplex at room temperature. Addition of 1 µL of 250 x SYBR Green I (~500 µM) to 100 µL of these solutions results in the dye selectively binding to the double-stranded DNA as well as green fluorescence. The fluorescence allows us to quantify the concentration of thymine-rich DNA in solution, from which the DNA incorporated into the gel can be deduced. The standard curve obtained using this method is shown in Figure 5.17. The curve shows a linear increase in the fluorescence as the concentration of thymine-rich DNA is increased from 0 to 240 nM. Therefore, this concentration region was used for quantification of samples with unknown acrydite-Hg-DNA concentrations. With the calibration curve, the DNA concentration in the soaking solution can be determined and the difference between added DNA and DNA in the soaking solution is the covalently bound thymine-rich DNA to the gel matrix. The fluorescence was obtained using a Molecular Device SpetraMax M5 plate reader with 485 nm excitation. The emission at 520 nm was collected with a cut-off filter at 515 nm.

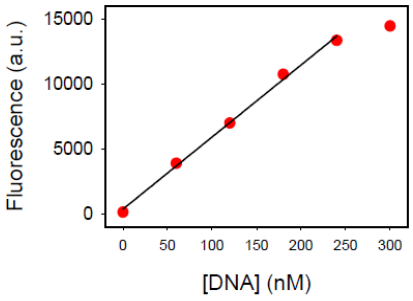

Figure 5.17 The standard curve for determining the concentration of thymine-rich DNA.

To determine the amount of DNA within the gel matrix, hydrogels (4%) with 10 μM non-acrydite thymine-rich DNA (the same DNA sequence as thymine-rich DNA but without the acrydite modification) were prepared. This DNA can only be entrapped inside the gel. Each prepared gel was transferred to a 15 mL tube and the liquid left in the well where the gel was formed was collected and subsequently transferred to the same tube. 3 mL buffer A was used to soak each gel for 8 hrs. The soaking buffer was collected. The gel was soaked for a second time for 8 hrs and buffer collected. To determine the DNA concentration in the soaking buffers c-DNA was added such that its final concentration was 300 nM and the buffer was adjusted to be identical to the above standard curve conditions. The DNA concentrations in the first soaking buffers were determined to be 131.8 nM and 214.1 nM, respectively, for thymine-rich DNA and non-acrydite thymine-rich DNA. In the second soaking solutions, the DNA was undetectable for thymine-rich DNA. However 1.5 nM of non-acrydite thymine-rich DNA was detected. Therefore, the first soaking is sufficient to remove most of the unbound DNA in both samples. The thymine-rich DNA concentration inside the gel was determined to be 4.7 μM and therefore, the amount of DNA incorporation was 47%. If no acrydite group was present then only 16% was entrapped suggesting that covalent attachment is crucial for achieving a high DNA concentration inside the gel.

5.5.2.2 Detection of Hg^{2+}.

In a typical experiment, each gel was soaked in 1 mL of buffer A containing Hg^{2+} or other metal ions. 2 μL of 250× concentrated (500 μM) SYBR Green I was added immediately. The mixtures were soaked for 1 hr at room temperature on a shaker. The gels were then excited with a handheld UV lamp at 365 nm at a distance ~10 cm from the gel and were imaged using a digital camera (Canon PowerShot SD 1200 IS). UV protection goggle was worn for visual observation.

To detect Hg^{2+} in 15 or 50 mL samples, the gels were transferred to appropriate conical tubes containing varying concentrations of Hg^{2+}. After soaking the gels overnight to allow Hg^{2+} binding, the gels were then transferred to 1.5 mL tubes and SYBR green I was added. For quantitative analysis, the gels were imaged with a gel documentation system (Alpha Innotech FluorChem FC2). The excitation wavelength was at 365 nm the emission was collected using a green filter and cooled CCD camera.

5.5.2.3 Flourometric analysis.

For the fluorescence spectra shown in Figure 5.4, 15 nM or 1 μM Hg-DNA was dissolved in 400 μL of buffer A. The molar ratio of SYBR Green I and DNA was maintained at 6:1. Spectra in the absence and presence of Hg^{2+} were collected using a PTI spectrofluorometer under 485 nm excitation at room temperature.

5.5.2.4 Quantification of Hg^{2+} in the supernatant.

To quantify Hg^{2+} removal, a sensor based on thymine-rich DNA and SYBR Green I was used. This sensor has a linear response to Hg^{2+} concentration over a range of 10 to 100 nM. The sensor solution was made by dissolving 30 nM thymine-rich DNA and 200 nM SYBR Green I in buffer A. To determine low concentrations of Hg^{2+} (< 100 nM), 10× sensor solution containing 300 nM thymine-rich DNA and 2 μM SYBR Green I was also prepared. In order to determine the kinetics of Hg^{2+} removal, hydrogels were soaked in 1 mL buffer A containing 1 μM Hg^{2+}. Three calibration solutions containing 1 μM, 100 nM or 10 nM Hg^{2+} in buffer A were also prepared at the same time. At designated time points, 10 μL of the supernatant solution or calibration solutions were transferred to a 96-well plate and 90 μL sensor solution was added. When the Hg^{2+} concentrations in the hydrogel soaking solution dropped to below 100 nM, 90 μL of the soaking solution and 10 μL of the 10× sensor solutions were mixed so that the final Hg^{2+} concentrations were still in the 10 to 100 nM range. Calibration was performed at each time interval. The fluorescence signals were read by a plate reader (SpectraMax M5) with excitation at 485 nm.

5.5.2.5 Hydrogel Regeneration.

After incubation with SYBR Green I and Hg^{2+}, the gels show green fluorescence. To regenerate the hydrogels, the gels were soaked in 1 mL of 1% HCl for 3 min. The HCl solution was discarded, and the gels were washed with 10 mL of water and subsequently soaked in 10 mL buffer A for 20 min. The gels were then soaked in 1 mL of 1% HCl and this process was repeated five times. After the fifth soaking in buffer A, an additional soaking in 10 mL of buffer A was performed for 1 hr. After that, the gels were imaged to ensure no fluorescence was observed. The regenerated gels were then used for Hg^{2+} detection.

5.5.2.6 DNase 1 assays.

DNase 1 was dissolved at a concentration of 10 mg/mL in 50% glycerol, 20 mM Tris-HCl at pH 7.5, and 1 mM $MgCl_2$. 2.5 μM of thymine-rich DNA was dissolved in the DNase reaction buffer (20 mM NaCl, 25 mM HEPES, pH 7.6 with 10 mM $MgCl_2$ and 10 mM $CaCl_2$). To 500 μL of this solution, 0.5 μL of the above 10 mg/mL DNase 1 was added and the resulting solution incubated at 37 °C in a dry bath. After 20 min, 50 μL of the mixture was transferred into another microcentrifuge tube and mixed with 2 μL of 250× SYBR Green I dye and 4 μM Hg^{2+} and immediately imaged.

For the thymine-rich DNA functionalized hydrogels, they were soaked in 1 mL of the DNase 1 reaction buffer. 1 μL of the above 10 mg/mL DNase 1 was added to each microcentrifuge tube was incubated at 37 °C for 1 hr. After soaking, the gels were washed with buffer A three times to remove DNase 1, and 1 μM Hg^{2+} and 2 μL of 250× SYBR Green I was added. After soaking for 1 hr at room temperature, the gels were imaged.

5.5.2.7 Hydrogel drying and rehydration.

To dry the DNA-functionalized hydrogels, the gels were soaked in 1 mL water for 1 hr twice. The gels were then transferred onto a plastic weighing boat and dried in air overnight. The mass of the gel before drying was around 80 mg. After drying, the mass reduced to ~3-4 mg. For rehydration, the dried gels were soaked in buffer A for 3 hrs at room temperature. The gel mass recovered to the original mass and the gels were ready for Hg^{2+} detection.

5.5.2.8 Detection Hg^{2+} in contaminated Lake Ontario Water Samples.

Lake Ontario water samples were collected from Colonel Samuel Smith Park in Toronto, Ontario, Canada. ICP-MS analysis showed no detectable mercury. Therefore, $Hg(ClO_4)_2$ was added to simulate contaminated water. For Hg^{2+} detection and removal, the water samples were transferred to conical tubes (15 mL each). Some of the tubes were spiked with varying amounts of Hg^{2+} to which a gel was added and soaked for one day. After soaking, the supernatants were collected and acidified with 1% nitric acid for ICP-MS analysis (performed by the Microanalysis Lab of the University of Illinois at Urbana-Champaign). For Hg^{2+} detection in Lake Ontario water samples, gels previously soaked were transferred to 1.5 mL microcentrifuge tubes and 1 mL buffer A containing 1 μM SYBR green I was added. After 1 hr, the gels were imaged.

5.5.3.0 DNA-functionalized microparticle hydrogel preparation.

Polyacrylamide hydrogel microparticles were prepared via emulsion polymerization.[165] The aqueous phase (2 mL total) contained 4 μL APS, acrylamide (0.18 g), bis-acrylamide (0.02 g) and 2 μM acrydite-modified DNA. The oil phase consisted of cyclohexane (2 mL) and 100 μL Span 80 as the surfactant. The aqueous phase was dispersed into the oil phase in a 10 mL glass vial. The solution was stirred at 800 rpm for 5 min in an ice bath to form an inverse suspension. After purging the emulsion with nitrogen gas for 2 min, the polymerization was initiated by adding TEMED (4 μL). The polymerization was continued for 4 h under 800 rpm stirring at room temperature. Afterwards, the stirring was stopped and the emulsion phase separated to allow for the removal of the cyclohexane layer. Each 100 μL of the aqueous phase was dissolved in 1 mL of ethanol. After 1 h soaking in ethanol, the solution was centrifuged for 15 min at 15000 rpm and ethanol was removed. The gel beads were soaked in 1 mL of water for 30 min and washed by centrifugation. This washing process was repeated 4 times in water to remove unreacted monomer and initiators. Finally, the gels were dispersed at a concentration of 10 mg/mL (considering only the dry mass of the gel). The size distribution of the hydrogel beads were obtained by measuring ~200 particles under an optical microscope.

5.5.3.1 Hg^{2+} detection.

For visual detection, 200 μL of gel beads were added to each tube containing 1.2 mL of buffer B (20 mM NaNO3, 10 mM HEPES, pH 7.6) with varying concentrations of Hg^{2+} and 100 nM SYBR Green I. The samples were incubated for 20 min, after which 1 mL of supernatant was removed. 250 nM of SYBR Green I was then added and the samples were observed using a blue light transilluminator (Invitrogen Safe Imager 2.0, excitation wavelength = 470 nm) and the fluorescence recorded using a digital camera (Canon PowerShot SD1200 IS). For imaging under a fluorescence microscope, 2 μL of the beads were spotted onto a glass slide and imaged using the cube for FAM fluorophore. The exposure time and other imaging conditions were set to be the same for all of the samples. Fluorescence intensity was quantified using Adobe Photoshop. The same procedure was used for the Lake Ontario samples.

5.5.3.2 Microparticle kinetics.

The kinetic experiment was carried out using a fluorometer (Eclipse, Varian) by exciting at 480 nm and monitoring the emission at 520 nm. Free DNA (20 nM) was dissolved in 600 μL of buffer B and its background fluorescence monitored for ~2 min before 100 nM SYBR Green I was added. After 5 min, 1 μM Hg^{2+} was added. For the gel microparticles, 20 μL of 10 mg/mL gel beads were dispersed in 600 μL of the same buffer and the same amount of SYBR Green I and Hg^{2+} was added. The cuvette was agitated before each measurement to ensure that the beads were homogeneously dispersed in buffer.

Chapter 6.0 Conclusions and Future Work

6.1 Conclusions and Future Work.

Bio-molecules can be used to control both the structure and property of nanomaterials. No biomolecule has been studied more often than DNA. In this thesis, we explored the use of DNA to functionalize soft materials such as liposomes and hydrogels. The majority of previous work has focused on DNA directed assembly of "hard" inorganic nanoparticles such as gold nanoparticles (AuNPs). In chapter 2 we demonstrated DNA-directed assembly of liposomes using a three component system via addition of DNA linker. This is the first systematic study on the physical properties of DNA-linked liposomes where various liposome formulations and DNA sequences have been studied. The melting transitions of these liposome assemblies as a function of lipid charge, size, fluidity, and attached DNA were systematically studied and compared with the analogous properties of AuNPs. While there are many similarities between assemblies of AuNPs and liposomes, important differences exist. For example, the melting temperature (T_m) of liposome assemblies are less affected by the interparticle separation or liposome size compared to AuNPs. These differences can be explained by the soft nature of liposomes. The fundamental understanding of such properties is expected to improve design of new liposome-based materials for both analytical and biomedical applications, particularly considering that liposomes have many attractive properties that are lacking in AuNP systems. In fact, with a large number of liposome-based drugs currently in phase 3 of their clinical trials has led to a separate FDA division making such fundamental studies imperative for *in vivo* and *in vitro* applications.[172a] A natural extension of our fundamental study in chapter 2 is to study the melting properties of AuNPs and liposome assemblies in a biological media which contain a variety of large macromolecules such as RNA, DNA and proteins that occupy 20-40% of a live cell's volume.[172b] These macromolecules strongly influence the rate of a reaction in a cell. Therefore, understanding how DNA-directed liposome and AuNPs assemblies behave in the presence of such molecular crowding allows us to gain further insight into how such systems would behave *in vivo* is currently lacking.

As an extension of our work in chapter 2, we prepared and characterized new DNA-linked hybrid nanostructure containing both soft and hard nanoparticles, in chapter 3. Liposomes alone, however, do not possess the unique and easily detectable properties of inorganic nanoparticles. Therefore, coupling liposomes and inorganic nanoparticles in a programmable manner can potentially afford single multifunctional nanostructures that combine the advantages of both particles. Such a system is useful for fundamental understanding of the interaction between light, AuNPs, and liposomes at the

nanoscale, since the length of linker DNA can be easily varied. Contrary to previous reports where AuNPs always promoted radiation induced liposome leakage, we are the first to have observed both promotion and protection effects, depending on the distance between the AuNPs and liposomes defined by DNA. We demonstrated controlled content release in our hybrid nanostructured material using UV light, in order to potentially use such assemblies as a theranostic systems. Theranostics deals with systems that simultaneously consists of diagnostic and therapeutic components.[173] The former component identifies the disease state such as metabolic/biochemical state, genotype, size, location, morphology, and chemical composition whereas the latter changes the outcome of the disease by introducing or releasing small molecules, proteins, RNA, drugs, ablation and surgery.

In chapter 4 and 5, we demonstrated that aptamers immobilized on soft materials have several advantages. In chapter 4, we demonstrated that even micromolar concentrations of functionalized adenosine aptamer split in half on a liposome surface can detect adenosine within a few seconds. In addition, the selectivity of the aptamer remains un-affected. This takes advantage of a fundamental property of liposomes that of DNA diffusion on a lipid bilayer. If DNA diffusion is eliminated by functionalization on silica nanoparticles, the adenosine sensor becomes non-responsive. A natural extension of our study is combining aptamer and liposome for targeted drug delivery. Many chemotherapeutic agents such as cisplatin have several drawbacks. For example, the drug lacks cancer specificity and causes severe side effects. One of the methodologies to deliver cisplatin more effectively involves using drug encapsulated liposomes functionalized with aptamers for cellular receptor recognition. Lu and coworkersreported cisplatin encapsulated liposomes with functionalized aptamers for cancer-cell-specific targeting. They demonstrated a method to turn-off the drug delivery via addition of a complementary DNA (cDNA).[174a] A 26-mer DNA aptamer with a cholesterol modification was used with a high binding affinity for nucleolin (NCL). The over expression of NCL in cell membranes has been linked to many cancers including breast cancer. Lu and coworkers showed an increase in death after four days by 59% of MCF-7 cells treated with their system whereas addition of cDNA resulted in 95% cell viability even after 4 days *in vitro*. Their system clearly demonstrated the combination of aptamer and liposome for effective treatment. Kang and coworkers linked a sgc8 aptamer specific for leukemia cells with a lipid modified PEG spacer and MPB-PE head group.[174a] A dual florouphore system where the aptamer is modified with a fluorophore and dye encapsulated liposome allowed them to study receptor binding and content delivery. Both binding and content release of dye was achieved after three hours of incubation with 250 aptamers bound per liposome. The specificity of sgc8 aptamer confirmed site specific delivery. Mann and coworkers attached a thiophosphate modified aptamer to an amine modified PEG

lipid. [174b] The aptamer targets E-selection, expressed in tumor vasculature. They studied intravenous administration of this system encapsulated with Rhodamine dye and found accumulation at the tumor site without decreasing the circulation half-life of the system. This system clearly demonstrates the importance of liposome and aptamers combinations in the potential treatment of diseases such as cancer *in vivo*.

For Hg^{2+} detection and removal, we immobilized thymine-rich DNA or Hg^{2+} aptamer in a polyacrylamide hydrogel. Hydrogels consists of a network of hydrophilic polymer and therefore, greater than 90% of their volume is occupied by water. Within these hydrogels, biomolecules can retain their native structure. Using this system we effectively detected and removed Hg^{2+} both in buffer and environmental water samples. The ability to increase sensitivity by using a larger sample volume distinguishes our gel-based sensors from others. We are one of the first to demonstrate detection and removal of Hg^{2+} simultaneously. To increase the response time from 1 hour in the case of monolithic hydrogels we prepared DNA-functionalized hydrogel microparticles, which showed much faster kinetics of signal generation due to the larger surface area. We demonstrated that within 10 minutes the microparticles could remove 200 nM Hg^{2+}.[175a] In addition, we have also successfully used such aptamer-functionalized microparticles for detection of adenosine in human blood serum since the gel protects the aptamer from degradation in the presence of serum enzymes.[175a] Our study highlights the importance of binding affinity for target analyte enrichment in immobilized sensors. The dissociation constant, K_d for Hg^{2+} and Pb^{2+} aptamers are in the low nM region and close to quantitative binding can be achieved. Therefore, immobilizing μM DNA probe inside the hydrogel could eventually accumulate μM metal ions enough to produce the signal necessary for visual detection. Using this immobilization method aptamers, proteins, and small molecule chelators can also be studied for environmental and biomedical applications.

An extension of our work in chapter 4 and 5 is to better understand raft or domain formation in cells using liposomes as model membranes. The cell membrane is no longer thought to be a homogeneous lipid bilayer composed of lipids, proteins and other biomolecules. In fact, the cell membrane is made-up of compartments or lipids that phase separate into a liquid ordered and dis-ordered domains.[175b] These rafts are vital for signaling, sensing and play an important role in pathogen invasion. Therefore, understanding the nature of raft formation in liposomes may allow deciphering the various pathways of biological molecules. To achieve this, liposome adsorbed onto a microhydrogel particle is being studied, since this allows for real-time fluorescence microscopy study. These types of liposome-hydrogel system are referred to as lipogels and are a natural extension of our study.

References.

1. Seeman, N. C. *Nature* **2003**, *421*, 427.
2. Lin, C.; Liu, Y.; Yan, H. *Biochemistry* **2009**, *48*, 1663.
3. Aldaye, F. A.; Palmer, A. L.; Sleiman, H. F. *Science* **2008**, *321*, 1795.
4. Alivisatos, A. P.; Johnsson, K. P.; Peng, X.; Wilson, T. E.; Loweth, C. J.; Bruchez, M. P., Jr; Schultz, P. G. *Nature* **1996**, *382*, 609.
5. Mirkin, C. A.; Letsinger, R. L.; Mucic, R. C.; Storhoff, J. J. *Nature* **1996**, *382*, 607.
6. Storhoff, J. J.; Mirkin, C. A. *Chem. Rev.* **1999**, *99*, 1849.
7. Liu, J.; Cao, Z.; Lu, Y. *Chem. Rev.* **2009**, *109*, 1948.
8. Rothemund, P. W. K. *Nature* **2006**, *440*, 297.
9. Zheng, J. P.; Birktoft, J. J.; Chen, Y.; Wang, T.; Sha, R. J.; Constantinou, P. E.; Ginell, S. L.; Mao, C. D.; Seeman, N. C. *Nature* **2009**, *461*, 74.
10. Park, S. Y.; Lytton-Jean, A. K. R.; Lee, B.; Weigand, S.; Schatz, G. C.; Mirkin, C. A. *Nature* **2008**, 451, 553.
11. Nykypanchuk, D.; Maye, M. M.; van der Lelie, D.; Gang, O. *Nature* **2008**, 451, 549.
12. Sharma, J.; Chhabra, R.; Cheng, A.; Brownell, J.; Liu, Y.; Yan, H. *Science* **2009**, 323, 112.
13. Tuerk, C.; Gold, L. *Science* **1990**, 249, 505.
14. Ellington, A. D.; Szostak, J. W. *Nature* **1990**, 346, 818.
15. Robertson, D. L.; Joyce, G. F. *Nature* **1990**, 344, 467.
16. a) Liu, J. *Soft Matter* **2011**, 7, 6757. b) *Bioconjugate Techniques, 2nd Edition* Greg T. Hermanson, Published by Academic Press, Inc., 2008.
17. a) Khorana H. G *Fed Proceedings* **1960**, 19, 931. b) McBride, J. L.; Caruthers, M. H. Tetrahedron Letters **1983**, 24, 245. c) Berner, S.; Muhlegger, K.; Seliger, H. *Nucleic Acids Res.* **1989**, 17, 853.

18. a) Seeman, N. C. *Acc. Chem. Res.* **1997**, 30, 357. b) Kallenbach, N. R.; Ma, R.-I.; Seeman, N. C. *Nature* **1983**, 305, 829. c) Ma, R.-I.; Kallenbach, N. R.; Sheardy, R. D.; Petrillo, M. L.; Seeman, N. C. *Nucleic Acids Res.* **1986**, 14, 9745. d) Zhang, Y.; Seeman, N. C. *J. Am. Chem. Soc.* **1992**, 114, 2656. e) Zhang, Y.; Seeman, N. C. *J. Am. Chem. Soc.* **1994**, 116, 1661. f) Shi, J.; Bergstrom, D. E. *Angew. Chem., Int. Ed. Engl.* **1997**, 36, 111. g) Coffer, J. L. *J. Cluster Sci.* **1997**, 8, 159. h) Murray, C. B.; Norris, D. J.; Bawendi, M. G. *J. Am. Chem. Soc.* **1993**, 115, 8706. i) Wang, Y.; Herron, N. *J. Phys. Chem.* **1991**, 95, 525. j) Weller, H. *Angew. Chem., Int. Ed. Engl.* **1993**, 32, 41. k) Braun, E.; Eichen, Y.; Sivan, U.; Ben-Yoseph, G. *Nature* **1998**, 391, 775. l) Cassell, A. M.; Scrivens, W. A.; Tour, J. M. *Angew. Chem., Int. Ed. Engl.* **1998**, 37, 1528. m) Storhoff, J. J.; Mirkin, C. A. *Chem. Rev.* **1999**, 99, 1849. n) Yang, D.; Campolongo, M. J.; Tran, T. N. N.; Ruiz, R. C. H.; Kahn, J. S.; Luo, D. *WIREs Nanomedicine and Nanobiotechnology* **2010**, 2, 648.

19. a) Keefe, A. D.; Pai, S.; Ellington, A. *Nature Reviews* **2010**, 9, 537. b) Shamah, S. M.; Healy, J. M.; Cload, S. T. *Acc. Chem. Res.* **2008**, 41, 130. c) Fitter, S.; James, R. *J. Biol. Chem.* **2005**, 280, 34193. d) Ng, E. W. M.; Shima, D. T.; Calias, P.; Cunningham Jr., E. T.; Guyer, D. R.; Adamis, A. P. *Nature Rev. Drug Discov.* **2006**, 5, 123. e) Huizenga, D. E.; Szostak, J. W. *Biochemistry* **1995**, 34, 656. f) Vianini, E.; Palumbo, M.; Gatto, B. *Bioorg. Med. Chem.* **2001**, 9, 2543. g) Stojanovic, M. N.; de Prada, P.; Landry, D. W. *J. Am. Chem. Soc.* **2000**, 122, 11547. h) Kato, T.; Takemura, T.; Yano, K.; Ikebukuro, K.; Karube, I. *Biochim. Biophys. Acta* **2000**, 1493, 12. i) Miyake, Y.; Togashi, H.; Tashiro, M.; Yamaguchi, H.; Oda, S.; Kudo, M.; Tanaka, Y.; Kondo, Y.; Sawa, R.; Fujimoto, T.; Machinami, T.; Ono, A. *J. Am. Chem. Soc.* **2006**, 128, 2172. j) Santoro, S. W.; Joyce, G. F. *Proc. Natl. Acad. Sci. U.S.A.* **1997**, 94, 4262. k) Willner, I.; Shlyahovsky, B.; Zayats, M.; Willner, B. *Chem. Soc. Rev.* **2008**, *37*, 1153. l) Liu, J.; Cao, Z.; Lu, Y. *Chem. Rev.* **2009**, *109*, 1948–1998. m) Wang, K. M.; Tang, Z. W.; Yang, C. Y. J.; Kim, Y. M.; Fang, X. H.; Li, W.; Wu, Y. R.; Medley, C. D.; Cao, Z. H.; Li, J.; Colon, P.; Lin, H.; Tan, W. H. *Angew. Chem. Int. Ed.* **2009**, *48*, 856. n) Navani, N. K.; Li, Y. *Curr. Opin. Chem. Biol.* **2006**, *10*, 272. o) Feldkamp, U.; Niemeyer, C. M. *Angew. Chem., Int. Ed.* **2006**, *45*, 1856. p) Fang, X.; Liu, X.; Schuster, S.; Tan, W. *J. Am. Chem. Soc.* **1999**, *121*, 2921. q) Yang, C. Y. J.; Pinto, M.; Schanze, K.; Tan, W. H. *Angew. Chem. Int. Ed.* **2005**, *44*, 2572-2576. r) Conlon, P.; Yang, C. Y. J.; Wu, Y. R.; Chen, Y.; Martinez, K.; Kim, Y. M.; Stevens, N.; Marti, A. A.; Jockusch, S.; Turro, N. J.; Tan, W. H. *J. Am. Chem. Soc.* **2008**, *130*, 336. s) Yang, C. Y. J.;

Lin, H.; Tan, W. H. *J. Am. Chem. Soc.* **2005**, *127*, 12772. t) Wang, L.; Yang, C. Y. J.; Medley, C. D.; Benner, S. A.; Tan, W. H. *J. Am. Chem. Soc.* **2005**, *127*, 15664. u) Tsourkas, A.; Behlke, M. A.; Bao, G. *Nucleic Acids Res.* **2002**, *30*, 5168. v) Shah, R.; El-Deiry, W. S. *Cancer Biology & Therapy* **2004**, *3*, 871. w) Tyagi, S.; Kramer, F. R. *Nat. Biotechnol.* **1996**, *14*, 303-308.

20. Torchilin, V. P. *Nature Review* **2005**; **4**, 145.
21. a) Jesorka, A.; Orwar, O. *Annu. Rev. Anal. Chem.* **2008**, 1, 801. b) Angelova, M.; Tsoneva, I. Chem. Phys. Lipids. 1999, 101, 123. c) Fischer, A.; Oberholzer, T.; Luisi, P. Biochim. Biophys. Acta. 2000, 1467, 177. d) Bangham, A.; Standish, M.; Watkins, J. *J. Mol. Biol.* **1965**, 13, 238. e) Toyran, N.; Severcan, F. *Chem. Phys. Lipids* **2003**, 123, 165. f) Romanowski, M.; Zhu, X.; Ramaswami, V.; Misicka, A.; Lipkowski, A.; Hurby, V.; O'Brien, D. *Biochim. Biophys. Acta* **1997**, 1329, 245. g) Braguini, W.; Cadena, S.; Carnieri, E.; Rocha, M.; de Oliveira, M. *Toxicol. Lett.* **2004**, 152, 191. h) Trombetta, D.;Arena, S.;Tomaino, A.; Tita, B.; Bisignano, G.; Pasquale, A.; Saija, A.; *Il Farmaco* **2001**, 56, 447. i) Grancelli, A.;Morros, A.; Caba˜nas, M.; Dom`enech, O.; Merino, S.; Vazquez, J.;Montero, M.; Vi˜nas, M.; Hern´andez-Borrell, J. *Langmuir* **2002**, 18, 9177. j) Edwards, K. A.; Baeumner, A. J. *Talanta* **2006**, 68, 1421. k) Edwards, K. A.; Wang, Y.; Baeumner, A. *J. Anal. Bioanal. Chem.* **2010**, 398, 2645.
22. Shimomura, M.; Sawadaishi, T. *Current Opinion in Colloid & Interface Science* **2001**, 6, 11.
23. Oldfield, E.; Chapman, D. *Febs Letters* **1972**, 23, 285.
24. Szoka, F.; Papahadjopoulos, D. *Annu. Rev. Biophys. Bioeng.* **1980**, 9, 467.
25. Hope, M. J.; Bally, M. B.; Mayer, L. D.; Janoff, A. S.; Cullis, P. R. *Chemistry and Physics of Lipids* **1986**, 40, 89.
26. Huang, C. H. *Biochemistry* **1969**, 8, 344.
27. Szoka, F.; Papahadjopoulos, D. *Proc Natl Acad Sci USA* **1978**, 75, 4194.
28. Angelova, M. I.; Soleau, S.; Meleard, P.; Faucon, J. F.; Bothorel, P. *Trends in colloid and interface science* vi. **1992**, 89.
29. Morales-Penningston, N. F.; Wu, J.; Farkas, E. R.; Goh, S. L.; Konyakhina, T. M.; Zheng, J. Y.; Webb, W. W.; Feigenson, G. W. *Biochimica Et Biophysica Acta-Biomembranes* **2010**, 1798, 1324.

30. Ohvo-Rekila, H.; Ramstedt, B.; Leppimaki, P.; Peter Slotte, J. *Progress in Lipid Research* **2002**, 41, 66.

31. Martin, R.; Yeagle, P. *Lipids* **1978**, 13, 594.

32. Veatch, S. L.; Keller, S. L. *J. Biophys.* **2003**, 85, 3074.

33. Karlsson, M.; Davidson, M.; Karlsson, R.; Karlsson, A.; Bergenholtz, J. *Annu. Rev. Phys. Chem.* **2004**, 55, 613.

34. a) Gupta, P.; Vermani, K.; Garg, S. *D. D. T.* **2002**, 7, 569. b) Wichterle, O.; Lim, D. *Nature* **1960**, 185, 117. c) Nayak, S.; Lyon, L. A. *Agnew. Chem. Int. Ed.* **2005**, 44, 7686. d) Hennink, W. E.; van Nostrum, C. F. *Adv. Drug. Delivery Rev.* **2002**, 54, 13. e) Dusek, K.; Prins, W. *Fortschr. Hochpolym.-Forsch* **1969**, 6, 1. f) Gombotz, W. R.; Wee, S. *Adv. Drug. Delivery Rev.* **1998**, 31, 267. g) Goosen, M. F. A.; OEShea, G. M.; Gharapetian, H. M.; Chou, S.; Sun, A. M. *Biotechnol. Bioeng.* **1985**, 27, 146. h) Lutolf, M. P.; Raeber, G. P.; Zisch, A. H.; Tirelli, N.; Hubbell, J. A. *Adv. Mater.* **2003**, 15, 888. i) Gacesa, P. *Carbohydr. Polym.* **1988**, 8, 161. j) Eagland, D.; Crowther, N. J.; Butler, C. J. *Eur. Polym. J.* **1994**, 30, 767. k) Mathur, A. M.; Hammonds, K. F.; Klier, Scranton, A. B. *J. Controlled Release* **1998**, 54, 177. l) Nagahara, S.; Matsuda, T. *Polym. Gels. Netw.* **1996**, 4, 111. m) Gallanger, S. M. *Current Protocols Essential Laboratory Techniques* **2008**, 7.3. n) Schild, H. G. *Prog. Polym. Sci.* **1992**, 17, 163. o) Heskins, M.; Guillet, J. E. *J. Macromol. Sci. Chem.* **1968**, 2, 1441. p) Peppas, N. A.; Hilt, J. Z.; Khademhosseini, A.; Langer, R. *Adv. Mater.* **2006**, 18, 1345. q) Peppas, N. A.; Bures, P.; Leobandung, W.; Ichikawa, H.; *Eur. J. Pharm. Biopharm.* **2000**, 50, 27. r) Gawel, K.; Barriet, D.; Sletmoen, M.; Stokke, B. T. *Sensors* **2010**, 10, 4381. s) Hendrickson, G. R.; Smith, M. H.; South, A. B.; Lyon, L. A. *Adv. Funct. Mater.* **2010**, 20, 1697.

35. a) Lent, C. S.; Isaksen, B.; Lieberman, M. *J. Am. Chem. Soc.* **2003**, *125*, 1056. b) Shipway, A. N.; Willner, I. *Chem. Commun.* **2001**, 2035. c) Weller, H.; Eychmüller, A. *Adv. Photochem.* **1995**, *20*, 165. d) Faraday, M. *Philos. Trans. R. Soc. London* **1857**, 147, 145. e) Turkevich, J.; Stevenson, P. C.; Hillier, J. *Discussions of the Faraday Soc.* **1951**, 11, 55. f) Frens, G. *Nature* **1973**, 105, 20. g) Daniel, M.-C.; Astruc, D. *Chem. Rev.* **2004**, 104, 293. g) Liu, J.; Lu, Y.; *Nat. Protoc.* **2006**, 1, 246. h) Hill, H. D.; Millstone, J. E.; Banholzer, M. J.; Mirkin, C. A. *ACS Nano* **2009**, 3, 418. i) Herdt, A. R.; Drawz, S. M.; Kang, Y. J.; Taton, T. A. *Colloids Surf. B* **2006**, 51, 130. j) Bhatt, N.; Huang, P.-J. J.; Dave, N.; Liu, J. *Langmuir* **2011**, 27, 6132. k) Storhoff, J. J.; Elganian, R.; Mucic, R. C.; Mirkin, C. A.; Letsinger, R. L. *J. Am. Chem. Soc.*

1998, 120, 1959. l) Elghanian, R.; Storhoff, J. J.; Mucic, R. C.; Letsinger, R. L.; Mirkin C.A. *Science* **1997**, 277, 1078. m) Cutler, J. I.; Auyeng, E.; Mirkin, C. A. *J. Am. Chem.* **2012**, 134, 1376. n) Alivisatos, A.P.; Johnsson, K. P.; Peng, X.; Wilson, T.E.; Loweth, C.J.; Bruchez, M. P. Jr.; Schultz, P. G. **Nature 1996**, 382, 609. o) Chen, W.; Bian, A.; Agarwal, A.; Liu, L.; Shen, H.; Wang, L.; Zu, C.; Kotov, N. A. *Nano Lett.* **2009**, 9, 2153. p) Sharma, J.; Chhabra, R.; Cheng, A.; Brownell, J.; Liu, Y.; Yan, H. *Science* **2009**, 323, 112. q) Lin, C.; Liu, Y.; Yan, H. *Biochemistry* **2009**, 48, 1663. r) Par,, S. Y.; Lytton-jean, A. K. R.; Lee, B.; Weigand, S.; Schatz, G. C.; Mirkin, C. A. *Nature* **2008**, 451, 553. s) Nykypanchuk, D.; Maye, M. M.; van der Lelie, D.; Gang, O. *Nature* **2008**, 451, 549. t) Macfarlane, R. J.; Lee, B.; Jones, M. R.; Harris, N.; Schatz, G. C.; Mirkin, C. A. *Science* **2011**, 334, 204.

36. Mirkin, C. A.; Letsinger, R. L.; Mucic, R. C.; Storhoff, J. J. *Nature* **1996** *382*, 607.
37. Alivisatos, A. P.; Johnsson, K. P.; Peng, X.; Wilson, T. E.; Loweth, C. J.; Bruchez, M. P.; Jr, Schultz, P. G. *Nature* **1996** *382*, 609.
38. a) Storhoff, J. J.; Mirkin, C. A. *Chem. Rev.* **1999** *99*, 1849. b) Jain, P. K.; Huang, X.; El-Sayed, I. H.; El-Sayed, M. A. *Acc. Chem. Res.* **2008** 41, 1578. c) Jain, P. K.; Lee, K. S.; El-Sayed, I. H.; El-Sayed, M. A. *J. Phys. Chem. B* **2006** 110, 7238. d) Kelly, K. L.; Coronado, E.; Zhao, L. L.; Schatz, G. C. *J. Phys. Chem. B* **2003** 107, 668. e) Link, S.; El-Sayed, M. A. *Annu. Rev. Phys. Chem.* **2003** 54, 331. f) Jain, P. K.; Huang, X.; El-Sayed, I. H.; El-Sayed, M. A. Biosystems Plasmonics **2007** 2,107. g) Wang, J.; Liu, G. D.; Merkoci, A. *J. Am. Chem. Soc.* **2003**, 125, 3214. h) Xiao, Y.; Patolsky, F.; Katz, E.; Hainfeld, J. F.; Willner, I. *Science* **2003**, 299, 1877. i) He, L.; Musick, M. D.; Nicewarner, S. R.; Salinas, F. G.; Benkovic, S. J.; Natan, M. J.; Keating, C. D. *J. Am. Chem. Soc.* **2000**, 122, 9071. j) Liu, J.; Lu, Y. *J. Am. Chem. Soc.* **2003**, 125, 6642. k) Giljohann, D. A.; Seferos, D. S.; Daniel, W. L.; Massich, M. D.; Patel, P. C.; Mirkin, C. A. *Agnew. Chem. Int. Ed.* **2010** 49, 3280.
39. Seeman, N. C. *Nature* **2003** *421*, 427.
40. Katz, E.; Willner, I. *Angew. Chem., Int. Ed.* **2004** *43*, 6042.
41. Feldkamp, U.; Niemeyer, C. M. *Angew. Chem., Int. Ed.* **2006** *45*, 1856.
42. a) Lu, Y.; Liu, J. *Acc. Chem. Res.* **2007** *40*, 315. b) Liu, J.; Lu, Y. *Angew. Chem., Int. Ed.* **2006**, 45, 90.
43. Aldaye, F. A., Palmer, A. L., and Sleiman, H. F., *Science* **2008** *321*, 1795.
44. Rosi, N. L., and Mirkin, C. A., *Chem. Rev.* **2005** *105*, 1547.

45. Cheng, W. L.; Campolongo, M. J.; Cha, J. J.; Tan, S. J.; Umbach, C. C.; Muller, D. A.; Luo, D. *Nat. Mater.* **2009** *8*, 519.
46. Lin, C.; Liu, Y.; Yan, H. *Biochemistry* **2009** *48*, 1663.
47. Ding, B. Q.; Deng, Z. T.; Yan, H.; Cabrini, S.; Zuckermann, R. N.; Bokor, J. *J. Am. Chem. Soc.* **2010** *132*, 3248.
48. Stearns, L. A.; Chhabra, R.; Sharma, J.; Liu, Y.; Petuskey, W. T.; Yan, H.; Chaput, J. C. *Angew. Chem. Int. Ed.* **2009** *48*, 8494.
49. a) Liu, J.; Cao, Z.; Lu, Y. *Chem. Rev.* **2009** *109*, 1948. b) Jin, R.; Wu, G.; Li, Z.; Mirkin, C. A.; Schatz, G. C. *J. Am. Chem. Soc.* **2003**, 125, 1643. c) Pavlov, V.; Xiao, Y.; Shlyahovsky, B.; Willner, I. *J. Am. Chem. Soc.* **2004**, 126, 11768. d) Stojanovic, M. N.; Landry, D. W. *J. Am. Chem. Soc.* **2002**, 124, 9678. e) Liu, J.; Lu, Y. *Adv. Mater.* **2006**, 18, 1667.
50. Zhao, W.; Brook, M. A.; Li, Y. *Chembiochem* **2008** *9*, 2363.
51. a) Storhoff, J. J.; Lazarides, A. A.; Mucic, R. C.; Mirkin, C. A.; Letsinger, R. L.; Schatz, G. C. *J. Am. Chem. Soc.* **2000** *122*, 4640. b) Long, H.; Kudlay, A.; Schatz, G. C. *J. Phys. Chem. B* **2006**, 110, 2918. c) Sabin, J.; Prieto, G.; Sarmiento, F. *Liposomes: Methods and Protocols, Volume 2: Biological Membrane Models, Methods in Molecular Biology* **2010**, 606, 189.
52. a) Jin, R.; Wu, G.; Li, Z.; Mirkin, C. A.; Schatz, G. C. *J. Am. Chem. Soc.* **2003** *125*, 1643. b) Kiang, C. -H. *Physica A* **2003**, 321, 164. c) Long, H.; Schatz, G. C. *Mat. Res. Soc. Proc.* **2002**, 735, C01. d) Reynolds, R. A.; Mirkin, C. A.; Letsinger, R. L. *Pure Appl. Chem.* **2000**, *72*, 229.
53. Storhoff, J. J.; Elghanian, R.; Mucic, R. C.; Mirkin, C. A.; Letsinger, R. L. *J. Am. Chem. Soc.* **1998** *120*, 1959.
54. Elghanian, R.; Storhoff, J. J.; Mucic, R. C.; Letsinger, R. L.; Mirkin, C. A. *Science* **1997** *277*, 1078.
55. a) Zhang, G. R.; Farooqui, F.; Kinstler, O.; Letsinger, R. L. *Tetrahedron Lett.* **1996** *37*, 6243. b) Beales P. A.; Vanderlick, T. K. *J. Phys. Chem. A.* **2007** *111*, 12372. c) Hadorn, M.; Eggenberger Hotz., P. *PLoS ONE* **2010** *5, 3*, e9886. d) Kessel, A.; Ben-Tal, N.; May, S. *Biophys J.* **2001**, 81, 643. d) Shohda, K.; Toyota, T.; Yomo, T.;

Sugawara, T. *Chem. Bio Chem.* **2003**, 4, 778. e) Beales, P. A.; Vanderlick, T. K. *J. Phys. Chem. B* **2009**, 113, 13678. f) Bunge, A.; Loew, M.; Pescador, P.; Arbuzova, A.; Brodersen, N.; Kang, J.; Dalhne, L.; Liebscher Jr, Hermann, A.; Stengel, G.; Huster, D. *J. Phys. Chem. B* **2009**, 113, 16425. g) Edwards, K. A.; Baeumner, A. J. *Anal. Bioanal. Chem.* **2006**, 386, 1335. h) Edwards, K. A.; Baeumner, A. J. *Anal. Bioanal. Chem.* **2006**, 386, 1613. i) Edwards, K. A.; Wang, Y.; Baeumner, A. J. *Anal. Bioanal. Chem.* **2010**, 398, 2645. i) Gartner, Z. J.; Bertozzi, C. R. *Proc. Natl. Acad. Sci. USA* **2009**, 106, 4606. j) Chandra, R. A.; Douglas, E. S.; Mathier, R. A.; Bertozzi, C. R.; Francis, M. B. *Agnew Chem. Int. Ed.* **2006** 45, 896. k) Wang, C. C.-Y.; Seo, T. S.; Li, Z.; Ruparel, H.; Ju, J. *Bioconjugate Chem.* **2003**, 14, 697.

56. a) Chan, Y. H. M.; van Lengerich, B.; Boxer, S. G. *Proc. Natl. Acad. Sci. U.S.A.* **2009** *106*, 979. b) Chan, Y. H. M.; van Lengerich, B.; Boxer, S. G. *Biointerphases* **2008**, 3, FA17. c) Pobbati, A. V.; Stein, A.; Fasshauer, D. *Science* **2006**, 313, 673.
57. Chan, Y. H. M.; Lenz, P.; Boxer, S. G. *Proc. Natl. Acad. Sci. U.S.A.* **2007** *104*, 18913.
58. Yoshina-Ishii, C.; Miller, G. P.; Kraft, M. L.; Kool, E. T.; Boxer, S. G. *J. Am. Chem. Soc.* **2005** *127*, 1356.
59. Yoshina-Ishii, C.; Boxer, S. G. *J. Am. Chem. Soc.* **2003** *125*, 3696.
60. Stengel, G.; Simonsson, L.; Campbell, R. A.; Höök, F. *J. Phys. Chem. B* **2008** *112*, 8264.
61. Stengel, G.; Zahn, R.; Höök, F. *J. Am. Chem. Soc.* **2007** *129*, 9584.
62. Jakobsen, U.; Simonsen, A. C.; Vogel, S. *J. Am. Chem. Soc.* **2008** *130*, 10462.
63. Jakobsen, U.; Vogel, S. *Methods in Enzymology; Liposomes, Pt F*, **2009** 233.
64. Wang, C. G.; Ma, Z. F. *Anal. Bioanal. Chem.* **2005** *382*, 1708.
65. Lozano, M. M.; Starkel, C. D.; Longo, M. L. *Langmuir* **2010** 26, 8517.
66. Chandra, R. A.; Douglas, E. S.; Mathies, R. A.; Bertozzi, C. R.; Francis, M. B. *Angew. Chem. Int. Ed.* **2006** *45*, 896.
67. Gartner, Z. J.; Bertozzi, C. R. *Proc. Natl. Acad. Sci. U.S.A.* **2009** *106*, 4606.
68. Loew, M.; Kang, L.; Dahne, L.; Hendus-Altenburger, R.; Kaczmarek, O.; Liebscher, J.; Huster, D.; Ludwig, K.; Bottcher, C.; Herrmann, A.; Arbuzova, A. *Small* **2009** *5*, 320.

69. Banchelli, M.; Bombelli, F. B.; Berti, D.; Baglioni, P.; Nejat, D. *Meth. Enzymol.* **2009** 249, Academic Press.
70. LaVan, D. A.; McGuire, T.; Langer, R. *Nat. Biotechnol.* **2003** *21*, 1184.
71. Collier, J. H.; Messersmith, P. B. *Annual Review of Materials Research* **2001** *31*, 237.
72. Liang, H. J.; Angelini, T. E.; Ho, J.; Braun, P. V.; Wong, G. C. L. *J. Am. Chem. Soc.* **2003** *125*, 11786.
73. Zhang, L. F.; Hong, L.; Yu, Y.; Bae, S. C.; Granick, S. *J. Am. Chem. Soc.* **2006** *128*, 9026.
74. Jesorka, A.; Orwar, O. *Annu. Rev. Anal. Chem.* **2008** *1*, 801.
75. Cao, Z. H.; Tong, R.; Mishra, A.; Xu, W. C.; Wong, G. C. L.; Cheng, J. J.; Lu, Y. *Angew. Chem. Int. Ed.* **2009** *48*, 6494.
76. a) Patolsky, F.; Lichtenstein, A.; Willner, I. *J. Am. Chem. Soc.* **1999** *122*, 418. b) Dave, N.; Liu, J. *ACS Nano* **2011**, 5, 1304.
77. Patolsky, F.; Lichtenstein, A.; Willner, I. *J. Am. Chem. Soc.* **2001** *123*, 5194.
78. Patolsky, F.; Lichtenstein, A.; Willner, I. *Angew. Chem., Int. Ed.* **2000** *39*, 940.
79. Chan, Y. H. M.; van Lengerich, B.; Boxer, S. G. *Biointerphases* **2008** *3*, FA17.
Thompson, M. P.; Chien, M.-P.; Ku, T.-H.; Rush, A. M.; Gianneschi, N. C. *Nano Lett.* **2010** *10*, 2690.
80. Hurst, S. J.; Hill, H. D.; Mirkin, C. A. *J. Am. Chem. Soc.* **2008** *130*, 12192.
81. Liu, J.; Lu, Y. *Nature Protocols* **2006** *1*, 246.
82. Hurst, S. J.; Lytton-Jean, A. K. R.; Mirkin, C. A. *Anal. Chem.* **2006** *78*, 8313.
83. Achalkumar, A. S.; Bushby, R. J.; Evans, S. D. *Soft Matter* **2010** *6*, 6036.
84. Pfeiffer, I.; Höök, F. *J. Am. Chem. Soc.* **2004** *126*, 10224.
85. Banchelli, M.; Betti, F.; Berti, D.; Caminati, G.; Bombelli, F. B.; Brown, T.; Wilhelmsson, L. M.; Norden, B.; Baglioni, P. *J. Phys. Chem. B* **2008** *112*, 10942.
86. Erkan, Y.; Halma, K.; Czolkos, I.; Jesorka, A.; Dommersnes, P.; Kumar, R.; Brown, T.; Orwar, O. *Nano Lett.* **2007** *8*, 227.
87. Bordi, F.; Cametti, C. *Colloid. Surface. B.* **2002** *26*, 341.
88. Lytton-Jean, A. K. R.; Mirkin, C. A. *J. Am. Chem. Soc.* **2005** *127*, 12754.

89. Xu, J.; Craig, S. L. *J. Am. Chem. Soc.* **2005** *127*, 13227.
90. Hammond, K.; Reboiras, M. D.; Lyle, I. G.; Jones, M. N. *Biochim. Biophys. Acta* **1984** *774*, 19.
91. Halling, K. K.; Ramstedt, B.; Nystrom, J. H.; Slotte, J. P.; Nyholm, T. K. M. *Biophys. J.* **2008** *95*, 3861.
92. a) Lee, J. S.; Stoeva, S. I.; Mirkin, C. A. *J. Am. Chem. Soc.* **2006** *128*, 8899. b) Lee, J. -S.; Seferos, D. A.; Giljohann, D. A.; Mirkin, C. A. *J. Am. Chem. Soc.* **2008**, 130, 5430. c) Miyake, Y.; Togashi, H.; Tashiro, M.; Yamaguchi, H.; Oda, S.; Kudo, M.; Tanaka, Y.; Kondo, Y.; Sawa, R.; Fujimoto, T.; Machinami, T.; Ono, A. *J. Am. Chem. Soc.* **2006**, 128, 2172.
93. Sun, Y.; Harris, N. C.; Kiang, C. H. *Plasmonics* **2007** *2*, 193.
94. Park, S. Y.; Stroud, D. *Physical Review B* **2003** *67*.
95. a) Keefe, A. D.; Pai, S.; Ellington, A. *Nat. Rev. Drug. Discov.* **2010**, 9, 537. b) Famulok, M.; Hartig, J. S.; Mayer, G. *Chem. Rev.* **2007**, 107, 3715. c) Cao, Z. H.; Tong, R.; Mishra, A.; Xu, W. C.; Wong, G. C. L.; Cheng, J. J.; Lu, Y. *Agnew Chem. Int. Ed.* **2009**, 48, 6494. d) Kang, H.; O'Donoghue, M. B.; Liu, H.; Tan, W. *Chem. Comm.* **2010**, 46, 249. e) Mann, A. P.; Bhavane, R. C.; Somasunderam, A.; Montalvo-Ortiz, B. L.; Ghaghada, K. B.; Volk, D.; Nieves-Alicea, R.; Suh, K. S.; Ferrari, M.; Annapragada, A.; Gorenstein, D. G.; Tanaka, T. *Oncotarget* **2011**, 2, 298.
96. a) Helenius, A.; Simons, K. *Biochim. Biophys. Acta* **1975**, 415, 29. b) Lash, J. *Biochim. Biophys. Acta* **1995**, 1241, 269. c) Lichtenberg, D.; Robson, R. J.; Dennis, E. A. *Biochim. Biophys. Acta, Biomembr.* **1983**, 737, 285. d) Link, S.; El-Sayed, M. A. **1999**, *J. Phys. Chem. B.* 103, 8410. e) Velluto, D.; Gasbarri, C.; Angelini, G.; Fontana, A. *J. Phys. Chem. B.* **2011**, 115, 8130. f) g) Edwards, K.A.; Baeumner, A. J. *Talanta* **2006**, 68, 1421. h) Ho, R.; Rouse, B.; Huang, L. *J. Biol. Chem.* **1987**, 262, 13979. i) Locascio-Brown, L.; Plant, A.; Durst, R. *Anal. Chem.* **1988**, 60, 792. i) Plant, A. *Photochem. Photobiol.* **1986**, 44, 453. j) Rule, G.; Montagna, R.; Durst, R. *Anal. Biochem.* **1997**, 244, 260. k) Ahn-Yoon, S.; DeCory, T.; Baeumner, A.; Durst, R. *Anal. Chem.* **2003**, 75, 2256. l) Park, S.; Durst, R. *Anal. Biochem.* **2000**, 280, 151. m) Ahn-Yoon, S.; DeCory,

T.; Baeumner, A.; Durst, R. *Anal. Bioanal. Chem.* **2004**, 378, 68. n) Tai, J.; Ewert, M.; Belliot, G.; Glass, R.; Monroe, S. *J. Virol. Method* **2003**, 110, 119. o) Hartley, H.; Baeumner, A. *Anal. Bioanal. Chem.* **2003**, 376, 319. p) Baeumner, A.; Schlesinger, N.; Slutzki, N.; Romano, J.; Lee, E.; Montagna, R. *Anal. Chem.* **2002**, 74, 1442. q) Zaytseva, N.; Montagna, R.; Lee, E.; Baeumner, A. *Anal. Bioanal. Chem.* **2004**, 380, 46.

97. a) Nir, S.; Nieva, J. L. *Progress in Lipid Research* **2000**, 39, 181. b) Hui, S.; Nir, S.; Stewart, T. P.; Boni, L. T.; Huang, S. K. *Biochim. Biophys. Acta.* **1988**, 941, 130. c) Nieva, J. L.; Nir, S.; Muga, A.; Goni, F. M.; Wilschut, J. *Biochemistry* **1994**, 33, 3201. d) Rapaport, D.; Peled, R.; Nir, S.; Shai, Y. *Biophys J.* **1996**, 70, 2503. e) Rex, S.; Schwarz, G. *Biochemistry* **1998**, 37, 2336. f) Lorin, A.; Noël, M.; Provencher, M. –E.; Turcotte, V.; Masson, C.; Cardinal, S.; Lagüe, Voyer, N.; Auger, M. *Biochemistry* **2011**, 50, 9409. g) Alonso, J. M.; Llácer, C.; Villa, A. O.; Figueruelo, J. E.; Molina, F. J. *Colloids and Surfaces A: Physicochemical and Engineering Aspects* **1995**, 95, 11. h) Levin, Y.; Idiart, M. A. *Physica A* **2004**, 331, 571.

98. a) Guo, X.; Szoka Jr., F. C. *Acc. Chem. Res.* **2003**, 36, 335. b) Drummond, D. C.; Zignani, M.; Leroux, J. *Prog. Lipid. Res.* **2000**, 39, 409. c) Asokan, A.; Cho, M. J. *J. Pharm. Sci.* **2002**, 91, 903. d) Chu, C. –J.; Szoka, F. C. *J. Liposome Res.* **1994**, 4, 361. e) Gerasimov, O. V.; Rui, Y. J.; Thompson, D. H. *Phase Transition. Vesicles*; Marcel Dekker: New York **1996**, 680. f) Thomas, J. L.; Tirrell, D. A. *Acc. Chem. Res.* **1992**, 25, 336. g) Yatvin, M. B.; Kreutz, W.; Horwitz, B. A.; Shinitzky, M. *Science* **1980,** 210, 1253. h) Drummond, D. C.; Meyer, O.; Hong, K.; Kirpotin, D. B.; Papahadjopoulos, D. *Pharmacol. Rev.* **1999**, 51, 691. i) Nir, S.; Nicol, F.; Szoka, F. C. *Mol. Membr. Biol.* **1999**, 16, 95. j) Boomer, J. A.; Thompson, D. H. *Chem. Phys. Lipids* **1999**, 99, 145. k) Thompson, D. H.; Gerasimov, O. V.; Wheeler, J. J.; Rui, Y.; Anderson, V. C. *Biochim. Biophys. Acta* **1996**, 1279, 25.

99. a) Bibi, S.; Lattmann, E.; Mohammed, A. R.; Perrie, Y. *J. of Microencapsulation* **2012**, 29, 262. b) Huang, S. –L.; Macdonald, R. C. *Biochim Biophys Acta* **2004**, 1665, 134. c) Schroeder, A.; Krost, J.; Barenholz, Y. *Chem. Phys. Lipids* **2009**, 162, 1. d) Smith, B.; Lyakhov, I.; Loomis, K.; Needle, D.; Baxa, U.; Yavlovich, A.; Capal, J.; Blumenthal, R.; Puri, A. *J. Control Release* **2011**, 153, 187. e) Winter, N. D.; Murphy, R. K. J.; Halloran, T. V. O.; Schatz, G. C. *J. Liposome Res.* **2011**, 21, 106. f) Needham, D.; Dewhirst, M. W. *Adv. Drug Deliv. Rev.* **2001**, 53, 285. g) Kono, K.; Nakai, R.; Morimoto, K.; Takagishi, T. *Biochim Biophys Acta* **1999**, 1416, 239. h) Chandaroy, P.; Sen, A.;

Hui, S. W. *J. Control Release*, **2001**, 76, 27. i) Kono, K. *Adv. Drug Deliv. Rev.* **2001**, 53, 307. j) Shum, P.; Kim, J, -M, Thompson, D. H. *Adv. Drug Deliv. Rev.* **2001**, 53, 273.

100. a) Melancon, M. P.; Zhou, M.; Li, C. *Acc. Chem. Res.* **2011**, 44, 947. b) Jokerst, J. V.; Gambhir, S. S. *Acc. Chem. Res.* **2011**, 44, 1050. c) Bardhan, R.; Lal, S.; Joshi, A., Halas, N. J. *Acc. Chem. Res.* **2011**, 44, 936. d) Link, S.; El-Sayed, M. A. **1999**, *J. Phys. Chem. B.* 103, 8410.

101. a) Wu, G. H.; Milkhailovsky, A.; Khant, H. A.; Fu, C.; Chiu, W.; Zasadzinski, J. A. *J. Am. Chem. Soc.* **2008**, *130*, 8175; b) Aili, D.; Mager, M.; Roche, D.; Stevens, M. M. *Nano Lett.* **2010**, *11*, 1401.

102. a) Kojima, C.; Hirano, Y.; Yuba, E.; Harada, A.; Kono, K. *Colloid. Surface. B.* **2008**, *66*, 246; b) Sau, T.K.; Urban, A. S.; Dondapati, S. K.; Fedoruk, M.; Horton, M. R.; Rogach, A. L.; Stefani, F. D.; Radler, J. O.; Feldmann, J. *Colloid. Surface. A.* **2009**, *342*, 92; c) Jin, Y. D.; Gao, X. H. *J. Am. Chem. Soc.* **2009**, *131*, 17774 d) Paasonen, L.; Laaksonen, T.; Johans, C.; Yliperttula, M.; Kontturi, K.; Urth, A. J. *Control. Release* **2007**, *122*, 86; e) Troutman, T. S.; Leung, S. J.; Romanowski, M. *Adv. Mater.* **2009**, *21*, 2334; f) Yaghmur, A.; Paasonen, L.; Yliperttula, M.; Urtti, A.; Rappolt, M. *J. Phys. Chem. Lett.* **2010**, *1*, 962; g) Paasonen, L.; Sipila, T.; Subrizi, A.; Laurinmaki, P.; Butcher, S. J.; Rappolt, M.; Yaghmur, A.; Urtti, A.; Yliperttula, M. *J Control Release* **2010**, *147*, 136; h) An, X.; Zhang, F.; Zhu, Y.; Shen, W. *Chem. Comm.* **2010**, *46*, 7202; i) Volodkin, D. V.; Skirtach, A. G.; Mohwald, H. *Angew. Chem. Int. Ed.* **2009**, *48*, 1807; j) Katz, J. S.; Burdick, J. A. *Macromolecular Bioscience* **2010**, *10*, 339; k) Anderson, L. J. E.; Hansen, E.; Lukianova-Hleb, E. Y.; Hafner, J. H.; Lapotko, D. O. *J. Control. Release* **2010**, *144*, 151; l) Fong, W.-K.; Hanley, T. L.; Thierry, B.; Kirby, N.; Boyd, B. J. *Langmuir* **2010**, *26*, 6136; m) Urban, A. S.; Fedoruk, M.; Horton, M. R.; Radler, J. O.; Stefani, F. D.; Feldmann, J. *Nano Lett.* **2009**, *9*, 2903; n) Troutman, T. S.; Barton, J. K.; Romanowski, M. *Adv. Mater.* **2008**, *20*, 2604.; o) Al-Jamal, W. T.; Kostarelos, K. *Nanomedicine* **2007**, 2, 85.; p) Hong, K.; Friend, D. S.; Glabe, C. G.; Papahadjopoulos, D. *Biochim. Biophys. Acta* **1983**, 732, 320.; q) Park, S.-H.; Oh, S.-G.; Mun, J.-Y.; Han, S.-S. *Colloids Surf. B* **2006**, 48, 112–118.

103. a) Mucic, R. C.; Storhoff, J. J.; Mirkin, C. A.; Letsinger, R. L. *J. Am. Chem. Soc.* **1998**, 120, 12674. b) Mirkin, C. A.; Letsinger, R. L.; Mucic, R. C.; Storhoff, J. J. *Nature* **1996**, 382, 607. c) Storhoff, J. J.; Mirkin, C. A. *Chem. Rev.* **1999**, 99, 1849. d) Kiely, C. J.; Fink, J.; Brust, M.; Bethell, D.; Schiffrin, D. J. *Nature* **1998**, 396, 444. e) Hutter, E.; Tokareva, I. *J. Am. Chem. Soc.* **2004**, 126, 15784. f) Sadasivan, S.; Dujardin, E.; Li, M.; Johnson, C. J.; Mann, S. *Small* **2005**, 1, 103. g) Liu, J.; Lee, J. H.; Lu, Y. *Anal. Chem.* **2007**, 79, 4120. h) Li, Y.; Zheng, Y.; Gong, M.; Deng, Z. *Chem. Comm.* **2012**, 48, 3727.

104. Elghanian, R.; Storhoff, J. J.; Mucic, R. C.; Letsinger, R. L.; Mirkin, C. A. *Science* **1997**, *277*, 1078.

105. a) Smith, H. L.; Howland, M. C.; Szmodis, A. W.; Li, Q.; Daemen, L. L.; Parikh, A. N.; Majewski, J. *J. Am. Chem. Soc.* **2009**, *131*, 3631; b) Yee, C. K.; Amweg, M. L.; Parikh, A. N. *J. Am. Chem. Soc.* **2004**, *126*, 13962.

106. Pack, D. W.; Ng, K.; Maloney, K. M.; Arnold, F. H. *Supramolecular Science* **1997**, *4*, 3.

107. Heldin, C.-H.; Östman, A. *Cytokine & Growth Factor Reviews* **1996**, *7*, 3.

108. Heldin, C. H.; Ostman, A.; Ronnstrand, L. *Biochimica Et Biophysica Acta-Reviews on Cancer* **1998**, *1378*, F79.

109. Periole, X.; Huber, T.; Marrink, S. J.; Sakmar, T. P. *J. Am. Chem. Soc.* **2007**, *129*, 10126.

110. Maloney, K. M.; Shnek, D. R.; Sasaki, D. Y.; Arnold, F. H. *Chem. Biol.* **1996**, *3*, 185.

111. Rapaport, D.; Shai, Y. *J. Biol. Chem.* **1992**, *267*, 6502.

112. Ellington, A. D.; Szostak, J. W. *Nature* **1990**, *346*, 818.

113. Tuerk, C.; Gold, L. *Science* **1990**, *249*, 505.

114. Wilson, D. S.; Szostak, J. W. *Annu. Rev. Biochem.* **1999**, *68*, 611.

115. a) Liu, J.; Cao, Z.; Lu, Y. *Chem. Rev.* **2009**, *109*, 1948.; b) Huizenga, D. E.; Szostak, J. W. *Biochemistry* **1995**, 34, 656. c) Lin, C. H.; Patel, D. *J. Chem. Biol.* **1997**, 4, 817. d) Hamaguchi, N., Ellington, A.; Stanton, M. *Anal. Biochem.* **2001**, 294, 126. e) Urata, H., Nomura, K., Wada, S.-i. and Akagi, M. *Biochem. Biophys. Res. Commun*. **2007**, 360, 459. f) Li, J. J.; Fang, X.; Schuster, S. M.; Tan, W. *Angew. Chem., Int. Ed.* **2000**, 39, 1049. g) Stojanovic, M. N., de Prada, P., Landry, D. W. *J. Am. Chem. Soc.* **2001**, 123, 4928. (h) Yang, C. J.; Jockusch, S.; Vicens, M.; Turro, N. J.; Tan, W. *Proc. Natl. Acad. Sci. U.S.A.* **2005**, 102, 17278.; (i) Ueyama, H.; Takagi, M.; Takenaka, S. *J. Am. Chem. Soc.* **2002**, 124, 14286.

116. Cho, E. J.; Lee, J.-W.; Ellington, A. D. *Annu. Rev. Anal. Chem.* **2009**, *2*, 241.

117. Li, D.; Song, S. P.; Fan, C. H. *Acc. Chem. Res.* **2010**, *43*, 631.

118. Navani, N. K.; Li, Y. *Curr. Opin. Chem. Biol.* **2006**, *10*, 272.

119. Willner, I.; Zayats, M. *Angew. Chem., Int. Ed.* **2007**, *46*, 6408.

120. Lubin, A. A.; Plaxco, K. W. *Acc. Chem. Res.* **2010**, *43*, 496.

121. Famulok, M.; Hartig, J. S.; Mayer, G. *Chem. Rev.* **2007**, *107*, 3715.

122. Chan, Y. H. M.; van Lengerich, B.; Boxer, S. G. *Proc. Natl. Acad. Sci. U.S.A.* **2009**, *106*, 979.

123. Yoshina-Ishii, C.; Miller, G. P.; Kraft, M. L.; Kool, E. T.; Boxer, S. G. *J. Am. Chem. Soc.* **2005**, *127*, 1356.

124. Achalkumar, A. S.; Bushby, R. J.; Evans, S. D. *Soft Matter* **2010**, *6*, 6036.

125. Stengel, G.; Zahn, R.; Hook, F. *J. Am. Chem. Soc.* **2007**, *129*, 9584.

126. Dave, N.; Liu, J. *Acs Nano* **2011**, *5*, 1304.

127. Jhaveri, S. D.; Kirby, R.; Conrad, R.; Maglott, E. J.; Bowser, M.; Kennedy, R. T.; Glick, G.; Ellington, A. D. *J. Am. Chem. Soc.* **2000**, *122*, 2469.

128. Stojanovic, M. N.; de Prada, P.; Landry, D. W. *J. Am. Chem. Soc.* **2000**, *122*, 11547.

129. Nutiu, R.; Li, Y. *J. Am. Chem. Soc.* **2003**, *125*, 4771.

130. Liu, J.; Lu, Y. *Angew. Chem., Int. Ed.* **2006**, *45*, 90.

131. Lu, N.; Shao, C. Y.; Deng, Z. X. *Chem. Comm.* **2008**, 6161.

132. Fahlman, R. P.; Sen, D. *J. Am. Chem. Soc.* **2002**, *124*, 4610.

133. Chen, S. J.; Huang, Y. F.; Huang, C. C.; Lee, K. H.; Lin, Z. H.; Chang, H. T. *Biosens. Bioelectron.* **2008**, *23*, 1749.

134. Wang, J.; Wang, L. H.; Liu, X. F.; Liang, Z. Q.; Song, S. P.; Li, W. X.; Li, G. X.; Fan, C. H. *Adv. Mater.* **2007**, *19*, 3943.

135. Xu, W. C.; Lu, Y. *Anal. Chem.* **2010**, *82*, 574.

136. Xiang, Y.; Tong, A. J.; Lu, Y. *J. Am. Chem. Soc.* **2009**, *131*, 15352.

137. Li, F.; Zhang, J.; Cao, X. N.; Wang, L. H.; Li, D.; Song, S. P.; Ye, B. C.; Fan, C. H. *Analyst* **2009**, *134*, 1355.

138. Freeman, R.; Li, Y.; Tel-Vered, R.; Sharon, E.; Elbaz, J.; Willner, I. *Analyst* **2009**, *134*, 653.

Liu, J. W.; Lu, Y. *Anal. Chem.* **2004**, *76*, 1627.

139. a) Li, Y.; Tanaka, T. *J. Chem. Phys.* **1990**, 92, 1365. b) Jones, C. D.; Lyon, L. A. *Macromolecules* **2000**, 33, 8301. c) Staudinger, H.; Husemann, E. *Ber. Dtsch. Chem. Ges. A* **1935**, 68, 1618. d) Tanaka, T. *Phys. Rev. Lett.* **1978**, 40, 820. e) Dusek, K.; Patterson, K. *J. Poly. Sci. Poly. Phys. Ed.* **1968**, 6, 1209. f) Moselhy, J.; Wu, X. Y.; Nicholov, R.; Kodaria, K. *J. Biomater. Sci. Polym. Ed.* **2000**, 11, 123. g) Duracher, D.; Sauzedde, F.; Elaissari, A.; Perrin, A.; Pichot, C. *Colloid Polym. Sci.* **1998**, 276, 219. h) Duracher, D.; Sauzedde, F.; Elaissari, A.; Pichot, C.; Nabzar, L. *Colloid Polym. Sci.* **1998**, 276, 920. i) Snowden, M. J.; Chowdhry, B. Z.;Vincent, B.; Morris, G. E. *J. Chem. Soc. Faraday Trans.* **1996**, 92, 5013. j) Tanaka, T.; Nishio, I.; Sun, S. T.; Ueno-Nishio, S. *Science* **1982**, 218, 467. k) Um, S. H.; Lee, J. B.; Park, N.; Kwon, S. Y.; Umbach, C. C.; Luo, D. *Nat. Mater.* **2006**, *5*, 797 l) Nagahara, S.; Matsuda, T. *Polymer Gels and Networks* **1996**, *4*, 111. m) Lin, D. C.; Yurke, B.; Langrana, N. A. *Engineering in Medicine and Biology, 2002. 24th Annual Conference and the Annual Fall Meeting of the Biomedical Engineering Society] EMBS/BMES Conference, 2002. Proceedings of the Second Joint*, **2002**, 621, 627.n) Liedl, T.; Dietz, H.; Yurke, B.; Simmel, F. *Small* **2007**, *3*, 1688. o) Liu, J. W., and Lu, Y. *Angew. Chem. Int. Ed.* **2006**, *45*, 90.; p) Huang, C.-C., Huang, Y.-F., Cao, Z., Tan, W., and Chang, H.-T. *Anal. Chem.* **2005**, *77*, 5735.; q) Pavlov, V., Xiao, Y., Shlyahovsky, B., and Willner, I. *J. Am. Chem. Soc.* **2004**, *126*, 11768.; r) Liu, J., Lu, Y. *Adv. Mater.* **2006**, *18*, 1667. s) Liu, J. W., Lee, J. H., Lu, Y. *Anal. Chem.* **2007**, *79*, 4120.; t) Yigit, M. V., Mazumdar, D., Kim, H.-K., Lee, J. H., Odintsov, B., Lu, Y. *ChemBioChem* **2007**, *8*, 1675. u) Yang, H. H.; Liu, H. P.; Kang, H. Z.; Tan, W. H. *J. Am. Chem. Soc.* **2008**, *130*, 6320.

140. a) Dorea, J. G.; Donangelo, C. M. *Clin. Nutr.* **2006**, *25*, 369. b) Nolan, E. M.; Lippard, S. J. *Chem. Rev.* **2008**, *108*, 3443.

141. Harris, H. H.; Pickering, I. J.; George, G. N. *Science* **2003**, *301*, 1203.

142. Tchounwou, P. B.; Ayensu, W. K.; Ninashvili, N.; Sutton, D. *Environ.Toxicol.* **2003**, *18*, 149.

143. Jarup, L. *Brit. Med. Bull.* **2003**, *68*, 167.

144. a) Nolan, E. M.; Lippard, S. J. *J. Am. Chem. Soc.* **2003**, *125*, 14270. b) Nolan, E. M.; Lippard, S. J. *J. Am. Chem. Soc.* **2007**, *129*, 5910. c) Yoon, S.; Albers, A. E.; Wong, A. P.; Chang, C. J. *J. Am. Chem. Soc.* **2005**, *127*, 16030. d) Wegner, S. V.; Okesli, A.; Chen, P.; He, C. *J. Am. Chem. Soc.* **2007**, *129*, 3474. e) Yoon, S.; Miller, E. W.; He, Q.; Do, P. H.; Chang, C. J. *Angew. Chem. Int. Ed.* **2007**, *46*, 6658. f) Hollenstein, M.; Hipolito, C.; Lam, C.; Dietrich, D.; Perrin, D. M. *Angew. Chem., Int. Ed.* **2008**, *47*, 4346.

145. a) Ono, A.; Togashi, H. *Angew. Chem., Int. Ed.* **2004**, *43*, 4300.; b) Simpson, R. B. *J. Am. Chem. SOC* **1964**, 86, 2069.; c) Kosturko, L.D. *Biochemistiy,* **1974** 13, 3949.

146. Tanaka, Y.; Oda, S.; Yamaguchi, H.; Kondo, Y.; Kojima, C.; Ono, A. *J. Am. Chem. Soc.* **2007**, *129*, 244.

147. Miyake, Y.; Togashi, H.; Tashiro, M.; Yamaguchi, H.; Oda, S.; Kudo, M.; Tanaka, Y.; Kondo, Y.; Sawa, R.; Fujimoto, T.; Machinami, T.; Ono, A. *J. Am. Chem. Soc.* **2006**, *128*, 2172.

148. a) Liu, J.; Lu, Y. *Angew. Chem., Int. Ed.* **2007**, *46*, 7587. b) Wang, Z.; Lee, J. H.; Lu, Y. *Chem. Comm.* **2008**, 6005. c)Wang, J.; Liu, B. *Chem. Comm.* **2008**, 4759. (d) Wang, H.; Wang, Y. X.; Jin, J. Y.; Yang, R. H. *Anal. Chem.* **2008**, *80*, 9021. e) Chiang, C. K.; Huang, C. C.; Liu, C. W.; Chang, H. T. *Anal. Chem.* **2008**, *80*, 3716. f) Liu, B. *Biosens. Bioelectron.* **2008**, *24*, 756. g) Ye, B.-C.; Ying, B.-C. *Angew. Chem., Int. Ed.* **2008**, *47*, 8386.

149. a) Lee, J.-S.; Han, M. S.; Mirkin, C. A. *Angew. Chem., Int. Ed.* **2007**, *46*, 4093. b) Liu, X. F.; Tang, Y. L.; Wang, L. H.; Zhang, J.; Song, S. P.; Fan, C. H.; Wang, S. *Adv. Mater.* **2007**, *19*, 1471. c) Liu, C. W.; Hsieh, Y. T.; Huang, C. C.; Lin, Z. H.; Chang, H. T. *Chem. Comm.* **2008**, 2242. (d) Xue, X. J.; Wang, F.; Liu, X. G. *J. Am. Chem. Soc.* **2008**, *130*, 3244. e) Li, D.; Wieckowska, A.; Willner, I. *Angew. Chem. Int. Ed.* **2008**, *47*, 3927. f) He, S. J.; Li, D.; Zhu, C. F.; Song, S. P.; Wang, L. H.; Long, Y. T.; Fan, C. H. *Chem. Comm.* **2008**, 4885. g) Lee, J.; Jun, H.; Kim, J. *Adv. Mater.* **2009**, *21*, 3674. h) Freeman, R.; Finder, T.; Willner, I. *Angew. Chem., Int. Ed.* **2009**, *48*, 7818. i) Li, T.; Li, B. L.; Wang, E. K.; Dong, S. J. *Chem. Comm.* **2009**, 3551. j) Lu, N.; Shao, C. Y.; Deng, Z. X. *Analyst* **2009**, *134*, 1822.

150. Office of Water. *Mercury update: impact on fish advisories*, EPA Fact Sheet EPA-823-F-01-011; U.S. Environmental Protection Agency: Washington, DC, 2001.

151. a) Liu, S.-J.; Nie, H.-G.; Jiang, J.-H.; Shen, G.-L.; Yu, R.-Q. *Anal. Chem.* **2009**, *81*, 5724. b) Wu, D. H.; Zhang, Q.; Chu, X.; Wang, H. B.; Shen, G. L.; Yu, R. Q. *Biosens. Bioelectron.*, *25*, 1025.

152. Feng, X.; Fryxell, G. E.; Wang, L. Q.; Kim, A. Y.; Liu, J.; Kemner, K. M. *Science* **1997**, *276*, 923.

153. a) Kara, A.; Uzun, L.; Besirli, N.; Denizli, A. *J. Hazard. Mater.* **2004**, *106*, 93. b) Li, N.; Bai, R. B.; Liu, C. K. *Langmuir* **2005**, *21*, 11780. c) Sonmez, H. B.; Senkal, B. F.; Sherrington, D. C.; Bicak, N. *React. Funct. Polym.* **2003**, *55*, 1. (d) Bicak, N.; Sherrington, D. C.; Senkal, B. F. *React. Funct. Polym.* **1999**, *41*, 69.

154. a) Kim, M.; Um, H. J.; Bang, S.; Lee, S. H.; Oh, S. J.; Han, J. H.; Kim, K. W.; Min, J.; Kim, Y.H. *Environ. Sci. Technol.* **2009**, *43*, 9335. b) Liu, X. J.; Qi, C.; Bing, T.; Cheng, X. H.; Shangguan, D. *Talanta* **2009**, *78*, 253.

155. Climent, E.; Marcos, M. D.; Martinez-Manez, R.; Sancenon, F.; Soto, J.; Rurack, K.; Amoros, P. *Angew. Chem. Int. Ed.* **2009**, *48*, 8519.

156. Ros-Lis, J. V.; Casasus, R.; Comes, M.; Coll, C.; Marcos, M. D.; Martinez-Manez, R.; Sancenon, F.; Soto, J.; Amoros, P.; El Haskouri, J.; Garro, N.; Rurack, K. *Chem. Eur. J.* **2008**, *14*, 8267.

157. Park, M.; Seo, S.; Lee, I. S.; Jung, J. H. *Chem. Comm.* **2010**, *46*, 4478.

158. Peppas, N. A.; Hilt, J. Z.; Khademhosseini, A.; Langer, R. *Adv. Mater.* **2006**, *18*, 1345.

159. Miyata, T.; Asami, N.; Uragami, T. *Nature* **1999**, *399*, 766.

160. Jen, A. C.; Wake, M. C.; Mikos, A. G. *Biotechnol. Bioeng.* **1996**, *50*, 357.

161. Olsen, K. G.; Ross, D. J.; Tarlov, M. J. *Anal. Chem.* **2002**, *74*, 1436.

162. Nayak, S.; Lyon, L. A. *Angew. Chem., Int. Ed.* **2005**, *44*, 7686.

163. Tsitsilianis, C. *Soft Matter* **2010**, *6*, 2372.

164. Liu, J. *Soft Matter* 2011, 7, 6757.

165. Liu, X. D.; Murayama, Y.; Matsunaga, M.; Nomizu, M.; Nishi, N. *Int. J. Biol. Macromol.* **2005**, 35, 193.

166. Nolan, E. M.; Lippard, S. *J. Chem. Rev.* **2008**, 108, 3443.

167. a) Ono, A.; Togashi, H. *Angew. Chem., Int. Ed.* **2004**, 43, 4300. b) Wang, J.; Liu, B. *Chem. Commun.* **2008**, 4759. c) Wang, Z.; Lee, J. H.; Lu, Y. *Chem. Commun.* **2008**, 6005. d) Chiang, C. K.; Huang, C. C.; Liu, C. W.; Chang, H. T. *Anal. Chem.* **2008**, 80, 3716. e) Lee, J.-S.; Han, M. S.; Mirkin, C. A. *Angew. Chem., Int. Ed.* **2007**, 46, 4093. f) Li, D.; Wieckowska, A.; Willner, I. *Angew. Chem., Int. Ed.* **2008**, 47, 3927. g) Liu, S.-J.; Nie, H.-G.; Jiang, J.-H.; Shen, G.-L.; Yu, R.-Q. *Anal. Chem.* **2009**, 81, 5724. h) Kong, R.-M.; Zhang, X.-B.; Zhang, L.-L.; Jin, X.-Y.; Huan, S.-Y.; Shen, G.-L.; Yu, R.-Q. *Chem. Commun.* **2009**, 5633. i) Guo, L.; Yin, N.; Chen, G. *J. Phys. Chem. C* **2011**, 115, 4837. k) Kiy, M. M.; Jacobi, Z. E.; Liu, J. *Chemistry Eur. J.* **2012**, 18, 1202.; l) Deng, L.; Zhou, Z. X.; Li, J.; Li, T.; Dong, S. J. *Chem. Commun.* **2011**, 47, 11065.

168. Pregibon, D. C.; Doyle, P. S. *Anal. Chem.* **2009**, 81, 4873.

169. Pregibon, D. C.; Toner, M.; Doyle, P. S. *Science* **2007**, 315, 1393.

170. Kawaguchi, H. *Prog. Polym. Sci.* **2000**, 25, 1171.

171. a) Alivisatos, A. P.; Johnsson, K. P.; Peng, X.; Wilson, T. E.; Loweth, C. J.; Bruchez, M. P., Jr; Schultz, P. G. *Nature* **1996**, *382*, 609.; b) Mirkin, C. A.; Letsinger, R. L.; Mucic, R. C.; Storhoff, J. J. *Nature* **1996**, *382*, 607.; c) Storhoff, J. J.; Mirkin, C. A. *Chem. Rev.* **1999**, *99*, 1849-1862.; d) Elghanian, R.; Storhoff, J. J.; Mucic, R. C.; Letsinger, R. L.; Mirkin, C. A. *Science* **1997**, *277*, 1078.; e) Storhoff, J. J.; Elghanian, R.; Mucic, R. C.; Mirkin, C. A.; Letsinger, R. L. *J. Am. Chem. Soc.* **1998**, *120*, 1959.; f) Rosi, N. L.; Mirkin, C. A. *Chem. Rev.* **2005**, *105*, 1547.

172. a) Torchilin, V. P. *Nature Review* **2005**; **4**, 145. b) Zimmerman, S. B.; Minton, A. P. *Annu. Rev. Biophys. Biomol.* **1993**, 22, 27.

173. a) Melancon, M. P.; Zhou, M.; Li, C. *Acc. Chem. Res.* **2011**, 44, 947. b) Jokerst, J. V.; Gambhir, S. S. *Acc. Chem. Res.* **2011**, 44, 1050. c) Bardhan, R.; Lal, S.; Joshi, A., Halas, N. J. *Acc. Chem. Res.* **2011**, 44, 936. d) Link, S.; El-Sayed, M. A. **1999**, *J. Phys. Chem. B.* 103, 8410.

174. a) Kang, H. Z.; O'Donoghue, M. B.; Liu, H. P.; Tan, W. H. *Chem. Comm.* **2010**, 46, 249. b) Mann, A. P.; Bhavane, R. C.; Somasunderam, A.; Montalvo-Ortiz, B. L.; Ghadhada, K. B., Volk, D.; Nieves-Alicea, R.; Suh, K. S.; Ferrari, M.; Annapragada, A. *Oncotarget* **2011**, 2, 298.

175. a) Helwa, Y.; Dave, N.; Froidevaux, R.; Samadi, A.; Liu, J. *ACS Applied Materials & Interfaces* **2012** 4, 2228. b) Simons, K.; Toomre, D. *Nature Reviews* **2000**, 1, 31.